PETROVIETNAM JOURNAL

An Official Publication of the Vietnam National Oil and Gas Group Vol. 6 - 2019

ISSN-0866-854X

PETROVIETNAM Vol 6 - 2019

PETROVIETNAM JOURNAL IS PUBLISHED MONTHLY BY VIETNAM NATIONAL OIL AND GAS GROUP

CONTACT ADDRESS
Floor M2, VPI Tower, Trung Kinh street, Yen Hoa ward, Cau Giay district, Ha Noi
*Tel: (+84-24) 37727108 * Fax: (+84-24) 37727107 * Email: tcdk@pvn.vn/pvj@pvn.vn*
Mobile: 0982288671

Cover photo: The Late Ordovician-Early Silurian deep water turbidites on the Co To island. Photo: Manh Toan

Publishing Licence No. 100/GP-BTTTT dated 15 April 2013 issued by Ministry of Information and Communications

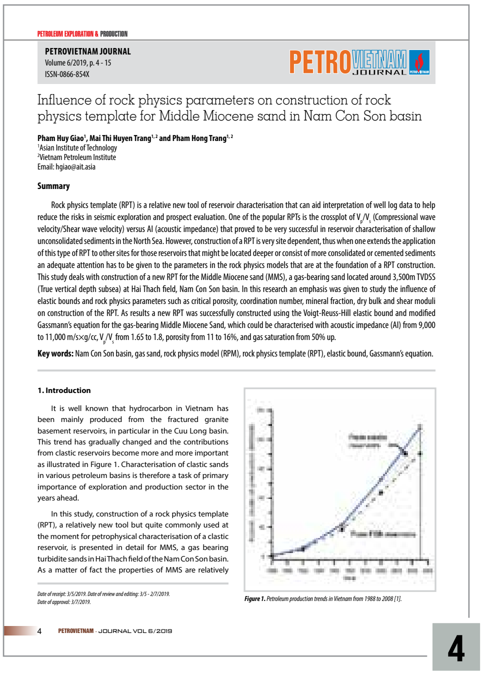
PETROLEUM EXPLORATION & PRODUCTION

PETROVIETNAM JOURNAL
Volume 6/2019, p. 4 - 15
ISSN-0866-854X

Influence of rock physics parameters on construction of rock physics template for Middle Miocene sand in Nam Con Son basin

4


PETROLEUM EXPLORATION & PRODUCTION

PETROVIETNAM JOURNAL
Volume 6/2019, p. 16 - 23
ISSN-0866-854X

Architecture, depositional pattern of syn rift sediments in the Northern Song Hong basin and its petroleum system association

16

SCIENTIFIC RESEARCH

PETROLEUM EXPLORATION & PRODUCTION

4. Influence of rock physics parameters on construction of rock physics template for Middle Miocene sand in Nam Con Son basin

16. Architecture, depositional pattern of syn rift sediments in the Northern Song Hong basin and its petroleum system association

24. Determination of contribution proportion of injection wells in oil production by interwell tracer method using partitioning organic compounds from crude oil

30. Oligocene combination/stratigraphic traps and their reservoir quality in Cuu Long basin, offshore Vietnam

41. Characterisation of acid treatment for damaged zone in fractured granitic basement of Bach Ho field

48. An applied machine learning approach to production forecast for basement formation - Bach Ho field

58. Predicting water influx for gas production wells of Lan Do field using material balance method

PETROLEUM TECHNOLOGIES & STRUCTURES

63. Corrosion threats and strategy to secure Mechanical integrity of Dung Quat refinery

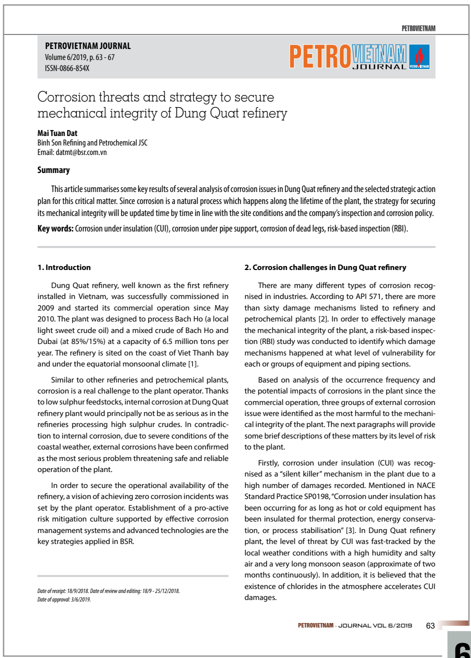
PETROVIETNAM

PETROVIETNAM JOURNAL
Volume 6/2019, p. 63 - 67
ISSN-0866-854X

Corrosion threats and strategy to secure mechanical integrity of Dung Quat refinery

Mai Tuan Dat
Binh Son Refining and Petrochemical JSC
Email: datmt@bsr.com.vn

Summary

This article summarises some key results of several analysis of corrosion issues in Dung Quat refinery and the selected strategic action plan for this critical matter. Since corrosion is a natural process which happens along the lifetime of the plant, the strategy for securing its mechanical integrity will be updated time by time in line with the site conditions and the company's inspection and corrosion policy.

Key words: Corrosion under insulation (CUI), corrosion under pipe support, corrosion of dead legs, risk-based inspection (RBI).

1. Introduction

Dung Quat refinery, well known as the first refinery installed in Vietnam, was successfully commissioned in 2009 and started its commercial operation since May 2010. The plant was designed to process Bach Ho (a local light sweet crude oil) and a mixed crude of Bach Ho and Dubai (at 85%/15%) at a capacity of 6.5 million tons per year. The refinery is sited on the coast of Viet Thanh bay and under the equatorial monsoonal climate [1].

Similar to other refineries and petrochemical plants, corrosion is a real challenge to the plant operator. Thanks to low sulphur feedstocks, internal corrosion at Dung Quat refinery plant would principally not be as serious as in the refineries processing high sulphur crudes. In contradiction to internal corrosion, due to severe conditions of the coastal weather, external corrosions have been confirmed as the most serious problem threatening safe and reliable operation of the plant.

In order to secure the operational availability of the refinery, a vision of achieving zero corrosion incidents was set by the plant operator. Establishment of a pro-active risk mitigation culture supported by effective corrosion management systems and advanced technologies are the key strategies applied in BSR.

Date of receipt: 18/9/2018. Date of review and editing: 18/9 - 25/12/2018.
Date of approval: 3/6/2019.

2. Corrosion challenges in Dung Quat refinery

There are many different types of corrosion recognised in industries. According to API 571, there are more than sixty damage mechanisms listed to refinery and petrochemical plants [2]. In order to effectively manage the mechanical integrity of the plant, a risk-based inspection (RBI) study was conducted to identify which damage mechanisms happened at what level of vulnerability for each or groups of equipment and piping sections.

Based on analysis of the occurrence frequency and the potential impacts of corrosions in the plant since the commercial operation, three groups of external corrosion issue were identified as the most harmful to the mechanical integrity of the plant. The next paragraphs will provide some brief descriptions of these matters by its level of risk to the plant.

Firstly, corrosion under insulation (CUI) was recognised as a "silent killer" mechanism in the plant due to a high number of damages recorded. Mentioned in NACE Standard Practice SP0198, "Corrosion under insulation has been occurring for as long as hot or cold equipment has been insulated for thermal protection, energy conservation, or process stabilisation" [3]. In Dung Quat refinery plant, the level of threat by CUI was fast-tracked by the local weather conditions with a high humidity and salty air and a very long monsoon season (approximate of two months continuously). In addition, it is believed that the existence of chlorides in the atmosphere accelerates CUI damages.

63

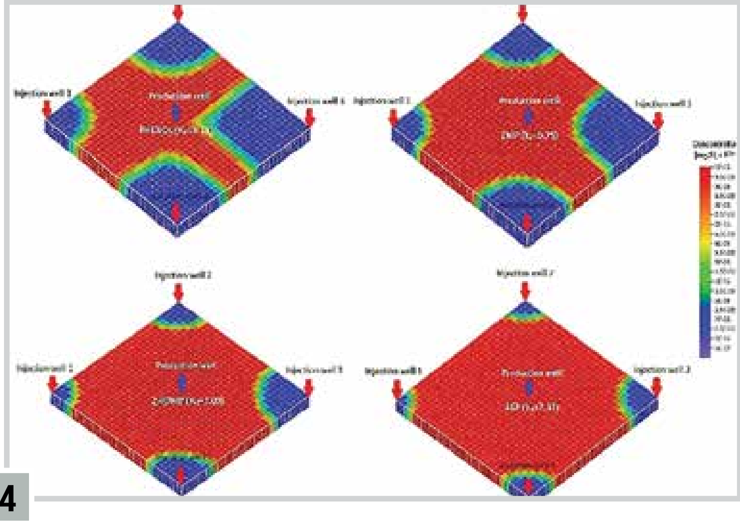

24

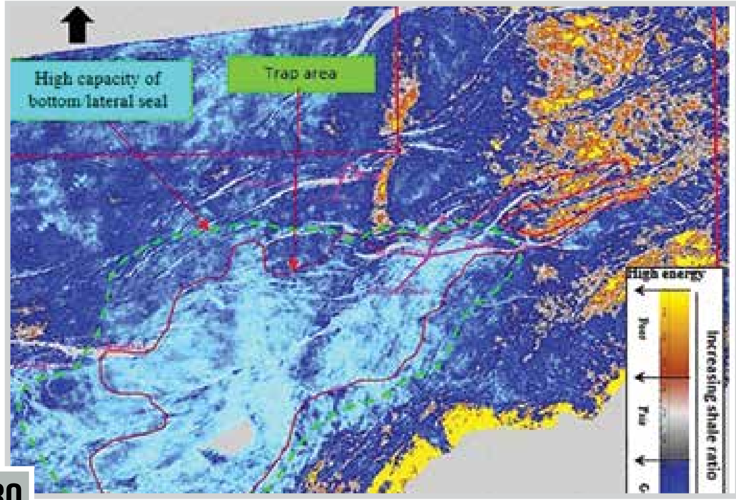

30

PETROLEUM SAFETY & ENVIRONMENT

68. Renewable energy business in oil companies - Case studies in Japan

PETROVIETNAM JOURNAL
Volume 6/2019, p. 4 - 15
ISSN-0866-854X

Influence of rock physics parameters on construction of rock physics template for Middle Miocene sand in Nam Con Son basin

Pham Huy Giao[1], Mai Thi Huyen Trang[1, 2] and Pham Hong Trang[1, 2]
[1]Asian Institute of Technology
[2]Vietnam Petroleum Institute
Email: hgiao@ait.asia

Summary

Rock physics template (RPT) is a relative new tool of reservoir characterisation that can aid interpretation of well log data to help reduce the risks in seismic exploration and prospect evaluation. One of the popular RPTs is the crossplot of V_p/V_s (Compressional wave velocity/Shear wave velocity) versus AI (acoustic impedance) that proved to be very successful in reservoir characterisation of shallow unconsolidated sediments in the North Sea. However, construction of a RPT is very site dependent, thus when one extends the application of this type of RPT to other sites for those reservoirs that might be located deeper or consist of more consolidated or cemented sediments an adequate attention has to be given to the parameters in the rock physics models that are at the foundation of a RPT construction. This study deals with construction of a new RPT for the Middle Miocene sand (MMS), a gas-bearing sand located around 3,500m TVDSS (True vertical depth subsea) at Hai Thach field, Nam Con Son basin. In this research an emphasis was given to study the influence of elastic bounds and rock physics parameters such as critical porosity, coordination number, mineral fraction, dry bulk and shear moduli on construction of the RPT. As results a new RPT was successfully constructed using the Voigt-Reuss-Hill elastic bound and modified Gassmann's equation for the gas-bearing Middle Miocene Sand, which could be characterised with acoustic impedance (AI) from 9,000 to 11,000 m/s×g/cc, V_p/V_s from 1.65 to 1.8, porosity from 11 to 16%, and gas saturation from 50% up.

Key words: Nam Con Son basin, gas sand, rock physics model (RPM), rock physics template (RPT), elastic bound, Gassmann's equation.

1. Introduction

It is well known that hydrocarbon in Vietnam has been mainly produced from the fractured granite basement reservoirs, in particular in the Cuu Long basin. This trend has gradually changed and the contributions from clastic reservoirs become more and more important as illustrated in Figure 1. Characterisation of clastic sands in various petroleum basins is therefore a task of primary importance of exploration and production sector in the years ahead.

In this study, construction of a rock physics template (RPT), a relatively new tool but quite commonly used at the moment for petrophysical characterisation of a clastic reservoir, is presented in detail for MMS, a gas bearing turbidite sands in Hai Thach field of the Nam Con Son basin. As a matter of fact the properties of MMS are relatively

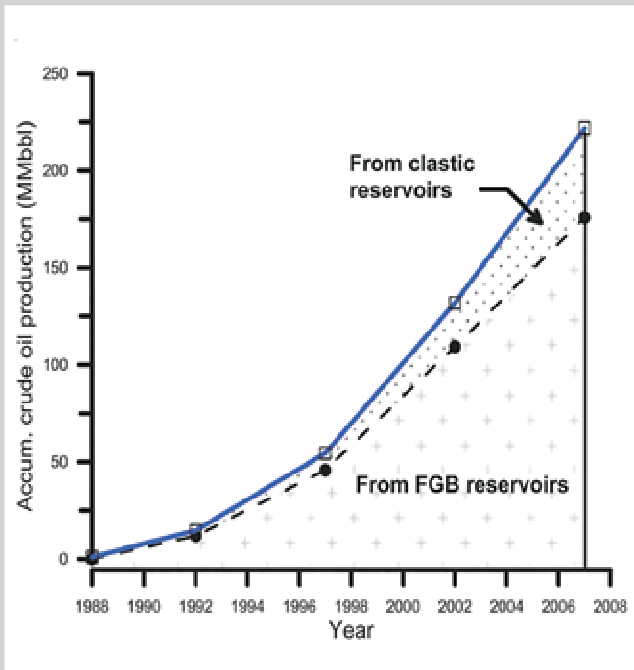

Figure 1. Petroleum production trends in Vietnam from 1988 to 2008 [1].

Date of receipt: 3/5/2019. Date of review and editing: 3/5 - 2/7/2019.
Date of approval: 3/7/2019.

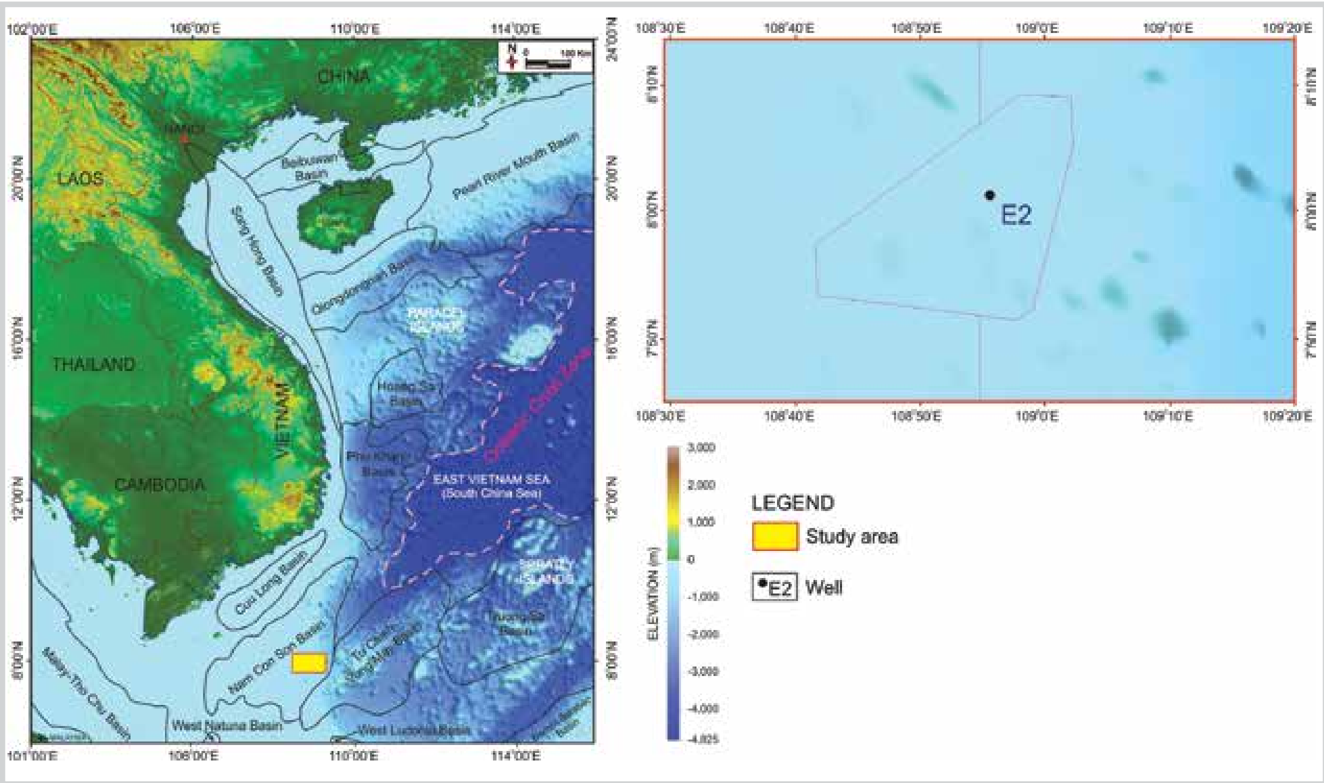

Figure 2. Nam Con Son basin (left inset) and the study well location (right inset) [2].

difficult to be identified on the conventional seismic data and post-stack inversion results owing to their complex lithology with appearance of calcite veins that would probably cause an increase in acoustic impedance (AI) of this sand. The objective of this study is to investigate the influences of rock physics parameters on construction of a RPT for MMS and propose a systematic procedure to apply it, taking into account the site-specific conditions of the study location.

2. Middle Miocene sand in Nam Con Son basin

The Nam Con Son basin lies on the continental shelf margin, offshore Vietnam. The basin type is of Cenozoic rift and regional subsidence [3]. It is bounded to the southwest by the Con Son swell and Khorat - Natuna arch, and to the west by the Tu Chinh - Vung May basin (Figure 2). The geological evolution of the Nam Con Son basin is closely related to the East Sea spreading and can be divided into main stages, i.e., syn-rift 1, inter-rift, syn-rift 2 and post-rift [2, 4, 5]. A seismic cross-section in Figure 3 shows geological sequences of the Nam Con Son basin consisting of Pre-Tertiary basement, Early Oligocene (T10), Late Oligocene (T20), Early Miocene (T30), Middle Miocene (T40, T50, T60, T65), and Late Miocene (T85). Rifting in Nam Con Son basin started during the Late Eocene to Early Oligocene, which was followed by seafloor spreading in the East Sea between the end of the Early Oligocene (32Ma) and the start of the Middle Miocene (15Ma) when it is characterised by thermal subsidence (sag phase) and widespread deposition of a thick package up to 2,000m of fluvial deltaic sediments. This sequence (T20 - T30) includes the paralic coals that are the main source rock of the basin petroleum system. Seafloor spreading in the East Sea stopped around 15Ma and was followed by a renewed rifting during the Middle Miocene. This phase propagated from North East to South West and is responsible for the structure and trap formation in the basin. The end of the Mid Miocene rifting event is marked by a pronounced unconformity (Middle Miocene unconformity), followed by the deposition of a thick post-rift ("sag phase") wedge, which includes the massive Plio-Pleistocene proto-Mekong shelf edge delta system, prograding from West to East. The rapid deposition of this package caused over-pressuring in the central basin, concentrated in a SSW-NNE oriented belt where the post-rift wedge is the thickest. The major discovery and production of hydrocarbons in the formations of basement, clastics and carbonates with age ranging from Pre-Cenozoic to Miocene are marked in the stratigraphic column of the Nam Con Son basin in Figure 4.

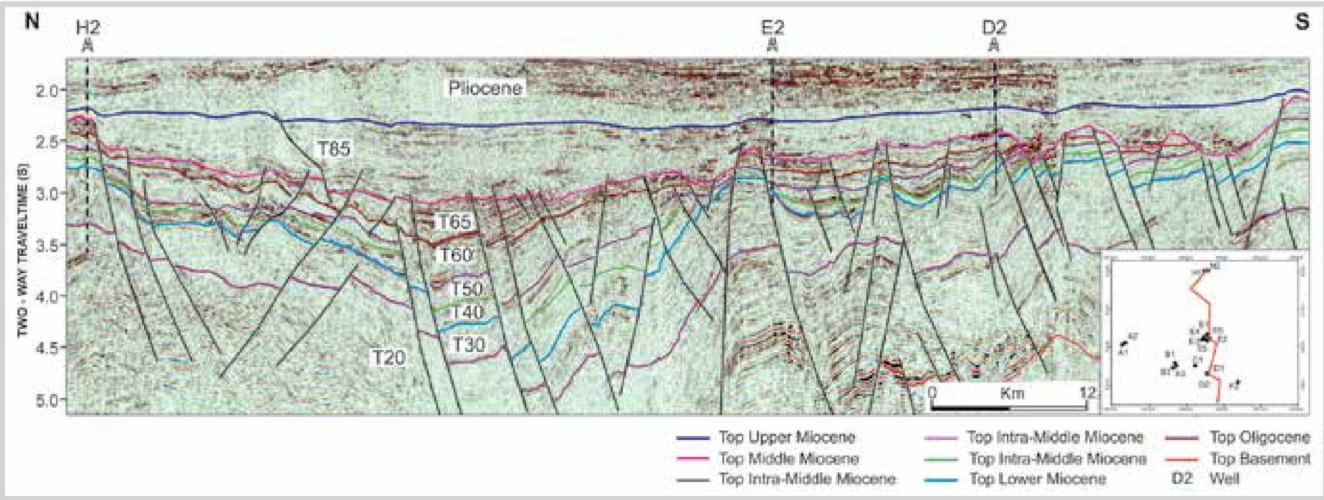

Figure 3. *A seismic section of the Nam Con Son basin [2].*

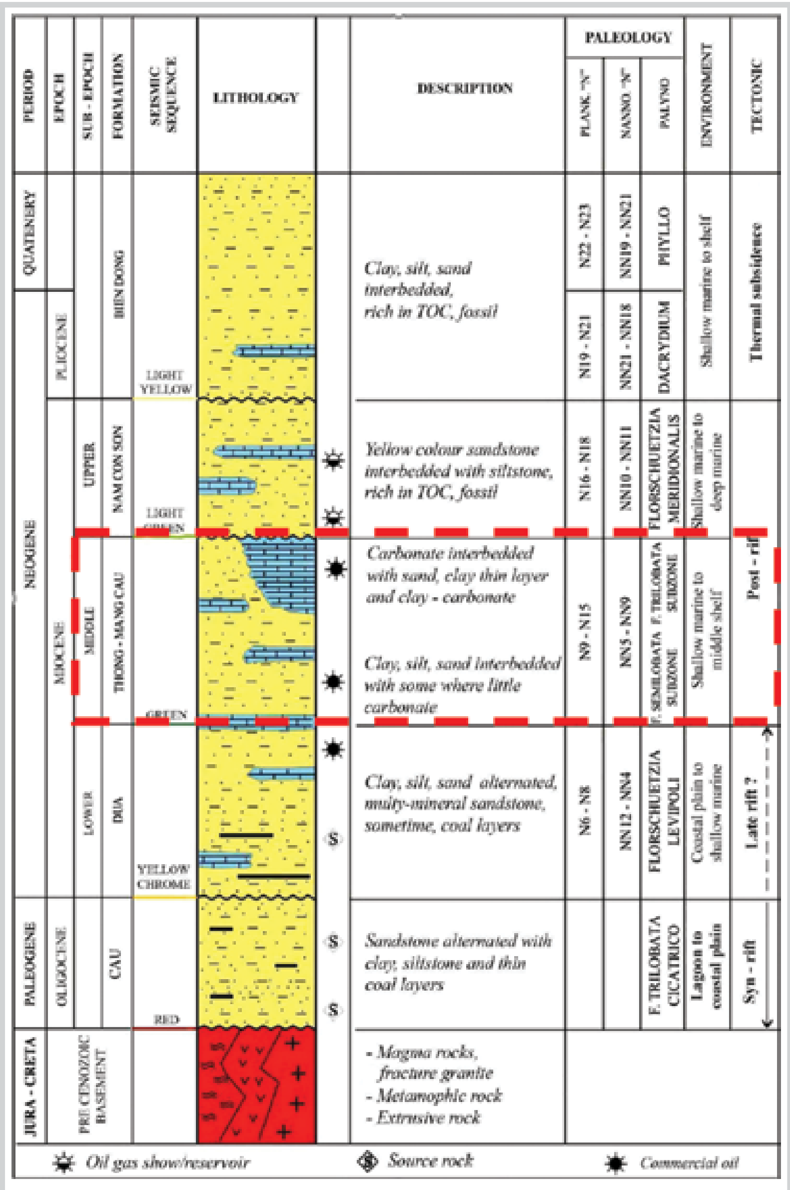

Figure 4. *Stratigraphic column of the Nam Con Son basin [6].*

Hai Thach field: The exploration and production activities in the Nam Con Son basin have led to discovery of many fields in various stratigraphic sequences including fractured basement (e.g. Dai Hung, Gau Chua), Oligocene (e.g. Rong Doi, Ca Rong Do), Lower Miocene (e.g. Rong Vi Dai, Ca Rong Do), Middle Miocene (e.g. Chim Sao, Dua, Dai Nguyet, Thien Ung, Mang Cau), Upper Miocene (e.g. Hai Thach, Moc Tinh, Lan Tay, Lan Do). Hai Thach field was discovered in 1995 by a BP (British Petroleum) exploration well drilled right on the Hai Thach horst structure, in which gas and condensate accumulations were found from multiple stacked reservoir units in Miocene, i.e. UMA10 (Upper Miocene), MMH10 (Mid Miocene), LMH10, LMH20 and LMH30 (Lower Miocene). Another BP well drilled on the eastern flank of the Hai Thach structure encountered additional HC-bearing sandstones in Upper Miocene (UMA15) and Middle Miocene (MMF10, MMF15 and MMF30). The appraisal and production wells confirmed gas and condensate presence in the MMF30 interval, which is the very target sand reservoir for RPT construction in this study as explained more in details in the following.

The Middle Miocene sand (MMS) belongs to the Thong - Mang Cau formation (Middle Miocene), which is widely distributed in the Nam Con Son basin and

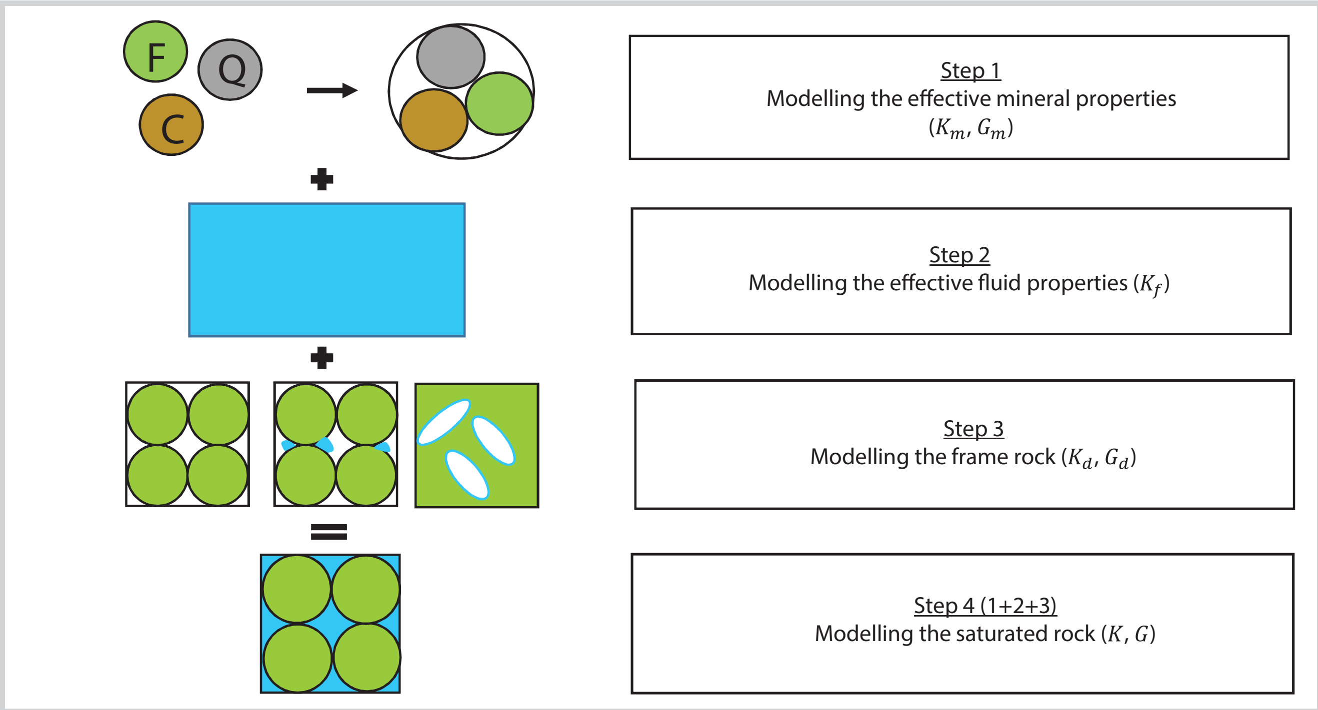

Figure 5. *Rock physics modelling process (modified from [7]).*

consists of two main parts, i.e. the lower part, mainly composed of fine to medium-grained quartz sandstone with carbonate cement, rich in glauconite and marine fossils interbedded with thin layers of claystone and carbonaceous shale; and the upper part, dominated with intercalation of light grey and milky white or sometimes reddish brown dolomitised carbonate and layers of greenish grey shale-siltstone, and fine-grained sandstone containing carbonate cement. Middle Miocene sediments were accumulated predominantly in open marine, outer shelf to bathyal depositional environments. On the flank area, reservoir quality is quite different from well to well. The sediments of reservoir interval (MMF30) were deposited as turbidites/slumps in the deep marine environment and have reservoir quality from fair to good, with average porosity from 14 to 16% and a net thickness from 25 to 43m TVD (True vertical depth). The resistivity readings show significant offset from the background, i.e., 10 to 20Ωm versus 2.0Ωm.

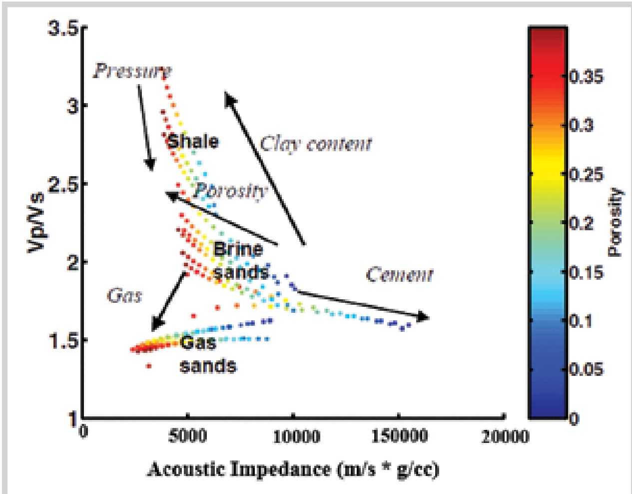

Figure 6. *RPT for North Sea Sand [8].*

3. Rock physics model (RPM) and rock physics template (RPT)

3.1. Rock physics model (RPM)

A rock physics model is a mathematical relation between elastic and intrinsic properties of a rock such as mineralogy, grain and pore geometry, porosity and connectivity. Rock physics modelling is the process to estimate bulk and shear moduli of mineral components, pore fluids, and rock frame, following the steps as shown in Figure 5. Some typical rock physics models that are commonly used in developing the rock physics templates can be seen in Equations 1 - 3.

3.2. Rock physics template (RPT)

Any chart or cross-plot between two types of elastic or geomechanical parameters based on which one can figure out the reservoir properties of interest such as lithology and fluid type, shale content, cementing type, porosity, permeability, hydrocarbon saturation, etc. can

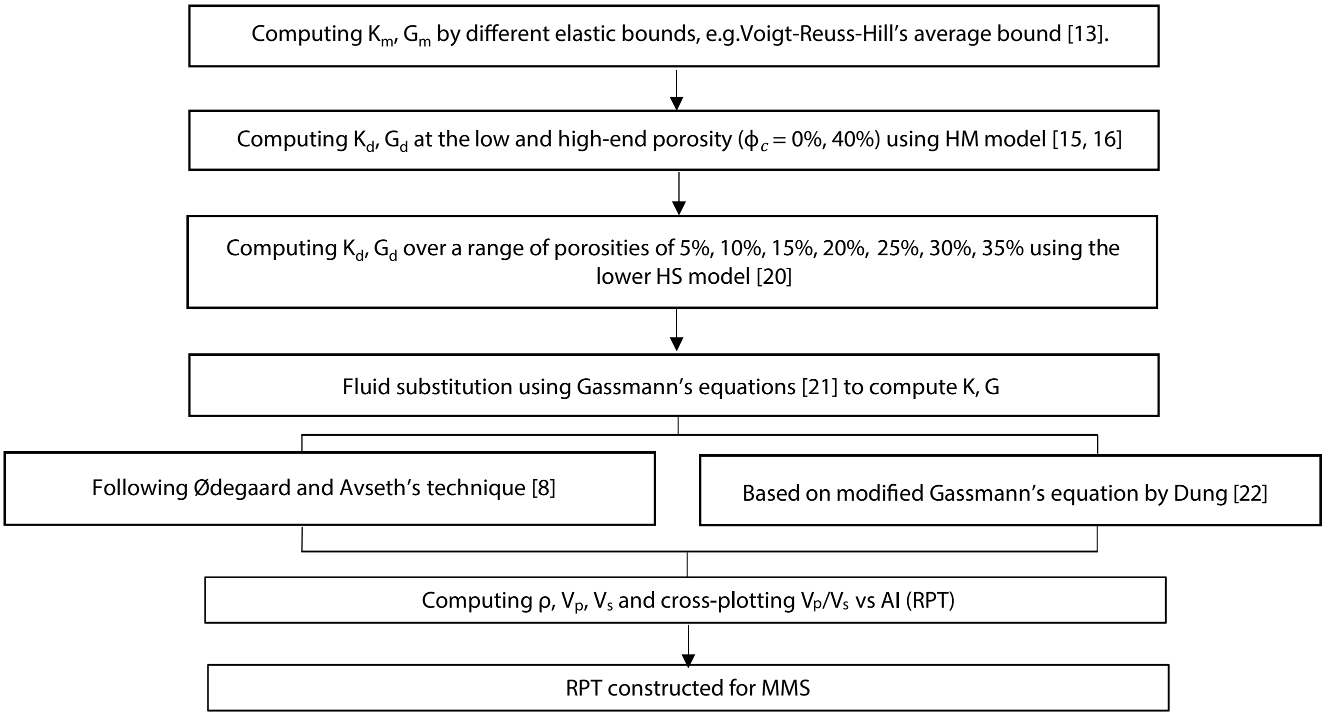

Figure 7. *Flow chart of the study.*

be considered as a rock physics template (RPT). One of the most popular RPTs at the moment is that proposed by [8] for North Sea Sand based on rock physics model of [9]. This RPT is a crossplot of V_p/V_s versus acoustic impedance (AI) of P-wave and can be used to estimate rock and fluid types of a reservoir as presented in Figure 6. Ødegaard and Avseth stated that "the rock physics templates provide an important interpretation tool that can improve communication between geologists and geophysicists and can help reduce risk in seismic exploration and prospect evaluation" [8]. The often-encountered problem in application of this technique is that the practical engineers tend to pay little attention to parameters involved in the rock physics models that are foundations for construction of RPT, ignoring their effects, and consequently the well data could not match with the RPT they constructed for the study site. It was made clearly that "a rock physics model should never be considered to be universal, but should be site specific and honor local geological factors. Geological constraints on rock physics models include lithology, mineralogy, burial depth, diagenesis, pressure and temperature. All these factors must be considered when generating rock physics templates for a given basin" [8]. In this study, the technique [8] was slightly modified to consider better the site conditions of Hai Thach field for construction of RPT for MMS as explained more in detail in the following sections.

4. Methodology

The flowchart to construct the RPT in this research follows that conducted by [10] as shown in Figure 7. In the first step, the bulk and shear mineral moduli (K_m, G_m) are calculated using one of the rock physic models shown in Equations 1a-d, known as the elastic bounds and plotted in Figure 8. To have properly calculated mineral moduli the fractions of each rock-forming constituent mineral are desired to be known, which are usually identified by the XRD (X-Ray Diffraction) analysis results as seen in Table 1a for the MMS core samples from the study well E2, Table 1b shows the moduli of some typical constituent minerals of a sandstone.

Voigt (1910) $$K_m = \sum_{i=1}^{N} f_i K_i \quad (1a)$$

$$G_m = \sum_{i=1}^{N} f_i G_i \quad (1b)$$

Reuss (1929) $$\frac{1}{K_m} = \sum_{i=1}^{N} \frac{f_i}{K_i} \quad (1c)$$

$$\frac{1}{G_m} = \sum_{i=1}^{N} \frac{f_i}{G_i} \quad (1d)$$

Hill (1952) $$K_m = \frac{1}{2}\left[\sum_{i=1}^{m} f_i K_i + \left(\sum_{i=1}^{m} \frac{f_i}{K_i}\right)^{-1}\right] \quad (1e)$$

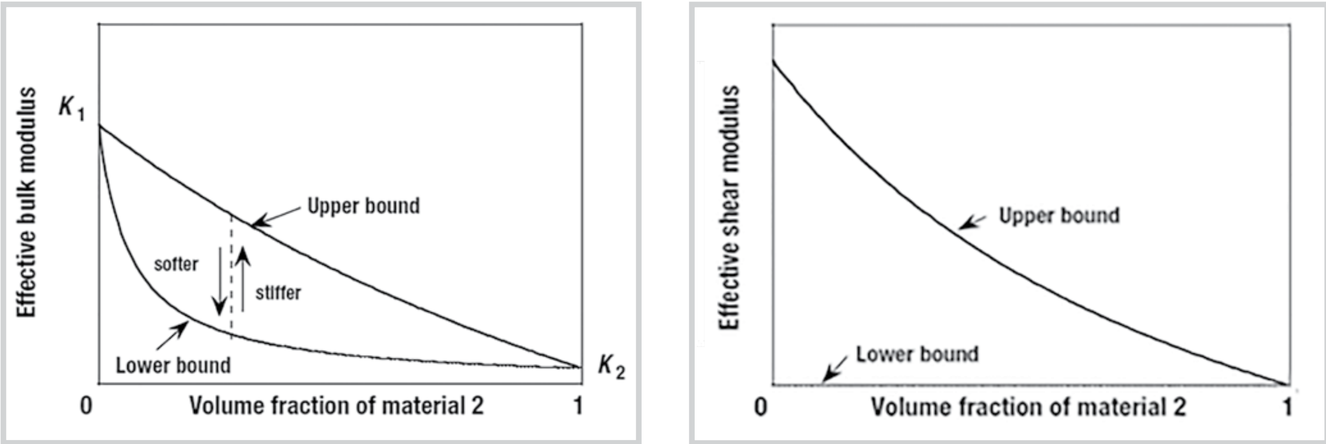

Figure 8. *The upper and lower elastic bounds: the upper bound in Equations 1a-b [11], the lower bound in Equations 1c-d [12] and the Voigt-Reuss-Hill average bound in Equations 1e-f [13].*

Table 1a. *Results of XRD analysis of some cores from the well E2*

Depth (m)	Quartz	Mica-clay	K-Feldspar	Plagioclase	Calcite	Dolomite	Siderite	Pyrite
3587.35	66	5.5	12	12	0.5	1.5	2.5	
3591.65	86.5	1	5.5	5.5	0.5		1	
3598.25	86.5	1	5.5	6				1
3601.25	85	2.5	4.5	7			1	
3610.35	68	5.5	6	9		3	8.5	
3612.35	72.5	7.5	5	10.5	0.5	2.5	1.5	
Percent (%)	77.42	3.83	6.42	8.33	0.5	2.33	2.9	1

Table 1b. *Moduli of some typical minerals [14]*

Mineral type	Quartz	Mica-clay	K-Feldspar	Plagioclase	Calcite	Dolomite	Siderite	Pyrite
Bulk moduli (GPa)	36.6	21	75.6	55	76.8	94.9	123.7	147.4
Shear moduli (GPa)	45	7	25.6	28	32	45	51	132.5
Density (g/cc)	2.65	2.58	2.62	2.56	2.71	2.87	3.96	4.93

$$G_m = \frac{1}{2}\left[\sum_{i=1}^{m} f_i G_i + \left(\sum_{i=1}^{m}\frac{f_i}{G_i}\right)^{-1}\right] \quad (1f)$$

Where: f_i, K_i, and G_i are the volume fraction, bulk modulus and shear modulus of the i^{th} constituent mineral, respectively; K_m, G_m are bulk and shear moduli of the rock matrix.

In the second step, the elastic moduli of the dry rock frame (K_d, G_d) are calculated using Hertz-Mindlin's model [15, 16] (also known as the HM model) for the low and high-end porosity corresponding to ϕ = 0% and 40%, respectively, based on Equations 2a-b:

$$K_{HM} = \left[\frac{n^2(1-\phi_c)^2 {G_m}^2}{18\pi^2(1-\nu_m)^2}P\right]^{\frac{1}{3}} \quad (2a)$$

$$G_{HM} = \frac{5-4\nu_m}{5(2-\nu_m)}\left[\frac{3n^2(1-\phi_c)^2 {G_m}^2}{2\pi^2(1-\nu_m)^2}P\right]^{\frac{1}{3}} \quad (2b)$$

$$\nu_m = \frac{3K_m - 2G_m}{2(3K_m + G_m)} \quad (2c)$$

$$P = g\int_0^Z (\rho_b - \rho_f)\, dz \quad (2d)$$

$$n = 20 - 34\phi + 14\phi^2 \quad (2e)$$

Where the critical porosity (ϕ_c) is an important parameter that is defined as the porosity above which the rock can exist only as a suspension. In this case the grains are not in contact anymore and are suspended in water and the stiffness of the sediment is determined by the pore fluid. Below the critical porosity, the stiffness of the rock is determined by the framework of contacting mineral grains. In sandstone critical porosity varies from 36% to 40%, and that is porosity of a random close pack of well-sorted rounded quartz grains. This is often the starting point for the formation of consolidated sandstones. In our study for MMS the critical porosity of 40% was used for calculation of K_d and G_d by Equations 2a-b. The critical porosity of different rock types may differ between them as seen in Table 2. Another important parameter in rock physics model is the co-ordination number or contact number (n), which is defined as the average number

Table 2. Critical porosity of some rock types [19]

Rock type	Critical Porosity (%)
Sandstones	40
Limestones	40
Dolomites	40
Pumice	80
Chalks	65
Rock salt	40
Cracked igneous rocks	5
Oceanic basalt	20
Sintered glass beads	40
Glass foam	90

of contacts per grain [14]. The contact number can be estimated by empirical relationships proposed by [17] or [18]. In this study, for the final RPT n was chosen equal to 8.64 corresponding to ϕ_c = 40%. The mineral Poisson's ratio (ν_m) is related to K_m and G_m as seen in Equation 2c. P is the effective pressure at the depth level of the target reservoir. ρ_b, ρ_f are bulk density and fluid density in g/cc, respectively, g is the gravitational acceleration equal to 9.81m/s^2, and z is the depth (m).

The next step in constructing the RPT is to calculate K_d and G_d for the range of porosities between two end values of 0% and critical porosity, say, ϕ = 5%, 10%, 15%, 20%, 25%, 30%, 35% using Equations 3a-c, which are Hashin-Shtrikman's model [20] or shortly known as the HS model:

$$K_d = \left[\frac{\frac{\phi}{\phi_c}}{K_{HM} + \frac{4}{3}G_{HM}} + \frac{1-\frac{\phi}{\phi_c}}{K_m + \frac{4}{3}G_{HM}}\right]^{-1} \quad (3a)$$

$$G_d = \left[\frac{\frac{\phi}{\phi_c}}{G_{HM} + Z} + \frac{1-\frac{\phi}{\phi_c}}{G_m + Z}\right]^{-1} - z \quad (3b)$$

$$z = \frac{G_{HM}}{6}\left[\frac{9K_{HM} + 8G_{HM}}{K_{HM} + 2G_{HM}}\right] \quad (3c)$$

In the 4th step, fluid substitution was conducted to calculate the saturated moduli (K, G) by Gassmann's equations [21] starting with Equations 4 - 5 below. In addition, the fluid bulk modulus (K_f) was calculated by Equation 6 following Reuss's lower elastic bound [12]:

$$\frac{K}{K_m - K} = \frac{K_d}{K_m - K_d} + \frac{K_f}{\phi(K_m - K_f)} \quad (4)$$

$$G = G_d \quad (5)$$

$$K_f = \left[\frac{S_w}{K_w} + \frac{1-S_w}{K_{hc}}\right]^{-1} \quad (6)$$

Once the elastic moduli are known, the elastic wave velocities are determined based on Equations 7 - 10, and finally a cross plot between V_p/V_s and AI can be constructed.

$$V_p = \sqrt{\frac{K + \frac{4}{3}G}{\rho_b}} \quad (7)$$

$$V_s = \sqrt{\frac{G}{\rho_b}} \quad (8)$$

$$\rho_s = (1-\phi)\rho_m + \phi\left[(1-S_w)\rho_g + S_w\rho_w\right] \quad (9)$$

$$AI = \rho_b V_p \quad (10)$$

Where: V_p, V_s are the saturated compressional and shear wave velocity (m/s), respectively; AI is acoustic impedance m/s×g/cc); ρ_s, ρ_m, ρ_w, ρ_g, are saturated density, matrix density, water density and gas density, respectively.

Regarding the calculation of mineral moduli using HM model (Equations 1a-f), both mono-mineral and multi mineral cases were studied. For the former case with Quartz being the only constituent mineral the input parameters used for calculation are shown in Table 3, while for the latter case K_m and G_m were determined based on the mineral fractions identified by the XRD analysis as shown in Table 1a.

Table 3. Input parameters for the mono-mineral case with Quartz being the only constituent mineral

Critical porosity ø = 40%	K_m = 36.6GPa
Coordinate number n = 8.64	G_m = 45GPa
Effective pressure P = 0.057GPa @ 3,548m TVDSS	ρ = 2.65g/cc

Notably, as indicated in Figure 7, to take into account the site-specific conditions of Hai Thach field, calculation of the dry modulus (K_d) in the second step can be done using a modified form of Gassmann's equation proposed by [22] as shown in Equations 11a-b. In this approach, the petrophysical parameters such as K, G, K_f, porosity were directly determined from well log analysis of the study well and introduced into Equation 11a to calculate the Biot coefficient (α), based on which K_d can be determined using Equation 11b as follows:

$$\left[\phi(K_m - K_f) - K_f\left(1 - \frac{K}{K_m}\right)\right]\alpha = \phi\left[(K_m - K_f) - K\left(1 - \frac{K_f}{K_m}\right)\right] \quad (11a)$$

$$\alpha = 1 - \frac{K_d}{K_m} \quad (11b)$$

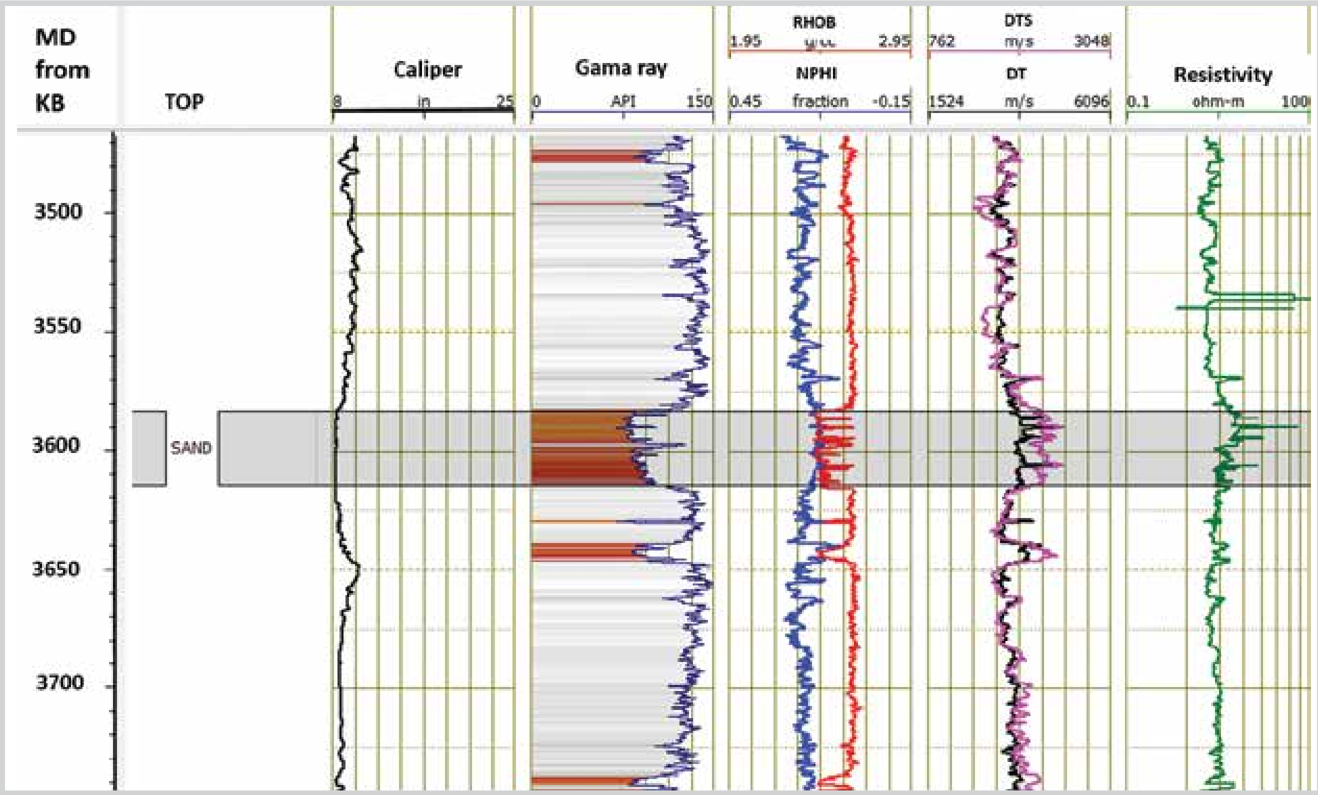

Figure 9. The MMS reservoir interval from 3,548.57 to 3,584.40m TVDSS, E2 well.

Table 4. The rock physics parameters used for estimation of K_d and G_d

Porosity = 0.14	Matrix	Dry rock frame
Effective pressure = 0.033 GPa	K_m = 36.52 GPa	K_d = 21.91 GPa
	G_m = 31.64 GPa	G_d = 12 GPa

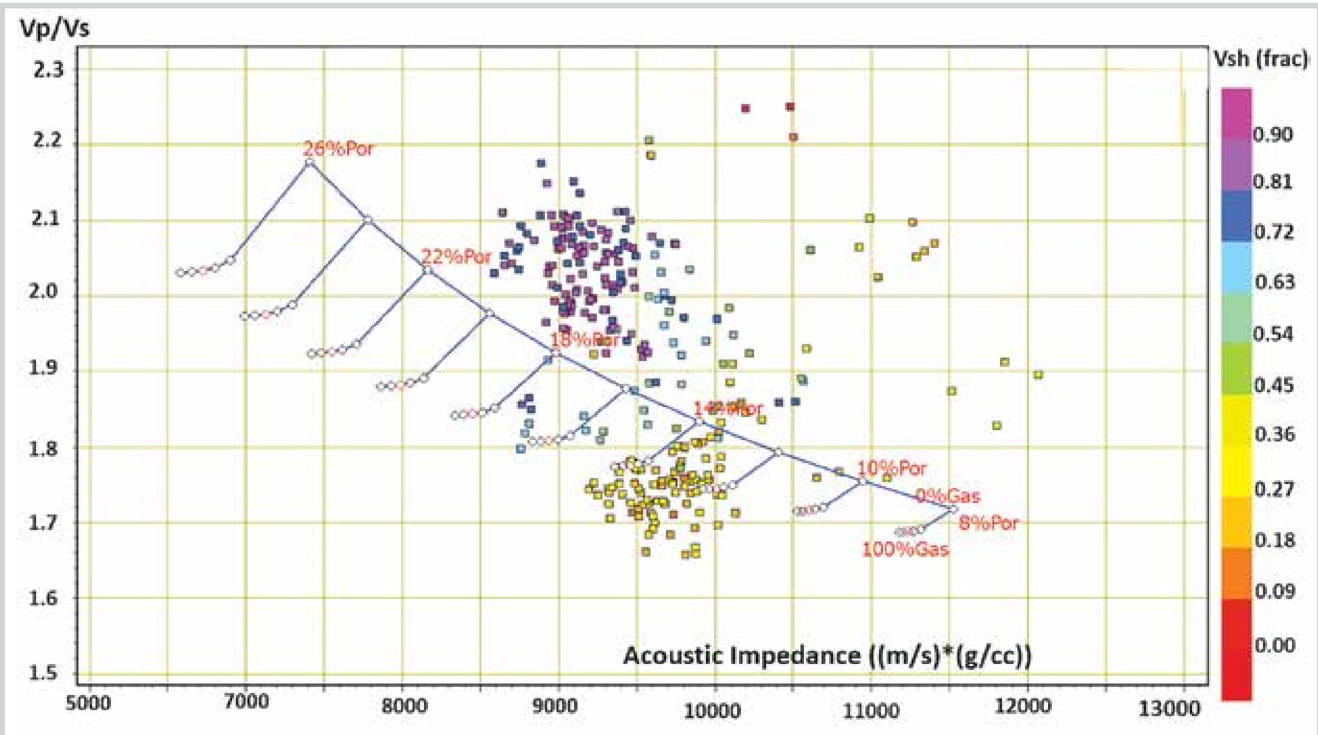

Figure 10. The RPT constructed for MMS method using Hampson-Russel software.

5. Results and discussions

5.1. Construction of RPT using Hampson-Russel software

Geoview is the main tool in HR (Hampson-Russell) software that can be used to analyse data and construct RPT. First, the well-log data of CAL (Caliper), GR (Gamma Ray), RHOB (Bulk density), NPHI (Neutron porosity), LLD (Depth resistivity), DT (Compressional wave slowness), DTS (Shear wave slowness) are loaded into Geoview through Data Explorer (Figure 9). The MMS has low GR from 80 to 90API (American Petroleum Institute), LLD from 3 to 10Ωm, NPHI from 0.09 to 0.18, RHOB from 2.42 to 2.65

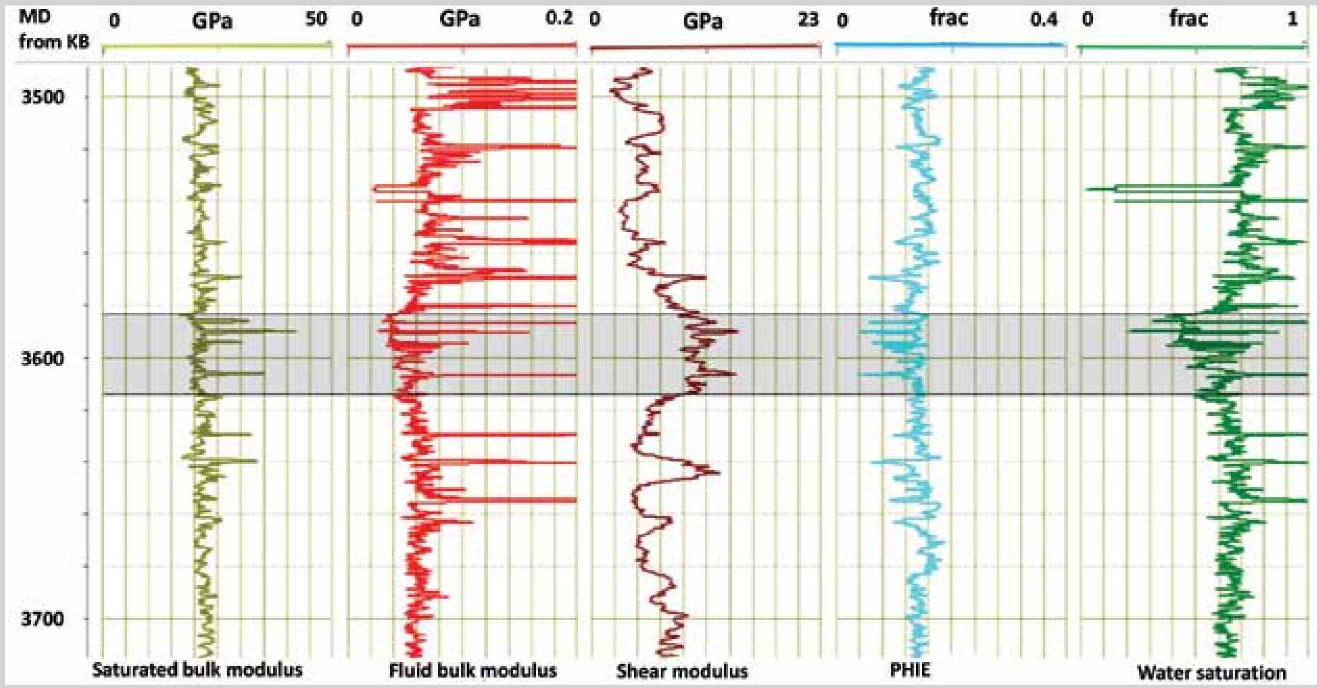

Figure 11. *Well-log based rock physics parameters for calculation of K_d using the modified Gassmann's equation form [22].*

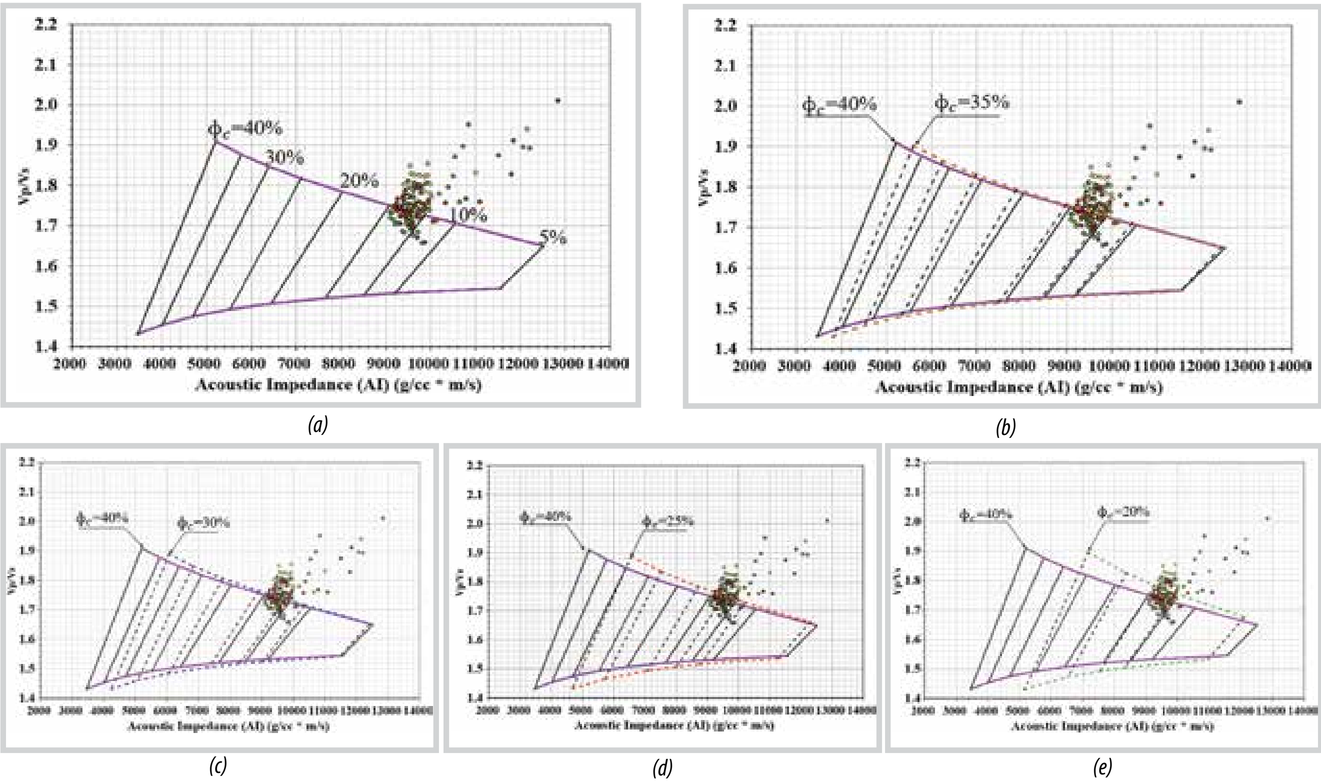

Figure 12. *Effect of change in critical porosity on RPT with ϕ_c = 0.4, 0.35, 0.3, 0.25, 0.20, respectively (Note: green points are of low GR, while yellow points are of high GR).*

g/cc, in addition a crossover between NPHI and RHOB was found. In the study well E2, the MMS reservoir (3,548.57 to 3,584.40m TVDSS) is interpreted having a net pay of 13.39m and moderate reservoir quality with 12% effective porosity, 20% of shale volume and 49% water saturation, respectively. Note that the effective porosity was calculated as the average of NPHI and PHID, and water saturation was estimated by Archie's laws.

In this analysis using Hampson-Russel software the average elastic moduli (K_m and G_m) were calculated using Reuss's lower elastic bound [12] in Equations 1c-d and with fraction of minerals shown in Table 1a. Results of rock physics template construction using Hampson Russel is shown in Figure 10 [23], where one can see that many MMS points lie beyond the 100% gas saturation (Sg = 100%). Thus, this RPT is still not good enough for characterisation of MMS and the answers are suspected to be found in selection of rock physics parameters, the problem that will be addressed in the immediately following section.

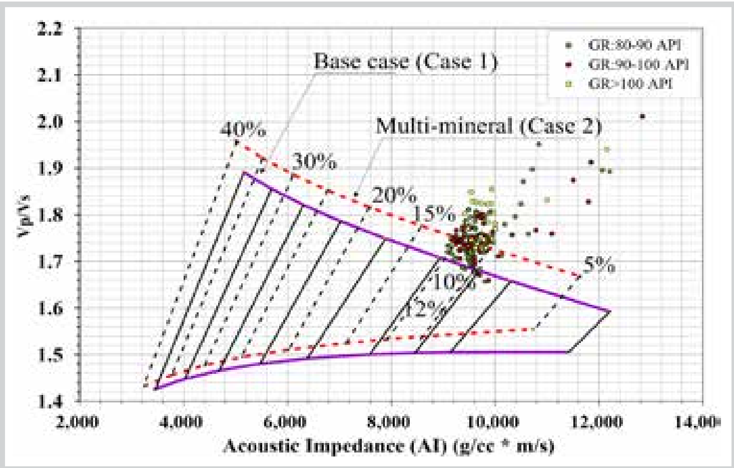

(a)

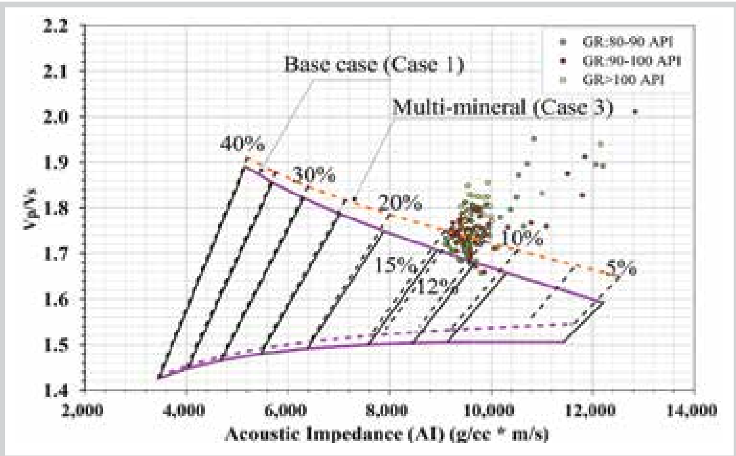

(b)

Figure 13. *Effects of K_m on construction of RPT: (a) case 2 vs. case 1; (b) case 3 vs. case 1.*

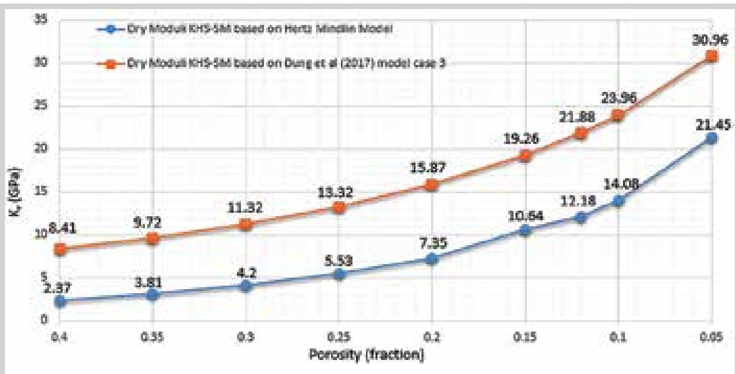

Figure 14. *Comparison of K_d calculated based on Hertz-Mindlin's model [15, 16] and Dung [22].*

5.2. Construction of RPT using a modified approach in this study

Well log analysis for the depth interval from 3,574.5 to 3,614m MD was revisited as shown in Figure 11 and gave the following petrophysical parameters of MMS, and namely: ø = 0.12, K = 21.84GPa, G = 12GPa, K_f = 0.042GPa, and K_d = 21.88GPa where K_d was calculated by modified Gassmann's equation by [21]. After a number of analyses the Voigt-Reuss-Hill's average elastic bound [13] was found to be the best to calculate the mineral moduli (K_m and G_m), which were estimated as 42.43GPa and 38.51GPa, respectively.

5.2.1. Influence of critical porosity (ϕ_c) on RPT construction

Normally for a sand reservoir the critical porosity (ϕ_c) is 40%. As seen in Table 2 this critical porosity can vary for different rock types. To see the effects of critical porosity on the RPT curves a number of charts were constructed for ϕ_c = 40, 35, 30, 25 and 20% as shown in Figure 12. It was observed that the change in critical porosity brings the change in the shape of RPT curves.

5.2.2. Influence of change in bulk and shear mineral moduli

To investigate the influence of the change in bulk and shear of mineral moduli on RPT construction, three cases were compared, and namely: i) case 1 or the base case (with matrix made of Quartz only); case 2 that is the case study by [23]; iii) and case 3 in this study with mineral fractions based on XRD results as shown in Table 1a. Figure 13a shows that in case 2 with K_m and G_m being estimated by using Reuss's bound [12] the porosity range is from 10 to 12%, while for case 3 that made use of the Voigt-Reuss-Hill's average bound [13] the porosity range is from 12 to 15% as seen in Figure 13b. The latter fits better with the well log analysis results. Thus, the results of XRD analysis are very important in calculating the mineral moduli beside selection of a good elastic bound.

5.2.3. Influence of change in dry bulk modulus of the rock frame (K_d)

Basically, this study found that a change in K_d would shift the RPT curves noticeably. Figure 14 shows a comparison of the dry rock framework moduli (K_d) calculated by Hashin-Shtrikman's model [20] based on Hertz Mindlin's model [15, 16] with those calculated using a modified form of Gassmann's equation as proposed by [22]. The latter method could give a consistently higher K_d as seen in Figure 14. The change in K_d could shift the RPT curves to fit better with well log data points as shown in Figure 15. Finally, a new RPT was successfully constructed for MMS as presented in Figure 16.

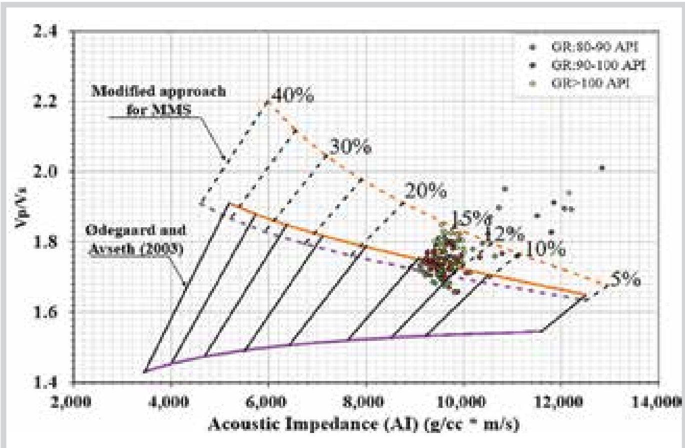

Figure 15. *Influence of K_d on RPT curve shifting.*

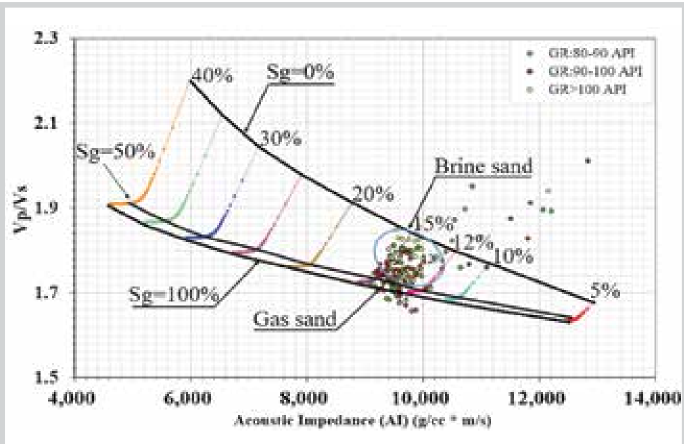

Figure 16. *The RPT constructed in this study for MMS.*

6. Conclusions and recommendations

Based on a detailed parametric analysis in this study it was found that the rock physics parameters such as critical porosity, co-ordination number, mineral fractions, the dry bulk and shear moduli etc. are very important in the construction of RPT for a certain site. Inadequate rock physics parameters could lead to uncertainties in characterisation of clastic reservoir, thus these parameters should be properly tested and estimated, taking into account the site-specific conditions. In this study a new RPT was successfully constructed using the Voigt-Reuss-Hill average elastic bound and a modified form of Gassmann's equation for the gas-bearing Middle Miocene sand at Hai Thach field. As results, the MMS is well characterised with acoustic impedance (AI) from 9,000 to 11,000 m/s×g/cc, and V_p/V_s from 1.65 to 1.80, porosity from 11 to 16%, and gas saturation from 50% up. It is recommended that the RPT construction procedure proposed in this study be applied for other gas-bearing sands in the Nam Con Son basin.

References

1. Pham Huy Giao. *Lithological zoning using the V_p/V_s Log curves*. The 21st Formation Evaluation Symposium of Japan (JFES 2015). Chiba, Japan. 13 - 14 October 2015.

2. Bui Viet Dung, Hoang Anh Tuan, Nguyen Van Kieu, Ha Quang Man, Nguyen Thi Thanh Thuy, Pham Thi Dieu Huyen. *Depositional environment and reservoir quality of Miocene sediments in the central part of the Nam Con Son basin, Southern Vietnam shelf*. Marine and Petroleum Geology. 2018; 97: p. 672 - 689.

3. Phan Trung Dien, Lars Henrick Nielsen, Claus Andersen, Do Van Nhuan. *Late Mesozoic to Cenozoic basin development along the North-West margin of the East Vietnam sea*. American Association of Petroleum Geologists Annual Convention. Salt Lake City, Utah. 1998.

4. C.K.Morley, R.King, R.Hillis, M.Tingay, G.Backe. *Deepwater fold and thrust belt classification, tectonics, structure and hydrocarbon prospectivity: A review*. Earth-Science Reviews. 2011; 104(1-3): p. 41 - 91.

5. Nguyen Quang Tuan, Tran Van Tri. *Seismic interpretation of the Nam Con Son basin and its implica-*

tion for the tectonic evolution. Indonesian Journal on Geoscience. 2016; 3(2): p. 127 - 137.

6. Vietnam Oil and Gas Group. *Petroleum geology and resources of Vietnam*. Science and Technical Publishing House, Hanoi. 2009.

7. Carl Reine. *Discovering a supermodel - A rock - Physics tutorial*. CSEG Recorder. 2017; 42(2): p. 20 - 25.

8. Ødegaard, P.Avseth. *Interpretation of elastic inversion results using rock physics templates*. 65th EAGE Conference & Exhibition. 2003.

9. Jack Dvorkin, Amos Nur. *Elasticity of high-porosity sandstones: Theory for two North Sea datasets*. Geophysics. 1996; 61(5): p. 1363 - 1370.

10. Pham Huy Giao, Pham Hong Trang, Mai Thi Huyen Trang. *Revisit of rock physics template (RPT) construction for petrophysical characterisation of a gas sand in the Nam Con Son basin, Vietnam*. Extended abstract submitted for the 2nd EAGE - VPI Conference on Reservoir Geoscience. Hanoi, Vietnam. 2 - 4 December, 2019.

11. W.Voigt. *Bestimmung der Elastizita¨tskonstanten des brasilianischen Turmalines*. Annual Review of Physical Chemistry. 1890; 41: p. 712 - 729.

12. A.Reuss. *Berechnung der fließgrenze von mischkristallen auf grund der plastizitätsbedingung für einkristalle*. ZAMM-Journal of Applied Mathematics and Mechanics/ Zeitschrift für Angewandte Mathematik und Mechanik. 1929; 9(1): p. 49 - 58.

13. R.Hill. *The elastic behavior of crystalline aggregate.* Proceedings of the Physical Society Section A. 1952; 65(5): p. 349 - 354.

14. Gary Mavko, Tapan Mukerji, Jack Dvorkin. *The rock physics handbook (2nd edition)*. Cambridge University Press. 2009.

15. Raymond David Mindlin. *Compliance of elastic bodies in contact*. Journal of Applied Mechanics. ASME. 1949; 16: p. 259 - 268.

16. Herinrich Hertz. *On the contact of elastic solids.* J. Reine Angew. Math. 1881; 92: p. 156 - 171.

17. William F.Murphy III. *Effects of microstructure and pore fluids on the acoustic properties of granular sedimentary materials*. Stanford University. 1982.

18. Per Avseth, Tapan Mukerji & Gary Mavko. *Quantitative seismic interpretation: Applying rock physics tools to reduce interpretation risk*. Cambridge University Press. 2010.

19. Amos M.Nur, Gary Mavko, Jack Dvorkin, Doron Gal. *Critical porosity: the key to relating physical properties to porosity in rocks*. SEG Technical Program Expanded Abstracts. Society of Exploration Geophysicists. 1995: p. 878 - 881.

20. Z.Hashin, S.Shtrikman. *A variational approach to the theory of the elastic behaviour of multiphase materials.* Journal of the Mechanics and Physics of Solids. 1963; 11(2): p. 127 - 140.

21. Fritz Gassmann. *Über die elastizität poröser medien*. Vierteljahrss-chrift der Naturforschenden Gesellschaft. Zurich. 1951; 96: p. 1 - 23.

22. Tran Trung Dung, Carl H.Sondergeld, Jean-Claude Roegiers. *Different forms of Gassmann equation and implications for the estimation of rock properties*. Petrovietnam Journal. 2017; 10: p. 23 - 29.

23. Mai Thi Huyen Trang. *Application of rock physic template in interpretation of elastic inversion results for the Middle Miocene sand in Nam Con Son basin, Vietnam*. Master Thesis. Asian Institute of Technology. Bangkok, Thailand. 2018.

PETROVIETNAM JOURNAL
Volume 6/2019, p. 16 - 23
ISSN-0866-854X

PETROVIETNAM JOURNAL

Architecture, depositional pattern of syn rift sediments in the Northern Song Hong basin and its petroleum system association

Nguyen Thu Huyen[1], Nguyen Tuan Anh[1], Tong Duy Cuong[1], Trinh Xuan Cuong[1], Bui Viet Dung[1], Vu Quang Huy[1], Bui Huy Hoang[1] Nguyen Trung Hieu[1], Tran Ngoc Minh[1], Nguyen Quang Tuan[1], Nguyen Thanh Tung[1], Nguyen Trung Quan[1], Micheal Fyhn[2] Lars Nielsen[2], Ioannis Abazit[2], Jussi Hovikoski[2], Ngo Van Hung[3], Hoang Anh Tuan[3]
[1]Vietnam Petroleum Institute (VPI)
[2]Geological Survey of Denmark and Greenland (GEUS)
[3]Vietnam Oil and Gas Group
Email: huyennt@vpi.pvn.vn

Summary

Rifting with syn rift sediments originally was formed during two tectonic phases in three stages. The syn rift deposits were composed of four units that have been identified by distinct seismic facies. The seismic expression of these syn rift units gives an idea about the linkage of their deposition with different stages of rift evolution. The lowermost units have wedge shaped reflection packages and hummocky internal reflection configuration, representing initial rifting in early rift stage. The overlying two units comprising divergent reflection, prograding pattern with aggradations on footwall represent climax rift stage and the topmost unit with sub-parallel reflection configuration represents the late phase. The units deposited during the rift climax stage have a good source rock potential, whereas the unit deposited in the late rift stage possesses favourable reservoir facies making a complete petroleum system within syn rift sediments.

Core data indicates the Late Oligocene deep lacustrine succession of mainly organic-rich, world class oil-prone source rocks interbedded with mudstones and sandstones. The pelagic deposition of mud and organic algae matters with excellent source rock characteristics was frequently interrupted by river-fed mud flows, bringing mud and terrestrial organic matter to the lake bottom forming mudstones with a low source rock potential. Occasionally, low and high density turbidities, debris and hybrid flows interrupted mud deposition transport sands into the deep lake bottom forming potential carrier beds and reservoir sandstones.

The syn rift petroleum system association by predicting reservoir and source rock intervals are fundamental to exploration and can therefore help formulating a predictive exploration model of the Northern Song Hong basin.

Key words: Northern Song Hong basin, syn rift, deep lacustrine, shallow lacustrine, initiation rift, climax rift, late rift.

1. Introduction

The study area is located in the Northern part of Song Hong basin, which is the largest basin along the Western East Sea margin extending from North of Hanoi underneath the Red River Delta (Song Hong Delta) and into the Gulf of Tonkin (Figure 1). Situated at the extension of the onshore Ailao Shan - Red River Shear Zone (ASRRSZ), the formation of the Song Hong basin is often considered to be linked with the Cenozoic continental-scale left-lateral motion taking place across the shear zone [1, 5]. The Paleogene rift system flooring the basin is little studied, however, but holds vital information to unravel the tectonic history of the ASRRSZ [1].

Based on a dense 2D with 3D seismic grid covering the Northern Song Hong basin and the well data, the Paleogene syn rift system of the study area has been mapped and analysed. By integrating the analytical results with all available geo-scientific knowledge, the Paleogene basin development was restored under the influence of two tectonic phases (Figure 2) and as following a model-driven within three stages of syn rift as initiation, climax and late (Figures 2 and 3). 4 markers have been identified in the syn rift section on the basis of log characters and bio-stratigraphic control (Figures 2 - 4). Equivalent seismic markers could be traced and were mapped regionally along with the top of the basement. The 4 syn rift units bounded by these seismic markers were named unit 1, unit 2, unit 3 and unit 4, from older to younger (Figures 2, 4 - 6). These unit tops were dated with the available paly-

Date of receipt: 11/12/2018. Date of review and editing: 11/12/2018 - 3/1/2019.
Date of approval: 3/6/2019.

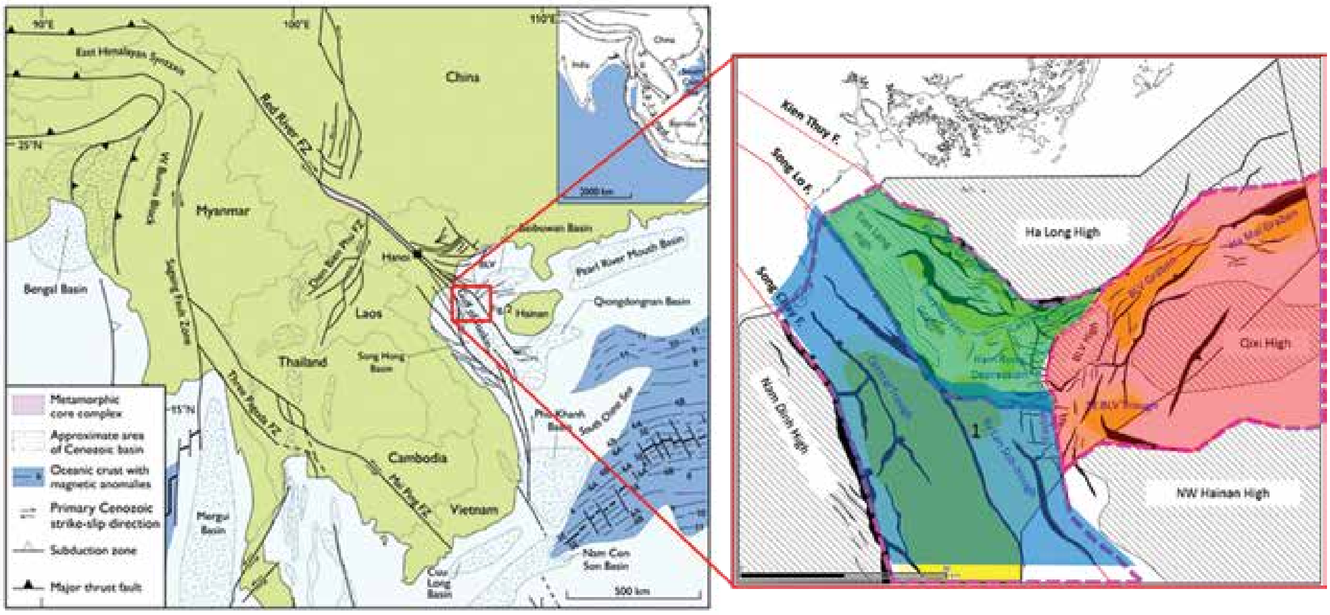

Figure 1. *Study area location map (left) and top basement structural map outline of the Northern Song Hong basin emphasising the main Paleogene faults, rift depressions and structural highs.*

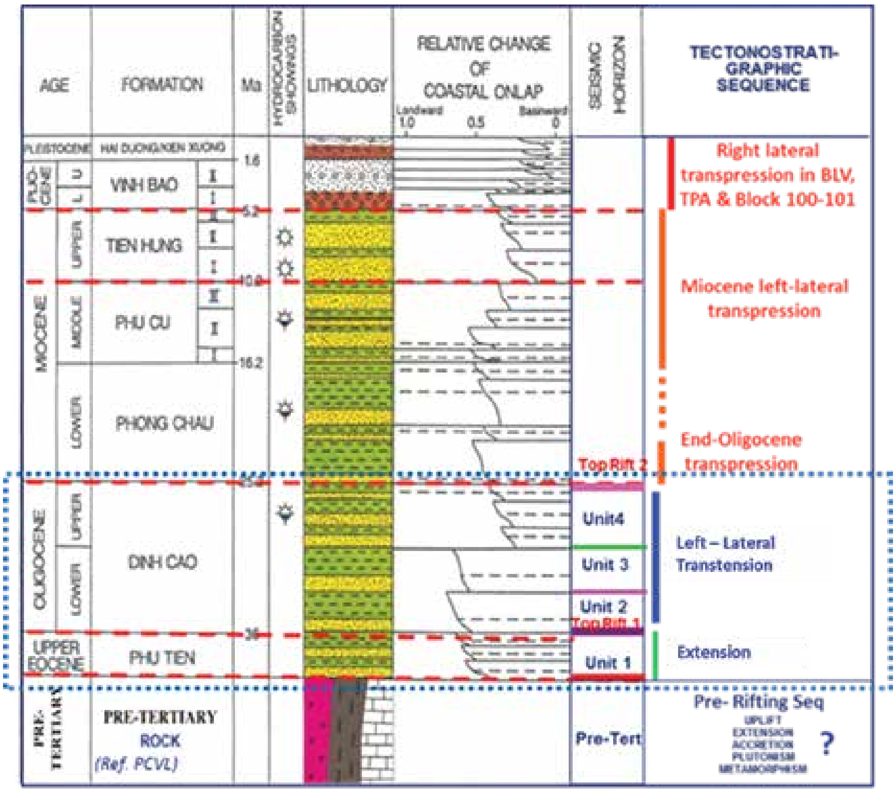

Figure 2. *Sequence stratigraphic column of the Northern Song Hong basin (modified from VPI).*

nological information. The tops of unit 1 (is also top Rift 1) and unit 4 (is also top Rift 2) (Figure 2) have been assigned as Phu Tien and Dinh Cao whereas unit 2 and unit 3 lie within Dinh Cao. These identified units have distinct seismic facies. The seismic facies within the units indicate their depositional environment associated with the stages of rifting. Unit 1 was deposited during the initial rift stage and distributed dominantly in the Northwestern part of the study area, however, no well records have been seen yet, it is only observed on the seismic data (Figures 3 and 4). It is difficult to observe unit 1 in the other parts. The climax rift stage persisted during deposition of unit 2 and unit 3, whereas, unit 4 was deposited during the late rift stage (Figures 2 - 5). It is observed that the potential and effective source is present in units 2 and 3, followed by unit 3 and better reservoir facies are developed in units 3 and 4. The good reservoir facies are also expected in the lower part of unit 2 where wedge sands and channels deposited in the initial stage of rifting. Therefore, the favourable petroleum system exists within the syn rift sediments [2, 4]. The basement structure map indicates three different sectors (Figure 1) which merged to form three stages at the initial, climax and late of rift (equivalent to 4 units of syn rift sediments) and were influenced by two tectonic phases (Figures 2 and 3). In the Northwestern sector (marked by green colour), alongate grabens and half grabens were strongly influenced by normal faults, bounded by the Tien Lang high and Ha Long shelf. Syn rift sediments are clearly

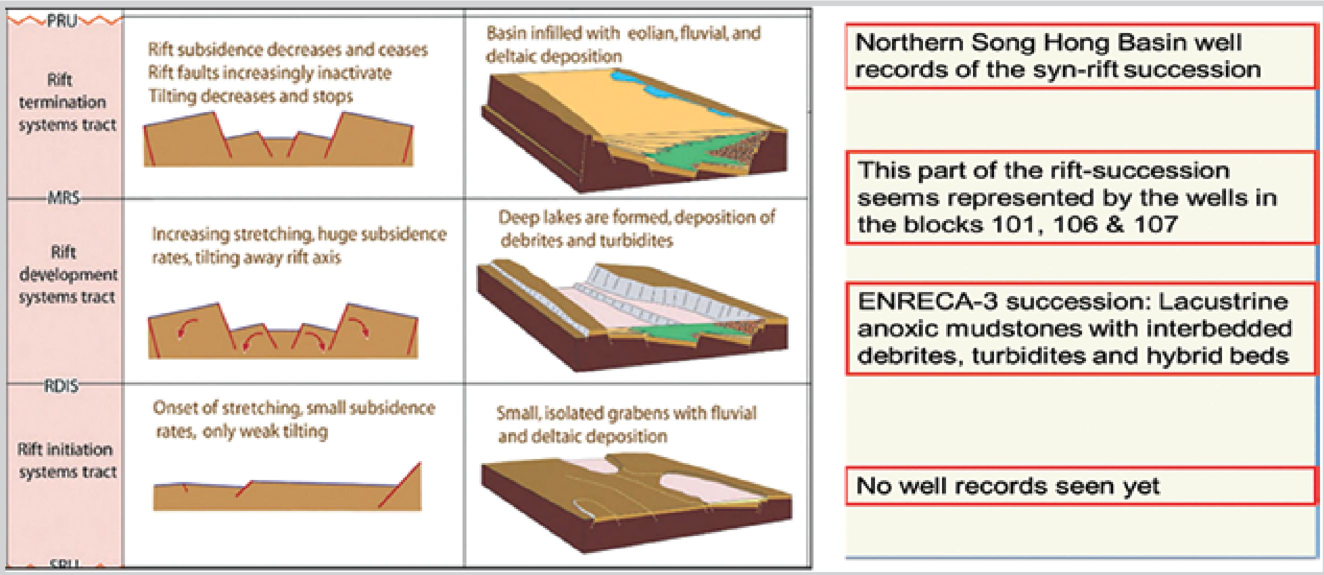

Figure 3. *The 3 stages of syn rift model in the Northern Song Hong basin (modified from [4]).*

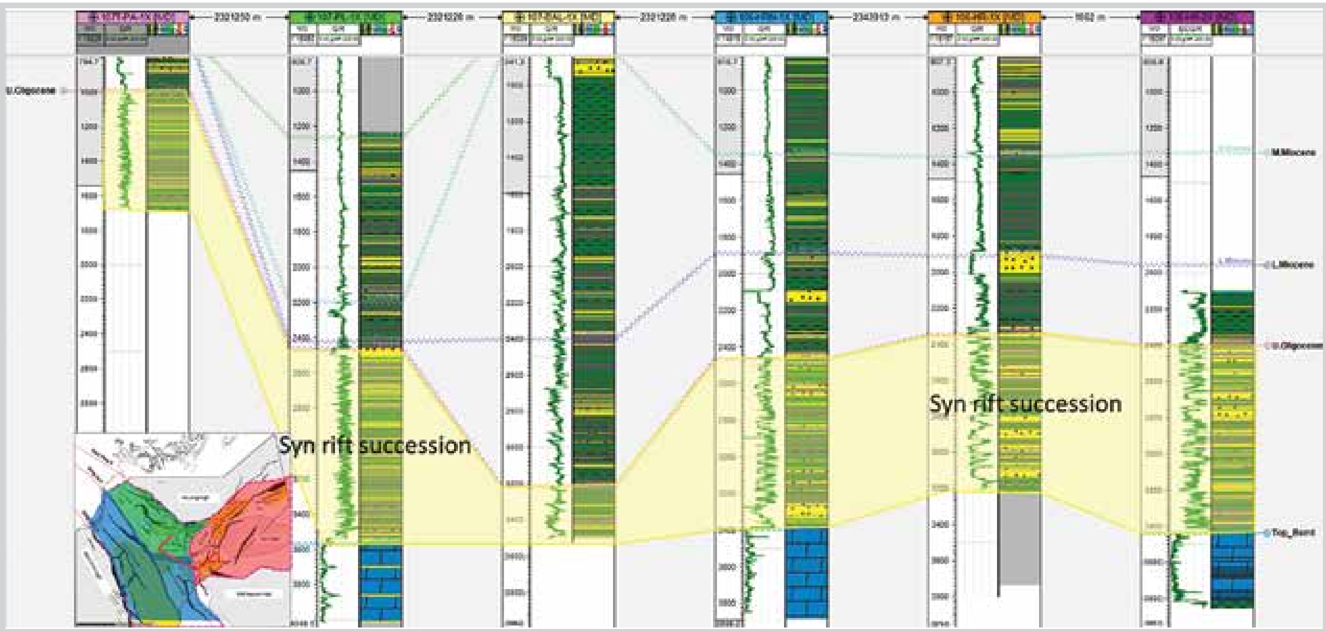

Figure 4. *Regional stratigraphic correlation.*

observed as four units which are more prominent and widespread in these grabens. In the area of the Eastern (marked by pink colour) and Western (marked by yellow colour) sectors, the syn rift sediments seem to be observed as 3 units because the rift climax stage prevailed during deposition of the upper part of unit 2 and unit 3. The Eastern sector which was earlier connected to the Western sector deepest low at the basement level got well differentiated as the rift progressed and becomes shallower and localised towards the South-Western margin. Moreover, Ham Rong - Ky Lan - BLV spur in the central part gradually becomes more prominent and widespread towards NW, bifurcating the two lows. The available core data indicates that the sediments were originally transported by fluvial drainage with considerable distance of transportation and deposited in the shallow marine setup. The sedimentation was later dominated by sandy debris flow along with intermittent bottom current activity in shallow marine condition [3].

2. Log correlation and seismic analysis

There are 16 wells encountering syn rift sediments in the Northern Song Hong basin which have been used for the studies. The regional stratigraphic correlation in direction along the axial part of three sectors of the study is shown in Figure 4. Log correlation combining with seis-

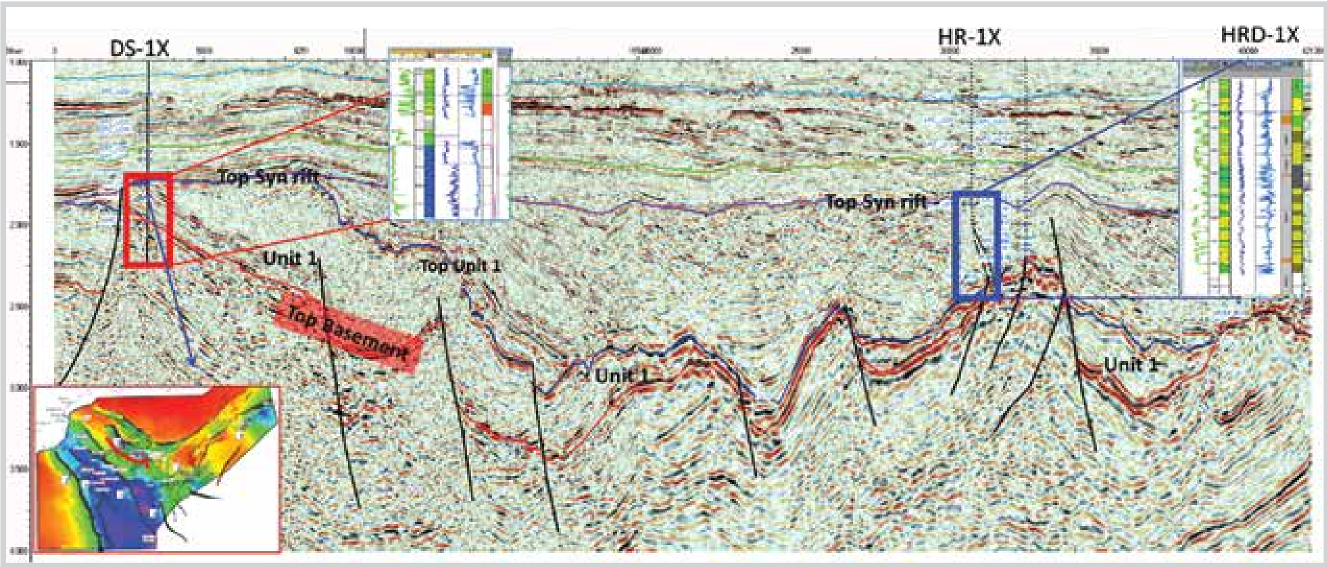

Figure 5. *Top syn rift is calibrated as top of Oligocene (top of Dinh Cao formation).*

mic profiles representing differential sectors (Figure 6) is analysed to understand the sedimentation of syn rift sediments. On the logs the top of syn rift is characterised by typical higher gamma, higher resistivity and low Δt values with respect to younger sediments. This typical syn rift top log marker is biostratigraphic calibrated as top of Oligocene (top of Dinh Cao formation) from palynological study [6].

The syn rift sediments are divided into four units, namely units 1, 2, 3 and 4. This division is primarily developed from the wells which encountered the Oligocene sediments in the Northern part of Song Hong basin. These units (except for unit 1 - it is mainly observed on the seismic data) are identified and correlated on the basis of distinct gamma trends and patterns (Figure 4). The tops of these units on well log are also correlated on the seismic section through these wells (Figures 4 - 6), where they are characterised by regionally developed strong reflectors. The tops of these units are also age calibrated where biostratigraphic data permitted.

The seismic characters showing different units within the syn rift sediments indicate the distinct stages of rift evolution and associated depositional system (Figures 6 and 7).

The Northern Song Hong area records an early stage of major NW-striking extensional faults stretching along the axis of the basin and delineating a major Paleogene syn-rift depocentre [1, 2]. The early stage of rift development is characterised by numerous fault bounding basins with displacement switching to major basin bounding fault during the rift climax. The phenomenon is well demonstrated in the Eastern sector (Ha Mai, BLV graben, SE BLV trough) and the Northwestern sector (Kien An, Thuy Nguyen, and Cam Pha graben) as grabens and troughs bounded by smaller faults seen on the basement levels finally switched to two major troughs having main displacement fault (Figures 1, 3 and 6).

In the period of initial rifting, stretching increased, the rate of fault displacement is relatively low while during the peak rift stage, the rate of fault displacement increases markedly with abundant sedimentation. In the initial rift stage, faulting is most active, and a significant topography is created. The patterns of lithofacies development are surprisingly consistent. Sediment supply to the basin is usually limited in this stage (It is only observed on the seismic data on significant highs, no well records have been seen yet) and, where the fault-driven subsidence rate is high the reflection geometry looks like an overall wedge shaped geometry. The hummocky discontinuous reflectors show a fluvial system. Prograding reflector geometry was in the very lowest fill, implying sedimentation was able to infill the space created through extension (Figure 6). The similar pattern is seen in unit 1 and the lower part of unit 2, which demonstrates the early rift stage during deposition.

During the climax rift stage, the maximum rate of displacement on fault causes sedimentation out paced by extension or exceeds subsidence and the basin topography gradually becomes filled with a lake deposit. This is typically most developed in syn-rift cycles, where shallow

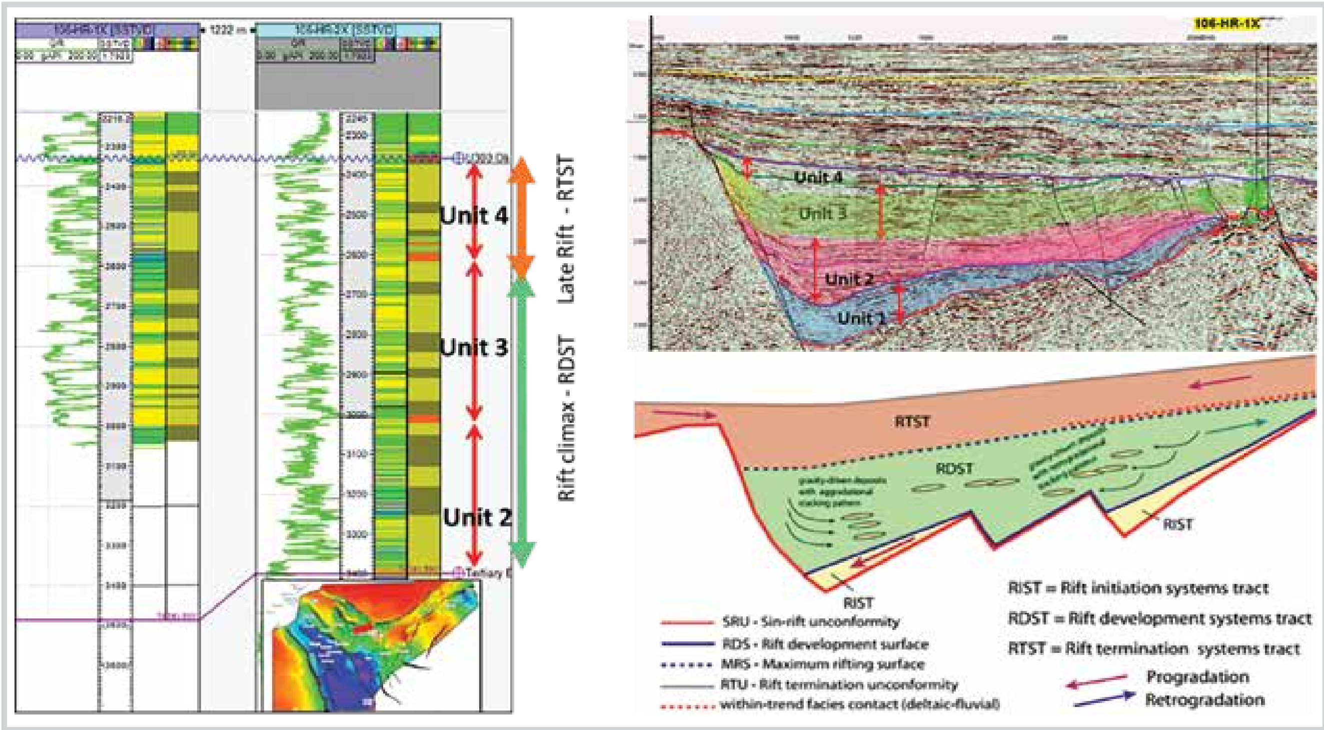

(a)

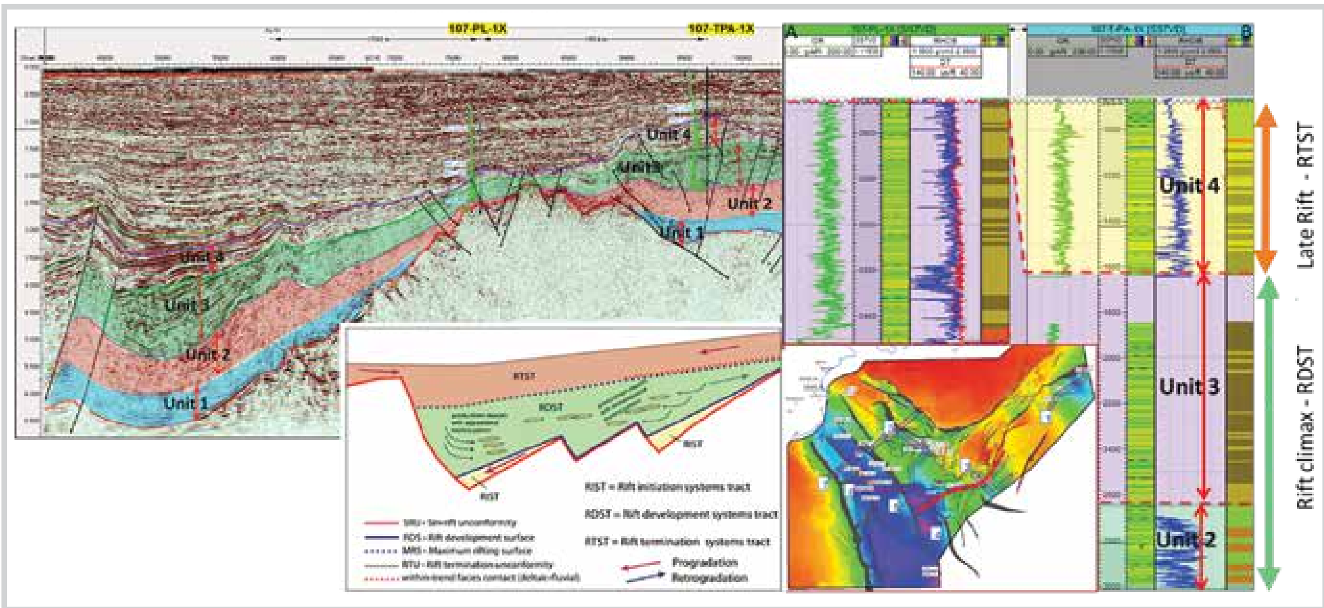

(b)

Figure 6. *Log correlation combining with seismic profiles through (a) Northwestern sector, (b) West Eastern sector.*

and deep lake fluvio-lacustrine to lacustrine source rocks of excellent quality are commonly developed. On the seismic section, the peak rift is characterised by an aggradation reflector with divergent forms related to continue tilting of the hanging wall during deposition (Figure 6). Units 2 and 3 were formed during rift climax with distinct seismic facies (Figure 6). The onset of peak rift started during the lower part of deposition of unit 2; the whole upper part of unit 2 and unit 3 are rift climax which has been deposited in mid and late peak rift stage and associated with the point at which transgression of the hanging wall slope occurs. The late peak rift is characterised on seismic section as a draping reflector that can be traced across the area onto the adjacent footwall and hanging wall crests (Figure 6).

The late rift stage corresponds to a period of waning fault activity, tilting decreases and stops when sediment

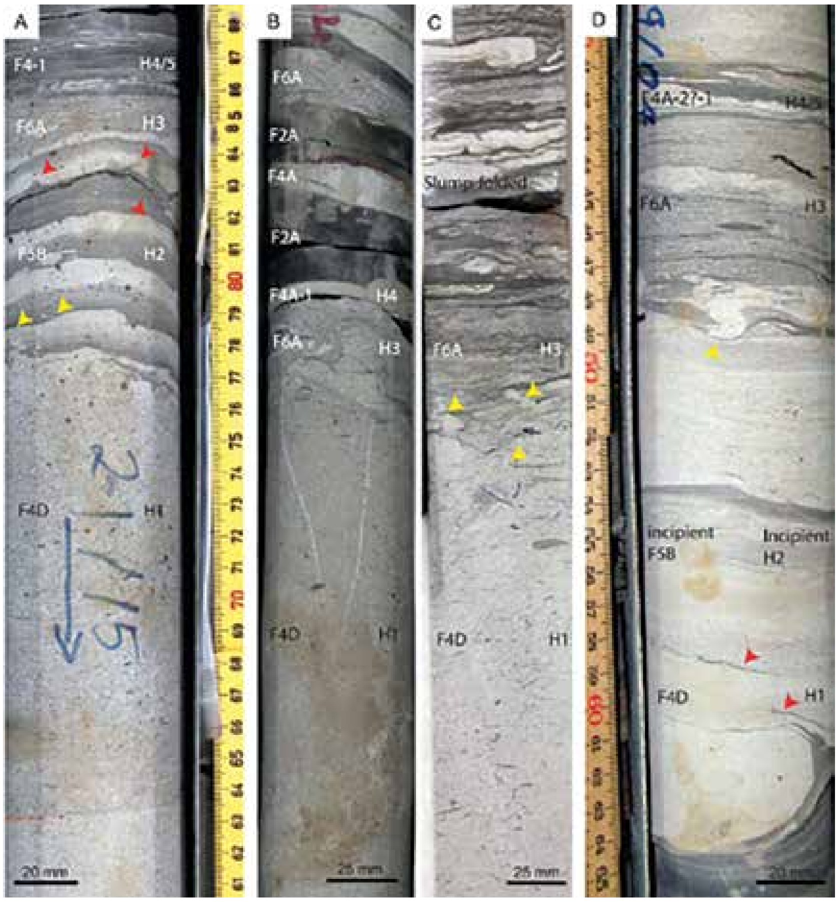

Figure 7. *Core segments from syn rift sediments of well ENRECA-3 [3, 7].*

supply keeps pace with subsidence resulting in the deposition of well sorted clastics which would act as good reservoir. Seismic pattern is observed as more continuous and parallel reflectors than the earlier sequences (Figure 6). Unit 4 had been deposited in the late syn rift stage and expected to have better reservoir characteristics.

3. Core analysis

The data derived from the core will be extrapolated to comparable successions elsewhere in the Northern Song Hong basin, where core data are not available. The core represents a unique window to deep lake deposition along the flanks of the Song Hong basin during the rift climax phase. The data indicates that several hundreds of metres thick of highly oil-prone petroleum source rock successions exist in the area and that source rock facies can be directly interbedded with thin sandstone successions potentially assisting oil expulsion.

The core data indicates that the sandstones of syn rift deposits show changes in flow type from turbidity current to debris flow during a single flow event, debrites and deposits of high-density turbidites (Figure 7). Core segments from syn rift sediments in Figure 7 show: A) Top part of an approximately 25-cm-thick structureless sandstone (F4D; H1) overlain by an interval of banded sandstone-muddy sandstone (F5B; H2), and further thin tabular unit comprising muddy sandstone (F6A; H3). In the top, H3 is sharply overlain by millimetre-scale heterolithic interlamination showing local pseudo nodular siltstone lenses (H4-5). Yellow arrows, water escape structures; red arrows, flame structures and mudstone injections; dashed red line, intra H1 boundary recording abrupt increase in organic-matter fragments. B) Top part of an approximately 22-cm-thick structureless sandstone (H1) overlain by chaotic muddy sandstone (H3), and ripple cross-laminated fine-grained sandstone topped by millimetre-scale clay drape (H4-H5). Top of the figure shows interbedded structureless clayey mudstone beds (fluid mud), ripple cross-laminated sandstone, and muddy sandstone (debrite) beds. (C) 25-cm-thick structureless sandstone (H1) overlain by a chaotic muddy sandstone interval (H3). The muddy sandstone is slump folded and mixed with well-sorted sandstone facies.

The ENRECA-3 core section is interpreted to have formed during rift climax in the Bach Long Vi graben, allowing the establishment of a deep lake due to the outpace of subsidence relative to sedimentation [3, 7]. Similar rift-climax sections will be identified in adjacent areas based on seismic sections and well data, which will be done in an attempt to predict the gross depositional outline of the syn rift sediments in the study areas (Figure 8), and thereby contribute to the prediction of source and reservoir rock intervals.

4. The syn rift association petroleum system

Source rock: This is typically developed best in units 2 and 3 in the climax syn-rift stage, where shallow and deep lake fluvial-lacustrine to lacustrine source rocks of excellent quality were commonly developed (Figures 3, 6 and 8). They contain good quality organic matter (up to 8.99% TOC, average: 3.33) which is present in the lacustrine of Dinh Cao formation [6]. Two distinct types of

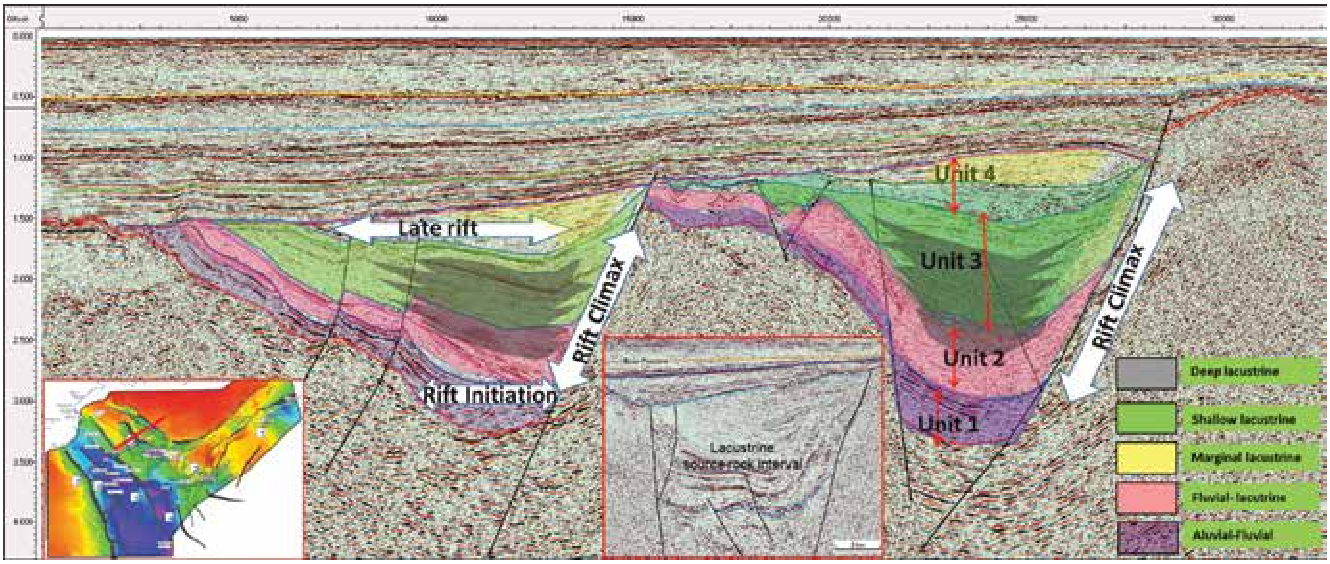

__Figure 8.__ Depositional outline of the syn rift sediments, lacustrine source rocks of excellent quality are commonly developed in the grabens of Northern Song Hong basin.

organic facies are identified within the source sediments as: 1) Type III organic matter (gas prone) in early mid phase of maturation; 2) Type III with minor type II organic matter (gas + sub. oil prone), in early phase of maturation.

The distribution pattern of effective source rock in the study area suggests that better source rock potential exists in the Northwestern sector of the Northern part of Song Hong basin (Figures 2 and 8) lying in the grabens identified in this study. Source rock accumulation can be explained by three syn rift phases and the potential source rocks and effective source are present in unit 2, and followed by the lower part of unit 3. Unit 2 has the best source rock potential as it was deposited during the climax rift stage.

Reservoirs: The integrated analysis of well data and seismic data has brought the presence of abundant reservoir facies in the syn rift sediment interbedded with source rock facies. The prediction depositional result (Figure 8) shows reservoir facies (fluvial, fluvial/lascutrine) development mainly in units 1, 2 and 3. The reservoir facies are also expected in unit 1 in fan wedges, channels as it was deposited in the early stage of rifting.

Traps: Structures and fault bounded closure in the syn rift sequences are prospective entrapments. Besides them, the important entrapment can be provided by stratigraphic traps formed by the wedge outs and pinch out of the syn rift reservoir strata. The wedge out phenomenon is observed at the faults shoulders and more characteristically at the paleo-highs at the grabens and troughs.

5. Conclusions

An attempt has been made to bring out a regional understanding of syn rift architecture by integrating available geo-scientific data and to analyse hydrocarbon prospectivity of syn rift sediments in the Northern Song Hong basin.

Rifting with syn rift sediments was formed along the two tectonic phases within 3 stages of syn rift. The 4 syn rift units bounded by these seismic markers named as units 1, 2, 3 and 4 from older to younger. These identified units have distinct seismic facies, which express their depositional environment associated with the stage of rifting. Most of unit 1 was deposited during the initial rift stage. The climax rift stage prevailed during deposition of unit 2 and unit 3, whereas, most of unit 4 were deposited during the late syn rift stage.

The available core data indicates that the sediments were transported by fluvial drainage with considerable length of transportation and deposited in the lake system. The sediments were dominated by sandy debris flow along with intermittent bottom current activity in lacustrine condition.

The syn rift associated petroleum system by predicting reservoir and source rock intervals are fundamental to exploration and can therefore help formulating a predictive exploration model of the Northern Song Hong basin such as: The reservoir characteristics of units 1, 2 and 3 was having moderate to good primary porosity, better reservoir facies are developed in units 3 & 4. The favourable reservoir facies are also expected in unit 1 in fans and channels deposited in the early stage of rifting; The potential source is present mainly in units 2 and 3. Unit 2 has the best source rock potential as it was deposited during the climax rift stage.

Acknowledgements

The authors express their gratitude to the leadership at all levels of PVN and VPI for permission to publish this paper and are grateful to experts of GEUS for giving them an opportunity to co-work on this project and providing guidance and encouragement during the collaboration of the PEXMOD project.

References

1. Michael B. W. Fyhn, Tong D. Cuong, Bui H. Hoang, Jussi Hovikoski, Mette Olivarius, Nguyen Quang Tuan, Nguyen Thanh Tung, Nguyen Thu Huyen, Trinh Xuan Cuong, Hans P. Nytoft, Ioannis Abatzis, Lars H. Nielsen. *Linking Paleogene rifting and inversion in the Northern Song Hong and Beibuwan basins, Vietnam, with left-lateral motion on the Ailao Shan-Red River shear zone.* Tectonics. 2018; 37(8): p. 2559 - 2585.

2. Harry Doust. *Petroleum systems in Southeast Asian Tertiary basins*. Bulletin of the Geological Society of Malaysia. 2017; 64(1): p. 1 - 16.

3. Jussi Hovikoski, Jens Therkelsen, Lars Henrik Nielsen, Jørgen A. Bojesen-Koefoed, Hans Peter Nytoft, Henrik I Petersen, Ioannis Abatzis, Hoang A. Tuan, Bui Thi Ngoc Phuong, Cao Van Dao, Michael Fyhn. *Density-flow deposition in a fresh-water lacustrine rift-basin, Paleogene Bach Long Vi graben, Vietnam*. Journal of Sedimentary Research. 2016; 86(8): p.982 - 1007.

4. J.J.Lambiase, W.Bosworth. *Structural controls on sedimentation in continental rifts*. Geological Society - Special Publication. 1995; 80: p. 117-144.

5. Christopher K. Morley. *Discussion of tectonic models for Cenozoic strike-slip fault affected continental margins of mainland SE Asia*. Journal of Asian Earth Sciences. 2013; 76: p. 137 - 151.

6. Tập đoàn Dầu khí Việt Nam. *Địa chất và tài nguyên Dầu khí Việt Nam*. Nhà xuất bản Khoa học và Kỹ thuật. 2016: trang. 233 - 283.

7. Henrik I Petersen, Michael Fyhn, Lars Henrik Nielsen, Ioannis Abatzis, Hoang Anh Tuan, Chu Duc Quang, Nguyen Thanh Tuyen, Phan Van Thang, Nguyen Thi Tham, Nguyen Kim Oanh. *World-class Paleogene oil prone source rocks from a cored lacustrine syn-rift succession, Bach Long Vi island, Song Hong basin, offshore Northern Vietnam*. Journal of Petroleum Geology. 2014; 37(4): p. 373 - 389.

PETROVIETNAM JOURNAL
Volume 6/2019, p. 24 - 29
ISSN-0866-854X

Determination of contribution proportion of injection wells in oil production by interwell tracer method using partitioning organic compounds from crude oil

Huynh Thi Thu Huong, Le Thanh Tai, Nguyen Huu Quang, Le Van Son
Centre for Applications of Nuclear Technique in Indusry, Vietnam Atomic Energy Institue
Email: huonghtt@canti.vn

Summary

Waterflooding is one of the most common secondary oil recovery methods because of its economic efficiency. In case where many injection wells contribute to the oil recovery process of a production well, contribution proportion will be an important parameter for management of water injection. Besides the well-known Interwell Tracer Tests using artificial tracers injected into the reservoir, the method of using partitioning organic compounds in crude oil as Natural Partitioning Interwell Tracers (NPITs) shows a great potential for evaluating the contribution proportion of injection wells in oil extraction process. The paper presents the research results to illustrate an idea of using NPITs for calculation of the contribution of injection wells to a production well in homogeneous single-layered reservoir on UTCHEM simulation data with Five-spot model and Direct-line model. The results showed that the calculated values of contribution proportion are different from modelling values between 1 - 2%.

Key words: NPITs, numerical model, contribution proportion, water injection.

1. Introduction

The interwell tracer method is well-known as an effective tool for studying flow dynamics in porous or fractured media of reservoirs. Besides the method using artificial tracers injected into the reservoir, organic compounds such as alkylphenols (APs) and aliphatic acids (AAs) are naturally existing in crude oil and able to dissolve into water phase depending on oil/water partition coefficient K_d used as natural partitioning interwell tracers (NPITs) for oil saturation and swept pore volume calculation [1, 2]. During oil displacement process by waterflooding, the concentration of NPITs decreases over time when diffusing from oil phase into water phase [3, 4]. In case the oil recovery process of a production well is contributed by many injection wells, the concentration of NPITs in water phase at the production well is the total concentration of NPITs contributed by component swept areas. The NPITs concentration curve of each swept area can be determined by deconvolution of the differential total concentration curve. Based on calculation of the mean residence time of NPITs in each swept area, it is possible to determine the contribution proportion of component swept areas.

The proposed method has been tried on the data simulated by UTCHEM in Five-spot model and Direct-line model of homogeneous single-layered reservoir.

2. Theory

Suppose that the reservoir consists of two phases of oil and water. The advection - dispersion - exchange transport of NPITs compound k between phases is given by the equation [2]:

$$\varphi \frac{\partial}{\partial t}\left(\sum_{p=1}^{n_p} S_p C_{kp}\right) + \nabla\left(\sum_{p=1}^{n_p}\left(C_{kp}\vec{u}_p - \varphi S_p \vec{K}_{kp} \times \nabla C_{kp}\right)\right) = 0 \quad (1)$$

In which, φ is porosity of media, $n_p = 2$ is number of phases (p = w: water phase, p = o: oil phase); S_p is saturation of phase p; C_{kp} is concentration of compound k in phase p [M/L^3]; K_{kp} is dispersion tensor of compound k in phase p [L^2/T]; u_p is velocity of phase p [L/T]; t is time [T].

Equation (1) can be solved with the following assumptions: the concentration of compound k between phases instantaneously reaches equilibrium while oil/water in contact, the partition coefficient K_d of compound k is constant, no mass transfer of compounds on the

Date of receipt: 2/8/2018. Date of review and editing: 3/8 - 6/12/2018.
Date of approval: 3/6/2019.

boundaries of studied zone except the boundaries of injection well and production well, the diffusion effect is ignored due to the high velocity of water, the degradation, absorption and interaction of compounds are not considered.

From Equation (1) Akasawa showed the expression of mean residence time of NPITs compound k [2]:

$$\bar{t}_k = \int_0^\infty [1 + (f_w + K_{dk} f_o)\, (\frac{C_{kw} - C_{kwI}}{C_{kwI}})]\, d\tau \tag{2}$$

In which, K_{dk} is the partition coefficient of compound k; f_w, f_o are fraction of water phase and oil phase in fluids at production well, respectively.

Let $C_{kA} = C_{kWI} + (f_w + K_{dko} \times f_o) \times (C_{kw} - C_{kwI})$ be the apparent concentration of compound k, mean residence time is given in equivalent form:

$$\bar{t}_k = \frac{1}{C_{kwI}} \times \int_0^\infty C_{kA}\, d\tau \tag{3}$$

The differential distribution of apparent concentration $C'_{kA} = \partial C_{kA}/\partial t$ has the form of chromatographic peak as illustrated in Figure 1, in which its mean residence time (4) is proven to be equal to the mean residence time of apparent distribution in Equation (3):

$$\bar{t}'_k = \frac{\int_0^\infty \frac{\partial C_{kA}}{\partial t} \times t dt}{\int_0^\infty \frac{\partial C_{kA}}{\partial t} dt} = \frac{1}{C_{kwI}} \times \int_0^\infty C_{kA}\, dt = \bar{t}_k \quad \left| \begin{array}{ll} C_{kA} = C_{kwI} & t = 0 \\ C_{kA} = 0 & t \to \infty \end{array} \right. \tag{4}$$

In case the oil recovery process of a production well is contributed by many injection wells, the concentration of NPITs in water phase at the production well is the total concentration of NPITs contributed by component swept areas. The differential distribution of apparent concentration of each swept area can be determined to calculate the mean residence time of NPITs in each swept area, therefore the contribution proportion of respective injection wells F_i is determined.

$$F_i = \frac{1}{1 + \bar{t}_{ki} \sum_{j \neq i} \frac{1}{\bar{t}_{kj}}} \tag{5}$$

Equation (5) is based on assumptions such as reservoir is homogeneous single-layered and the distances between the injection wells and the production well are the same.

3. Simulation results

UTCHEM (The University of Texas's Chemical Simulator) is a software for simulating multiphase and multicomponent reservoir model developed by Texas University. UTCHEM allows simulation of advection - dispersion and exchange of solutes between phases in reservoir media, including the leaching process of organic compound from oil phase to water phase during oil production [5].

UTCHEM was used to run 3D reservoir model with two water injection patterns: Five-spot pattern - common pattern in stratified sediment reservoir and Direct-line

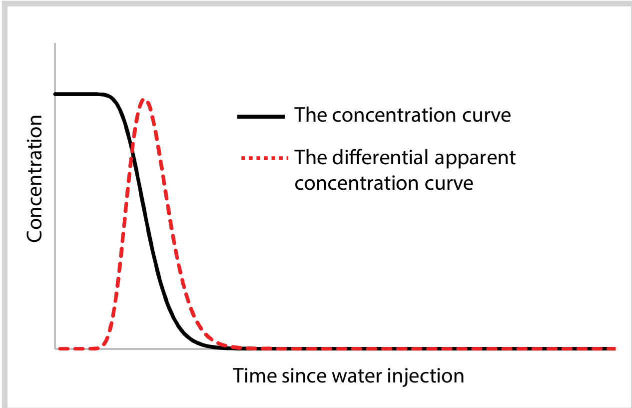

Figure 1. *Illustrating the apparent concentration curve of NPITs compound and its differential curve. The differential distribution of apparent concentration is in the form of a chromatogram.*

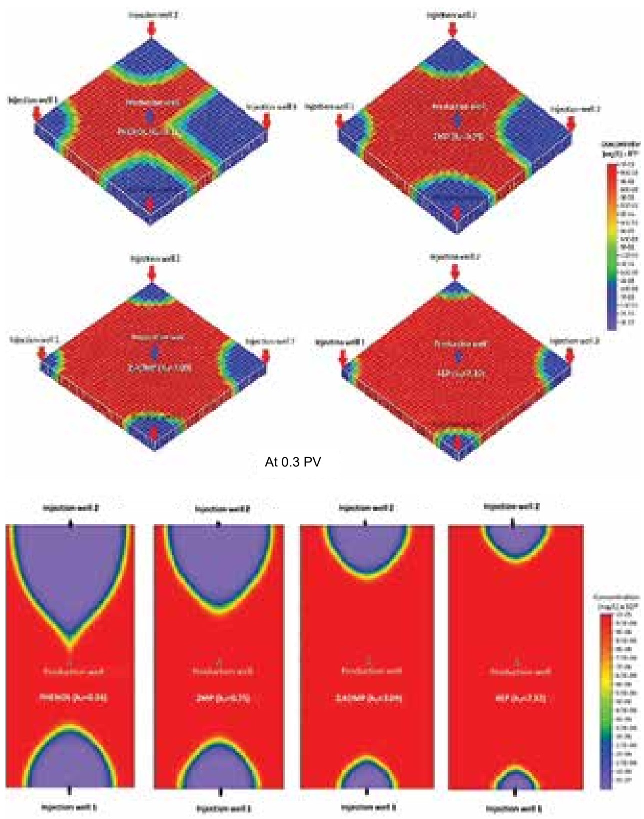

Figure 2. *Concentration distribution in space of phenol, 2-methylphenol, 2,4-dimethylphenol, 4-ethylphenol at 0.3 PV in Five-spot model and Direct-line model.*

pattern - typical pattern in edge water injection or gravity injection.

The models have initial oil saturation of 0.65 and initial water saturation of 0.35.

The Five-spot model includes 4 injection wells and a production well having the size of 132m x 132m x 15m divided into 33 x 33 x 4 grid cells. The total flow rate is 261.36m^3/day with contribution proportion of injection wells equal to 10:20:30:40 (%).

The Direct-line model includes 2 injection wells and a production well having the size of 102m x 204m x 8m divided into 25 x 51 x 4 grid cells in corresponding ratio

Table 1. *The partition coefficient K_d of NPITs used in the models*

NPITs	Partition coefficient $K_d = C_o/C_w$	Initial concentration in oil (mg/L)	Initial concentration in water (mg/L)
Phenol	0.16	1.6	10
4-Methylphenol	0.58	5.8	10
2-Methylphenol	0.75	7.5	10
4-Propylphenol	1.34	13.4	10
3,4-Dimethylphenol	1.61	16.1	10
2,4-Dimethylphenol	3.09	30.9	10
4-Ethylphenol	7.37	73.7	10

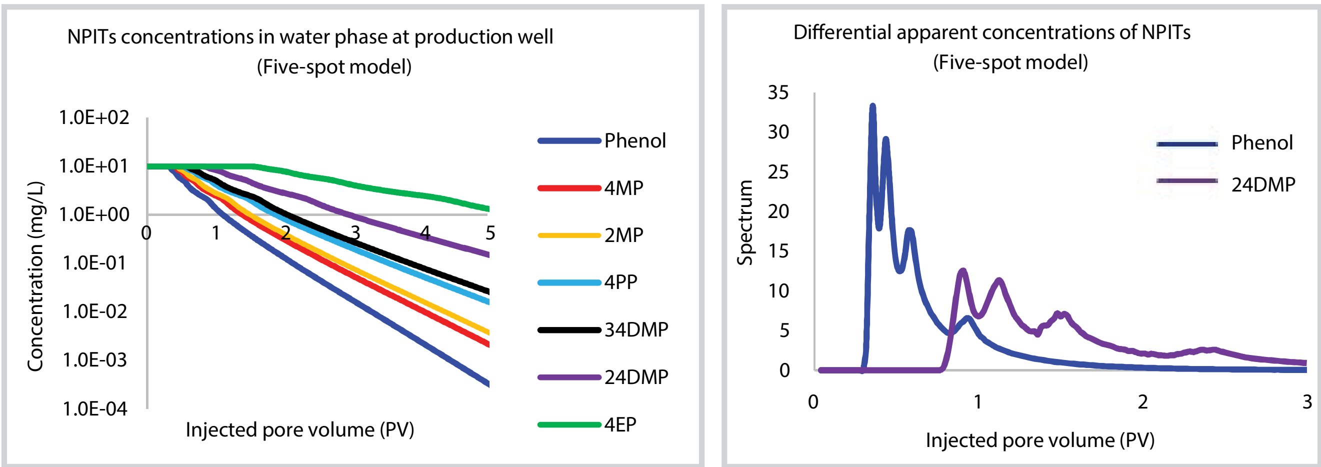

(a) *(b)*

Figure 3. *NPITs concentration curves in water phase at production well of Five-spot model (a) and its differential apparent concentration (b) of phenol (K_d = 0.16) and 2,4-dimethylphenol (K_d = 3.09). The chromatogram shows the effect of four swept areas on NPITs concentration at production well.*

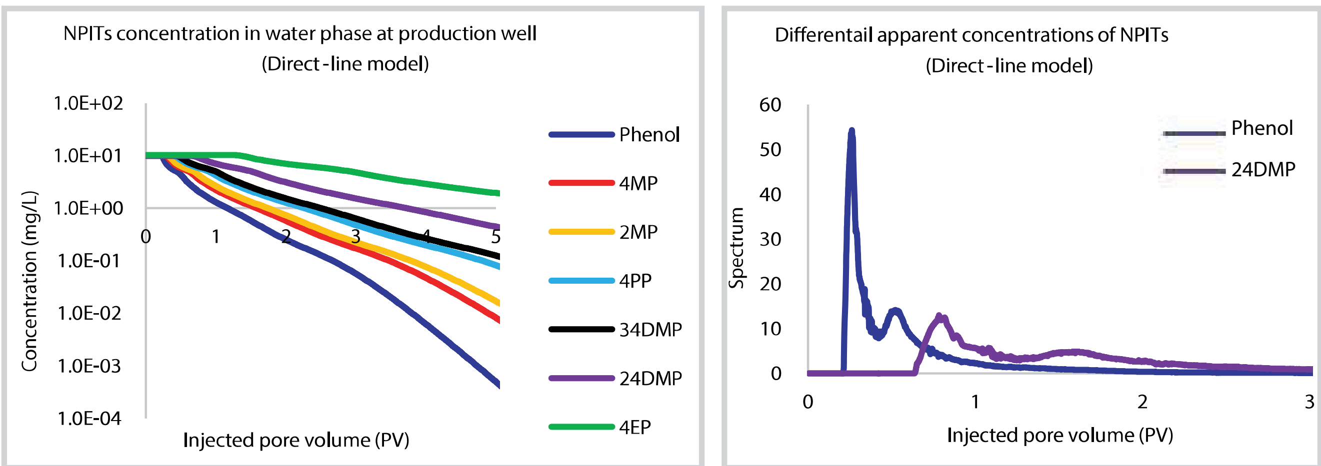

(a) *(b)*

Figure 4. *NPITs concentration curves in water phase at production well of Direct-line model (a) and its differential apparent concentration (b) of phenol (K_d = 0.16) and 2,4-dimethylphenol (K_d = 3.09). The chromatogram shows the effect of two swept areas on NPITs concentration at production well.*

of length to width d/a = 2. The total flow rate is 200m³/day with contribution proportion of injection wells equal to 30:70 (%).

The general parameters of the models are:

- Porosity φ = 0.2, water viscosity μ_w = 0.7cp, oil viscosity μ_o = 4cp;

- Longitudinal and transverse dispersivity are α_{DL} = 0.03m, α_{DT} = 0.003m;

- Relative permeability curve is described by Corey model with critical water saturation S_{cwr} = 0.3, residual oil saturation S_{or} = 0.35, water endpoint: 0.15, oil endpoint 0.85, water exponent: 1.5, oil exponent: 2, endpoint mobility ratio: 1.

The NPITs initial concentration in oil phase and water phase and its partition coefficient between phases determined in the experimental data of Tracer Lab of CANTI are listed in Table 1. All compounds are supposed to have the same density, alkane number and chemical properties but different partition coefficient.

The waterflooding lasts 10 PV of the model to obtain the whole concentration curves of the NPITs at the production well. The concentration of NPITs between phases instantaneously achieves equilibrium while oil/water are in contact. Figure 2 illustrates NPITs concentration distribution of the models at 0.3 PV. Figures 3a and 4a show NPITs concentration curves at the production well decreased over time, in which the greater K_d the slower reduction of concentration. The Levenberg-Marquart (LM) algorithm and Exponential Modified Gauss (EMG) function were applied to determine the differential apparent concentration curve of each swept area. The corresponding differential apparent concentrations illustrated in Figures 3b and 4b have the form of overlapping chromatographic peaks, in which the mean residence time of each peak equal to the mean residence time of NPITs representing the injection mode of the respective swept area.

Figures 5 and 6 show the results of applying LM algorithm to separate the overlapping chromatographic

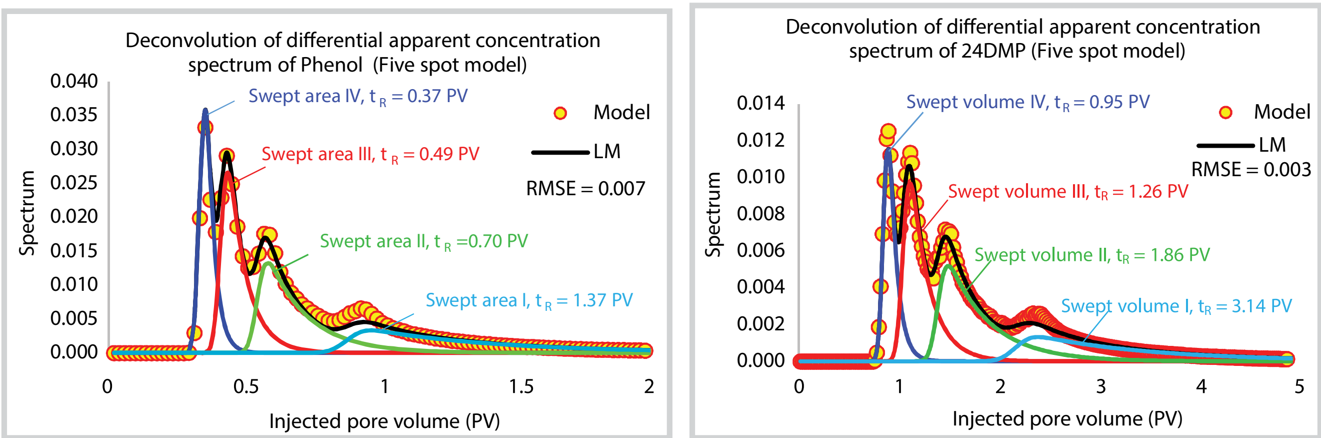

Figure 5. *Differential apparent concentration of phenol (K_d = 0.16) and 2,4-dimethylphenol (K_d = 3.09) of Five-spot model is obtained after using LM algorithm. The mean residence time t_R of NPITs in each swept area is determined by using corresponding chromatographic peak.*

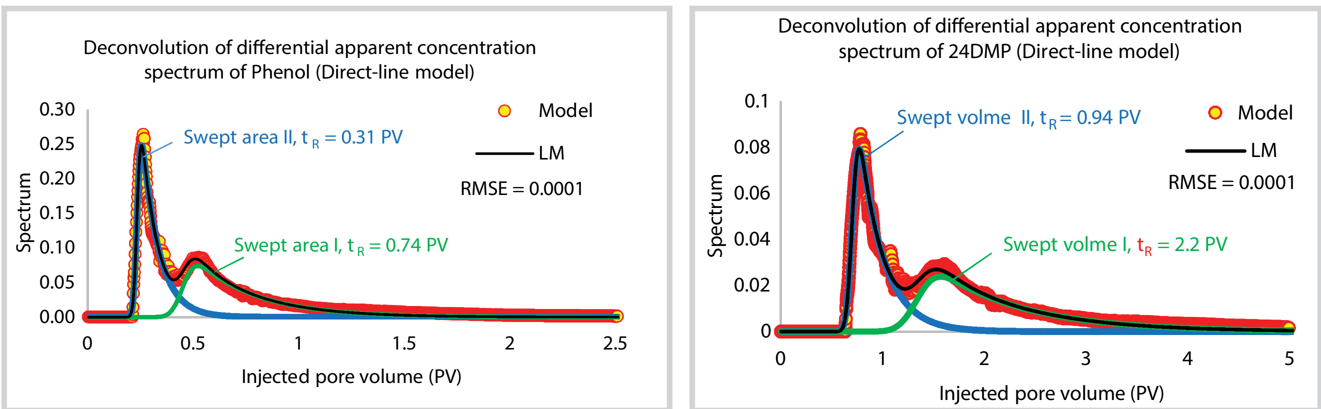

Figure 6. *Differential apparent concentration of phenol (K_d = 0.16) and 2,4-dimethylphenol (K_d = 3.09) of the Direct-line model is obtained after using LM algorithm. The mean residence time t_R of NPITs in each swept area is determined by using corresponding chromatographic peak.*

Table 2. The results of calculating the contribution proportion of injection wells of Five-spot model and Direct-line model

Model	Five spot model				Direct-line model	
Swept area	I	II	III	IV	I	II
Contribution ratio of swept areas of models (%)	10	20	30	40	30	70
The mean residence time of NPITs in swept areas $\bar{t}$ (PV) calculated from Equation (4). The contribution proportion of injection wells F (%) calculated from Equation (5) and the difference from model value d (%) are given below.						
Phenol (K_d = 0.16)						
$\bar{t}$ (PV)	1.37	0.70	0.49	0.37	0.74	0.31
F (%)	10.6	20.6	29.8	39.0	29.7	70.3
d (%)	0.6	0.4	0.2	1.0	0.3	0.3
4MP (K_d = 0.58)						
$\bar{t}$ (PV)	1.65	0.88	0.60	0.46	0.92	0.40
F (%)	10.9	20.4	29.7	39.0	30.2	69.8
d (%)	0.9	0.0	0.3	1.0	0.2	0.2
2MP (K_d = 0.75)						
$\bar{t}$ (PV)	1.77	0.95	0.65	0.49	1.06	0.45
F (%)	10.9	20.3	29.7	39.0	29.7	70.2
d (%)	0.9	0.3	0.3	1.0	0.3	0.2
4PP (K_d = 1.34)						
$\bar{t}$ (PV)	2.18	1.18	0.81	0.61	1.37	0.59
F (%)	11.0	20.3	29.6	39.1	30.3	69.7
d (%)	1	0.3	0.4	0.9	0.3	0.3
34DMP (K_d = 1.61)						
$\bar{t}$ (PV)	2.37	1.29	0.88	0.66	1.50	0.63
F (%)	11	20.2	29.6	39.2	29.6	70.4
d (%)	1	0.2	0.4	0.8	0.4	0.4
24DMP (K_d = 3.09)						
$\bar{t}$ (PV)	3.14	1.86	1.26	0.95	2.20	0.94
F (%)	11	20.1	29.6	39.3	29.9	70.1
d (%)	1	0.1	0.4	0.7	0.1	0.1
4EP (K_d = 7.37)						
$\bar{t}$ (PV)	5.72	3.49	2.37	1.78	4.16	1.86
F (%)	12.1	19.8	29.2	38.9	30.9	69.1
d (%)	2.1	0.2	0.8	1.1	0.9	0.9

peaks of phenol (K_d = 0.16) and 2,4-dimethylphenol (K_d = 3.09). The mean residence time of NPITs in each swept area can be determined by using corresponding chromatographic peak. The greater K_d the greater mean residence time of NPITs in each swept area and vice versa. The results of calculating the contribution proportion of injection wells of the Five-spot model and the Direct-line model are presented in Table 2.

The calculated contribution proportion values are different from the model values in range of 1 to 2% for all NPITs in both models. The compounds having K_d smaller than 3 allow for the calculation from 0 to 3 PV whereas those having K_d more than 3 need greater observation time period. The results show the applicability of the interwell tracer method using NPITs for evaluating the contribution proportion of injection wells in oil extraction process on both the Five-Spot and Direct-line models.

4. Conclusions

The movement of partitioning organic compounds (NPITs) in the case of many injection wells contributing to the oil recovery process of a production well is simulated on the UTCHEM software with the Five-spot model and the Direct-line model. The contribution proportion of swept areas can be determined by using mean residence time of NPITs in corresponding swept area. The calculated values are then compared with the model to assess the feasibility of the method.

The NPITs having K_d smaller than 3 are more suitable to calculate contribution proportion values at the stage of up to 3 PV of injection volume, while other NPITs having K_d greater than 3 are more suitable to longer injection period.

Acknowledgements

This research work has been implemented through Project CS/17/06-01 under the grant of Vietnam Atomic Energy Institute (VINATOM).

References

1. R.Sinha, K.Asakawa, G.A.Pope, K.Sepehmoori. *Simulation of natural and partitioning interwell tracers to calculate saturation and swept volumes in oil reservoirs*. SPE/DOE Symposium on Improved Oil Recovery, Tulsa, Oklahoma. 17 - 21 April, 2004.

2. Kazuhiro Asakawa. *A generalized analysis of partitioning interwell tracer tests*. University of Texas. 2005.

3. Nguyễn Hồng Phan, Nguyễn Hữu Quang, Tô Bá Cường, Huỳnh Thị Thu Hương, nnk. *Phát triển mô hình mô phỏng quá trình vận động của các chất chỉ thị tự nhiên (NPIT) để đánh giá trữ lượng dầu trong khai thác*. Viện Năng lượng Nguyên tử Việt Nam.

4. To Ba Cuong, Nguyen Hong Phan, Nguyen Huu Quang. *Interwell tracer method using partitioning compounds naturally existing in crude oil for determination of residual oil saturation*. Petrovietnam Journal. 2016; 10: p. 38 - 43.

5. Center for Petroleum and Geosystems Engineering, University of Texas. *Reservoir engineering research program: Volume II - Technical documentation for UTCHEM - 9.0 - A three-dimensional chemical flood simulator.* 2000.

PETROVIETNAM JOURNAL
Volume 6/2019, p. 30 - 40
ISSN-0866-854X

Oligocene combination/stratigraphic traps and their reservoir quality in Cuu Long basin, offshore Vietnam

Nguyen Dinh Chuc[1, 3], Mai Thanh Tan[2], Tran Van Xuan[3], Tran Nhu Huy[1]
[1]Petrovietnam Exploration Production Corporation
[2]Ha Noi University of Mining and Geology
[3]Ho Chi Minh City University of Technology, VNU-HCMC
Email: chucnd@pvep.com.vn

Summary

Cuu Long basin is a Cenozoic rift basin located in the Southeastern shelf of Vietnam with high potential of oil and gas. Up to date, most production in the Cuu Long basin is contributed from structural traps, making them more and more depleted after years of exploitation. Exploration activities in the Cuu Long basin, therefore, are shifting towards nonstructural traps including stratigraphic and/or combination ones.

By integrating exploration methods such as seismic sequence stratigraphy and seismic attribute interpretation, petrophysical and petrographical analysis, this article discusses the assessments of combination/stratigraphic trap types within the Oligocene section in the Cuu Long basin, including (i) identification of several trapping mechanisms and (ii) some evaluations of the trap's reservoir quality utilising the database of some 2D/3D seismic sections, several wells and unpublished reports. The research results show that the key forming factor for primary stratigraphic traps of sand body is lithology change and the one for pinch-out stratigraphic traps is tapering off of sand layers landward or toward the horsts. The reservoir quality of these traps ranges from moderate to good. Further detailed studies on reservoir distribution and sealing capacity of these trap types, however, need to be carried out to fully evaluate hydrocarbon potential of these stratigraphic/combination traps, and minimise risks in exploration drilling.

Key words: Stratigraphic trap, trapping mechanism, reservoir quality, Cuu Long basin.

1. Introduction

Cuu Long basin is a matured basin with high density of exploration and production activities. So far, it is the most important sedimentary basin which contributes greatly to Vietnam's annual petroleum production. The major targets for petroleum exploration and production in the Cuu Long basin have been Pre-Cenozoic fractured basement highs and sandstones in Oligocene as well as in Early and Middle Miocene time. Most of these Cenozoic targets are related to structural traps of tectonically formed anticlines.

In recent years, petroleum production from structural traps in the Cuu Long basin has been gradually declining, and exploration for new structural traps is facing technical difficulties, limited potential and commercial issues. Thus, petroleum exploration needs to focus on more potential but more complicated targets such as stratigraphic/combination traps.

Exploration and appraisal activities in recent years have increasingly discovered more hydrocarbons in the Oligocene section of the Cuu Long basin, thus showing a higher potential of Oligocene targets. Some of them were discovered in combination/stratigraphic traps, such as Ca Tam, Song Ngu, Kinh Ngu Trang Nam, etc. These demand further attention to explore the nonstructural traps.

There were several researches conducted in the Cuu Long basin to search for non-structural traps [1 - 4]. Some of them focused on the Southeastern part of the Cuu Long basin and showed that there existed pinch-out traps in Oligocene deposits along the Northwestern slope of Con Son swell. However, these traps were not paid sufficient attention in petroleum exploration due to low petroleum potential or insufficient petroleum

Date of receipt: 4/5/2018. Date of review and editing: 4/5 - 16/10/2018.
Date of approval: 3/6/2019.

system. As the result, these non-structural traps are ordinarily considered as secondary targets in exploration in the Cuu Long basin.

Recently, exploration activities in the Southeastern margin of the Cuu Long basin have identified several stratigraphic traps formed by appropriate changes in rock facies. Their existence has been confirmed through several wells. These are new exploration targets in the Southeastern part of the Cuu Long basin. These findings have opened up a new direction for petroleum exploration of potential stratigraphic/combination traps in the Southeastern part of the Cuu Long basin [5]. Nevertheless, prospecting these non-structural traps is a difficult task due to the complex distribution and the large range of exploration risks. Therefore, additional studies and assessments of recently discovered nonstructural traps need to be carried out in order to support future exploration and appraisal programmes in the Cuu Long basin.

This paper focuses on the identification of several trap types ascertained in the Oligocene section and their distribution as well as main risks in exploration using various methods of seismic stratigraphy and seismic attribute analysis in conjunction with well log interpretation and other geological data. Further discussions on reservoir's qualities of combination/stratigraphic traps are also mentioned with some examples in the Southeastern margin of the Cuu Long basin in order to support the exploration of non-traditional target and appraisal of the discovered structural traps in this area as well.

2. Geological settings

2.1. Basin evolution

Cuu Long basin is a Cenozoic rift basin located in the Southeastern shelf of Vietnam. The geological evolution of the Cuu Long basin is divided into three periods: pre-rift, syn-rift and post-rift [1, 6]:

First period (pre-rift): From Jurassic to Paleogene was the period of formation and uplifting of basement. This was the levelling period of the paleo-topography before creation of the Cuu Long basin [1].

Second period (syn-rift): This period took place from Late Eocene to Early Miocene. A series of NE-SW faults were formed due to vigorous subduction and extension activities [1]. The Cuu Long basin was formed during this period and underwent two rifting phases: true rift phase from Middle Eocene to Oligocene and late rift phase in Early Miocene [6].

Third period: Thermal subsidence from Middle Miocene to the Quaternary [1].

2.2. Structural elements

The Cuu Long basin has an oval shape, elongating along Northeast-Southwest direction and is divided into five secondary structural units including: Bac Lieu differentiated trough, Ca Coi differentiated trough, Cuu Long uplifted zone, Phu Quy uplifted zone (the extension of Con Son swell), and Cuu Long main trough [1]. Cuu Long main trough (secondary structure unit) is subdivided into smaller (tertiary) structural units including Northeastern trough, West Bach Ho trough, Northwestern monocline, Central high, Northwestern high, Eastern high, Northeastern differentiated zone, Southwestern differentiated zone, East Bach Ho trough, Opal - Amethyst high and Southeastern monocline (Figure 1).

2.3. Stratigraphy

Stratigraphic column of the southeastern area as well as the whole Cuu Long basin can be summarised as follows (Figure 2) [1]:

Pre-Tertiary basement: The Pre-Tertiary basement in the Cuu Long basin is mostly magnetic intrusive rocks with main lithologies of granite, granite - gneiss, granodiorite, diorite, adamellite, monzodiorite, gabbro, monzogabbro. The metamorphic rocks are also encountered in some places [1].

Lower Tra Tan - Tra Cu formation - Oligocene E: This continental sediment consists of shale, siltstone and sandstone which were deposited unconformably on the Pre-Tertiary basement. It is distributed widely across the southeastern area and divided into two sub-units:

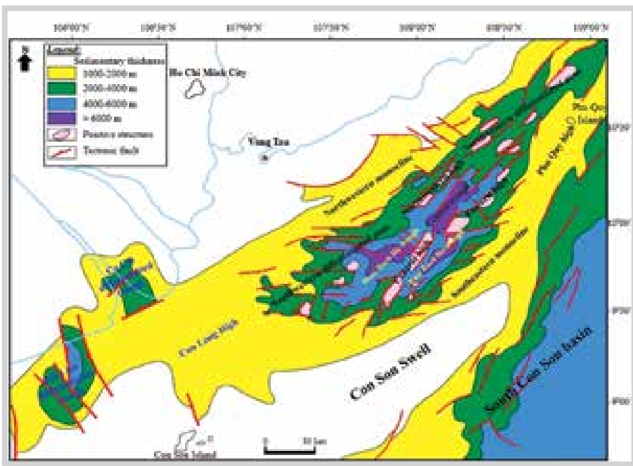

Figure 1. *Structural provenances of Cuu Long basin [1].*

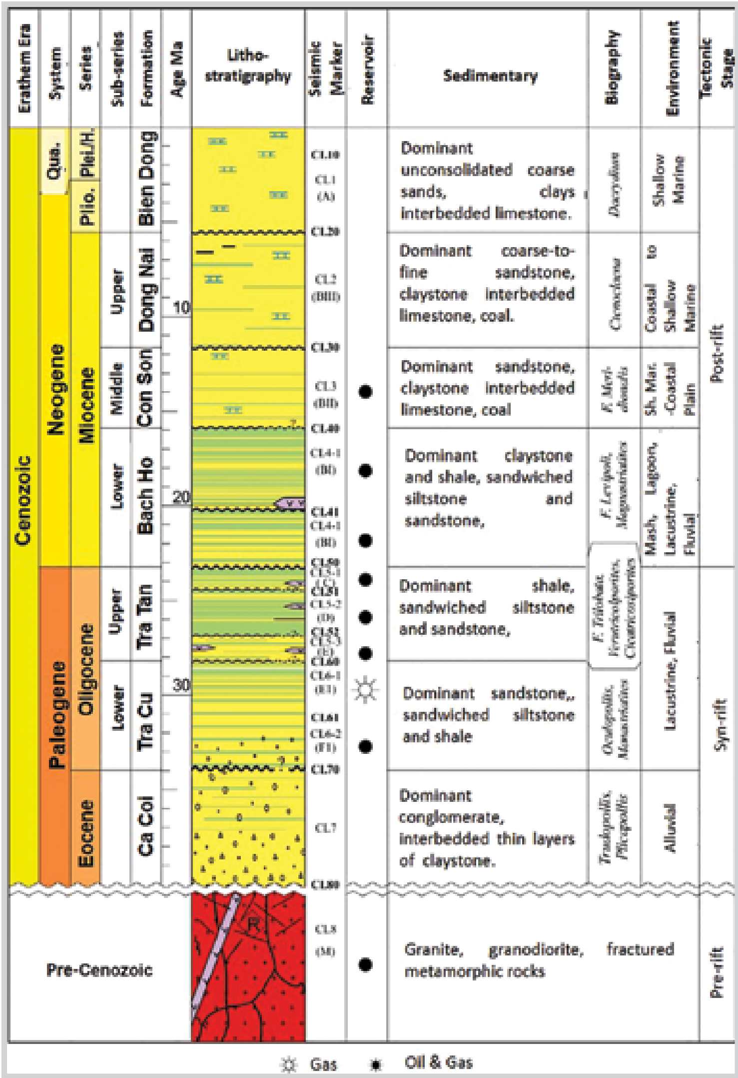

Figure 2. Generalised litho-stratigraphic column of Cuu Long basin [1].

Oligocene E Lower in the lower part and Oligocene E Upper in the upper part. The lower one is dominated by medium- to coarse-grained sandstones composed of mostly granitic fragments and feldspars, interbedded with hard organic-rich black shale layers. The other one is composed majorly of fine to medium grained sandstones interbedded with gray shale layers. In addition, magma intrusions such as dykes, composed majorly of andesite/basalt were found occasionally [1].

Upper Tra Tan formation - Oligocene D: It is majorly organic-rich brown shale deposited in lacustrine environment, occasionally interbedded with local layers of coal or sandstone [1]. However, toward the Eastern boundary of the sub-basin (close to Con Son swell), thick layers of sandstone were deposited on top of Oligocene D shale.

Upper Tra Tan formation - Oligocene C: This section is the mixtures of fine-grained sandstones and lacustrine brown shale [1].

Bach Ho formation - Miocene BI: This stratigraphic sequence is divided into two sub-units Miocene BI.1 (lower part) and Miocene BI.2 (upper part). Miocene BI.1 is composed mainly of sandstone-dominant fluvial-deltaic deposits with small intercalation of shale deposited in floodplain or some brackish environments, while Miocene BI.2 is composed mainly of sandstone interbedded with shale/claystone, occasionally shallow marine siltstone and limestone. The top section of Miocene BI is Bach Ho shale, a thick and continuous shale layer, acting as a regional seal for the whole Cuu Long basin [1].

2.4. Petroleum systems

Two matured source rocks in the Cuu Long basin are shales in Lower Oligocene + Eocene (?) and in Upper Oligocene [1]. The reservoirs in the Cuu Long basin are fractured granitoid basements and Cenozoic sandstones aged from Early Oligocene to Early Miocene. Besides, there could be Middle Miocene sandstone reservoir in the Eastern area of the Cuu Long basin [1]. The seals in the Cuu Long basin are confirmed to include five shale layers. The most important one is Rotalia shale in Bach Ho formation. The other four are shales in Con Son, Bach Ho, Tra Tan (C and D sequences) and in Tra Cu formation [1]. In the Cuu Long basin, the traps are defined to be structural, stratigraphic and combination ones. They were mostly formed during syn-rift and early post-rift periods. Migration timing of Lower Oligocene source rock started in Early Miocene and reached max in late of Middle Miocene. The migration timing of Upper Oligocene source rock started in Late Miocene. These timings occurred later than those of trap formation, thus making it favourable for hydrocarbons to be trapped [1].

3. Data and methodology

3.1. Database

This research was accomplished utilising several 2D/3D seismic surveys and petrophysical data from some wells in the Cuu Long basin. Data of regional geology and results of some unpublished reports were also included as database for this research.

3.2. Methodology

In this article, we utilise an integrated approach of different exploration methods to assess various Oligocene traps in the Cuu Long basin. These methods are seismic sequence stratigraphy, seismic attribute analysis, petrophysical interpretation, petrographical analysis, and biostratigraphy, etc. Seismic sequence stratigraphy is based on analysis of patterns of seismic reflectors and analysis of sequences and system tracts [7, 8]. Seismic attribute analysis is based on the application of different attributes to enable the interpretation of depositional environment as well as the identification of internal patterns in stratigraphic units [9, 10]. Petrophysical analysis allows detailed interpretation of geologic sections and provides information on lithology, facies, reservoir characteristics as well as sequence stratigraphy [11]. Other supporting methods including petrographic analysis and paleo-biostratigraphy play an important role in the interpretation of depositional environments.

3.3. Depositional model in the study area

The Cuu Long basin is a continental rifting basin during the Oligocene epoch [1, 12]. Various researches show that tectonics and climate are two of the factors controlling the sedimentary and petroleum systems in rift basins [13, 14]. Tectonics also affects the trap types formed in these basins. Several authors [15, 16] have indicated that climate during Oligocene time in the Cuu Long basin was seasonal with more arid conditions in Early Oligocene and more humid ones in Late Oligocene times (Figure 3a). The depositional model for sedimentary system in the study area is illustrated in Figure 3b [13]. During wet seasons, the water level rose and caused most of the area to submerge (possibly up to dashed black line in Figure 3a), then creating opportunities for shale layers to form and act as both source and seal for traps at the East-Southeastern margin of the Cuu Long basin. During dry seasons, the water level felt back low making the lake's area retracted (light blue area in Figure 3a). The area between the highest and the lowest water level had sedimentary facies of fluvial deposits, mudflats, sandy alluvial fan that were detrital-deposit reservoirs of different trap types in the research area. In some locations on the slope less affected by post-depositional tectonic activities, these deposit materials could form potential stratigraphic traps. In the areas that were affected by post-depositional tectonics without truncation, the traps formed would be structural type. Other conditions could cause combination traps to be formed.

4. Results and discussion

4.1. Trap types, forming mechanisms and their distributions

A series of hydrocarbon fields and discoveries in the Oligocene section have been identified by exploration and appraisal drilling in the Cuu Long basin. They appear to trend in the main axis of the Cuu Long basin. Integrated studies and oil and gas exploration in recent years have shown that oil and gas accumulations exists in both structural and stratigraphic traps such as facies change, pinch-outs or truncations. These traps have different trapping mechanisms, risks and different distributions in the Cuu Long basin. Detailed delineations of the structural ones could be found in various papers. This section reviews several trap types and forming mechanisms as well as their main risks in the Cuu Long basin, focusing on the stratigraphic/combination traps.

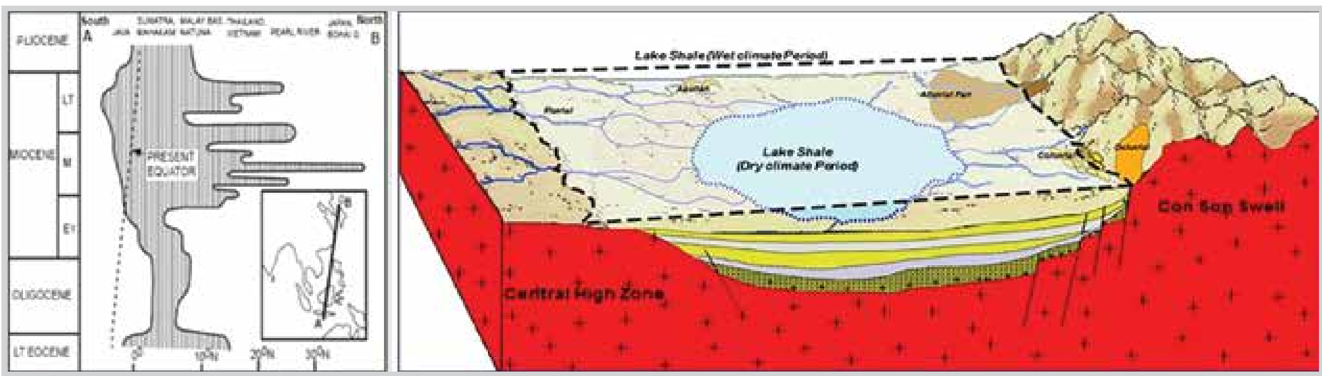

(a) (b)

Figure 3. *Illustration of Cuu Long basin's eastern sub-basin depositional model under wet and dry paleo-climate conditions [15] (a); Schematic and simplified distribution of tropical rain forest climate in SE and East Asia during Tertiary [13] (b).*

4.2. Structural traps

These trap types developed mainly over the pre-rift basement highs (Figure 4a). The trap forming mechanism is determined to be the consequences of post-depositional tectonic activities forming anticlines or draping over the existing topography highs. Tectonic inversion can be a favourable conditions for structural traps to form. These traps are sealed at the top by a number of overlying shale layers (Figure 4a). Lateral seals of these structural traps are 4-way closure types or fault-dependent trap types in which a tectonic seal is created on the downdip of the structures (Figure 4b). The structural traps distribute widely in the Cuu Long basin but mostly in the centre of the basin. Main risks in exploring these trap types are mostly related to sealing, especially fault seal. In some places, source rock and migration complexities could add additional risk into prospecting these trap types due to long distances from the source areas in the Cuu Long basin.

4.3. Stratigraphic traps

4.3.1. Facies change

This kind of stratigraphic trap was identified in some places in the southeastern areas of the Cuu Long basin such as Kinh Ngu Trang Nam (in Oligocene C sequence), SoN (in Oligocene D sequence) and Ca Tam (Oligocene D) [5, 17]. The trap is interpreted to be sand bodies that could be sand fans as the case in KTN prospect or channel sands as in SoN case (Figure 5). Lithology changes from coarse-grained to contemporaneously deposited fine-grained sediments are the key factor to form these stratigraphic traps.

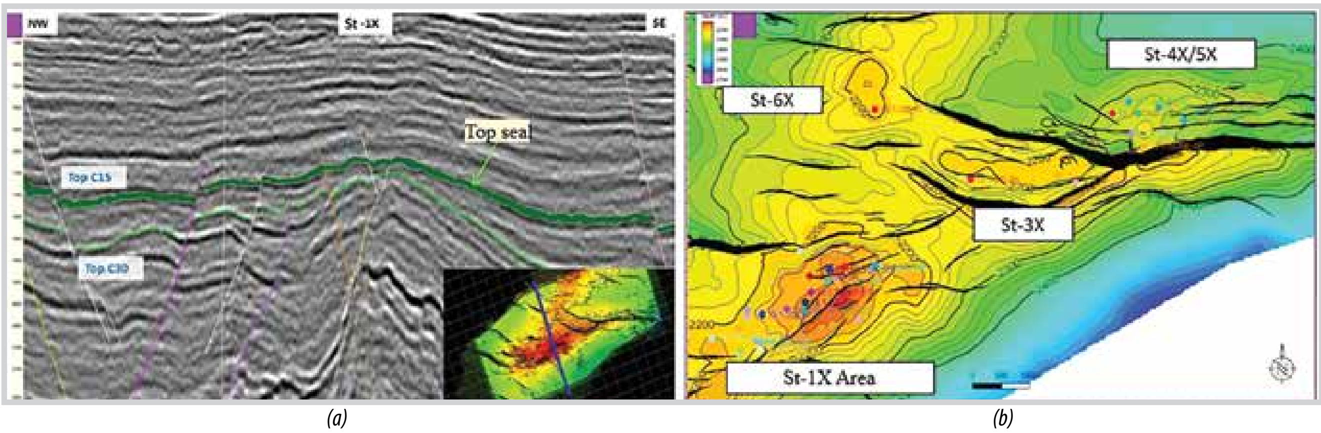

Figure 4. Seismic section though an anticline formed by post-depositional tectonics (a); Depth map of a structural trap showing four-way closure (b).

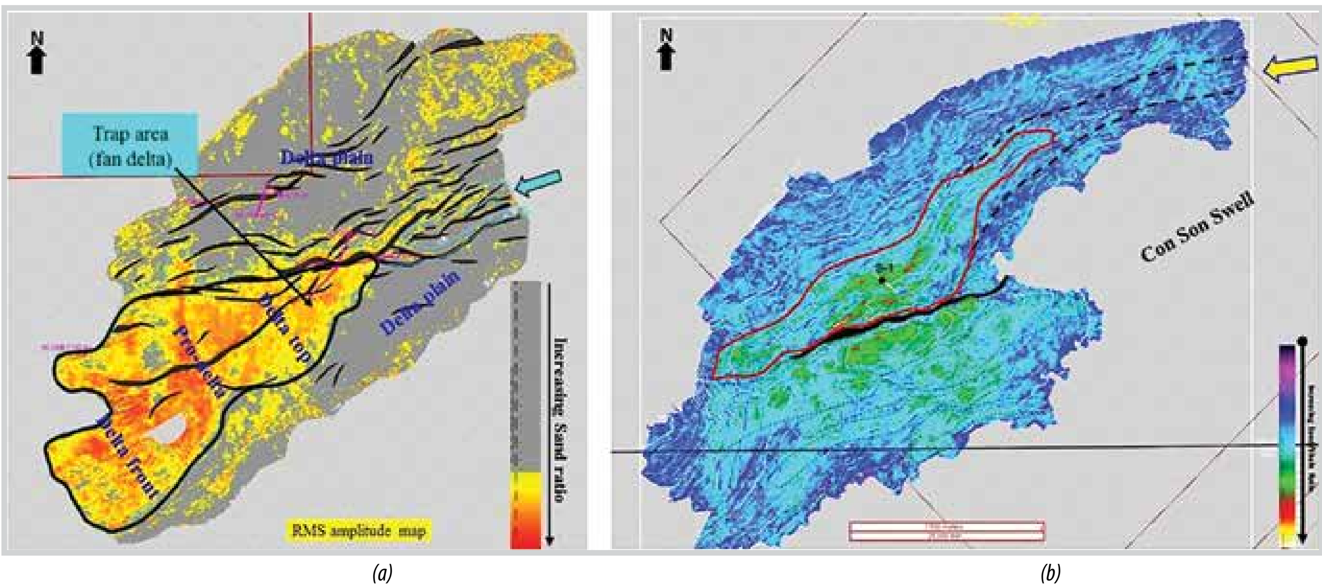

Figure 5. Interpretation of stratigraphic traps in Block 09-2/09: Fan trap deposited in deltaic environments during lowstand stage of water level (a); Channel sands deposited during high-stand stage of water level (b). The trapping mechanism is interpreted to be lithology changes from coarse-grained sediments to fine-grained sediments.

The overlying fine-grained sediments that were deposited during the highstand stage of water level act as top seal for these traps. Lateral and bottom seals for the traps are fine-grained sediments (Figure 6).

Well data analysis shows that the overlying strata of the trap consist mainly of shale/clay interbedded with minor sandstones with thickness of more than 17m deposited in flood plain environment (Figure 7) [5]. The underlying strata consist of very thick brown shale layers deposited in lacustrine environment. These Oligocene D shales are believed to be very good seal in the Cuu Long basin. These analyses show that both top and bottom seals for this stratigraphic trap are interpreted to be the best type.

Seismic attribute analysis is applied to predict the distribution of seals for this trap. It could be inferred from seismic attribute map (Figure 8) that there is high possibility of shale distribution of both overlying and underlying strata over the trap area. This reveals that the trap has good sealing capacity at both top and bottom positions.

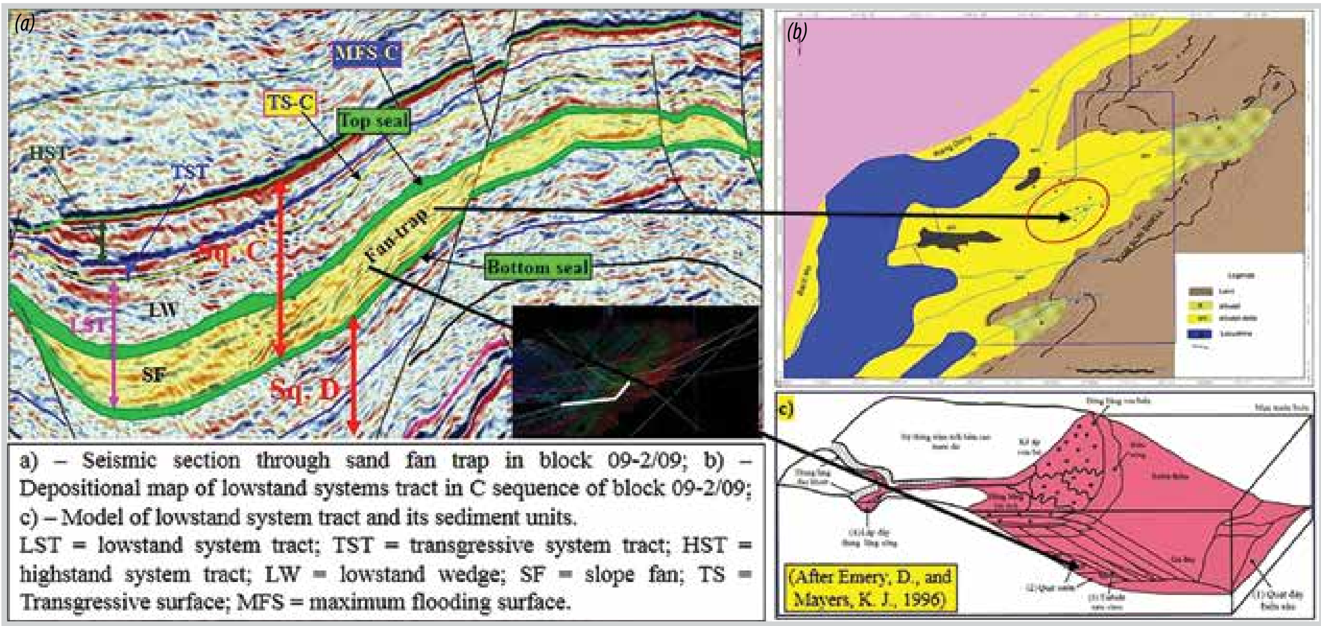

Figure 6. *Seismic section through a stratigraphic fan trap that is interpreted to have formed during lowstand stage of water level in deltaic environment (a); Depositional environment map of lowstand systems track in C sequence (b); Model of lowstand systems track and its sediment units (c).*

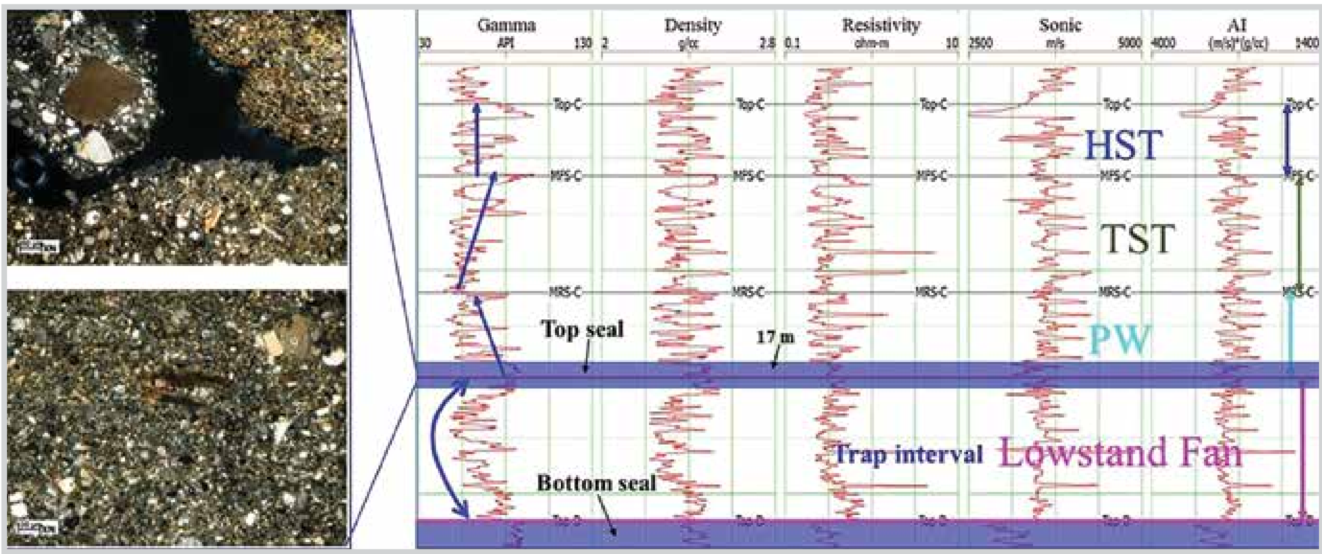

(a) (b)

Figure 7. *Well data analysis of stratigraphic fan trap in Block 09-2/09: Petrographical analysis of overlying strata showing mostly shale/claystones interbedded with minor sandstones (a) [18]; Petrophysical interpretation showing about 17m top seal and thick Oligocene D shale acting as bottom seal (b).*

Based on evidence derived from seismic data analysis (Figures 9a and b), this stratigraphic trap is predicted to be distributed along the Eastern margin of Cuu Long basin where there is a steep slope (Figure 9c). To discover this type of trap, explorationists need to predict thoroughly a number of significant factors including depositional environmental and lithological changes as well as evaluate the petroleum system with great care for the lateral and bottom seals.

4.3.2. Other stratigraphic traps

- Pinch-out traps

This kind of stratigraphic trap was identified in some places at the southeastern margin of Cuu Long basin. They were formed due to the tapering off of sand layers landward or toward the horsts. These sand layers were overlain by finer-grained sediments deposited in during the highstand stage of water level that acted as top seal for these traps. The bottom seal is determined to be the underlying shale layers or the ones in Oligocene D sequence. The lateral seal could be facies change into contemporaneously fine-grained sediments or tectonic sealing such as fault sealing or structural closing (Figure 10a). For the latter case, the trap becomes

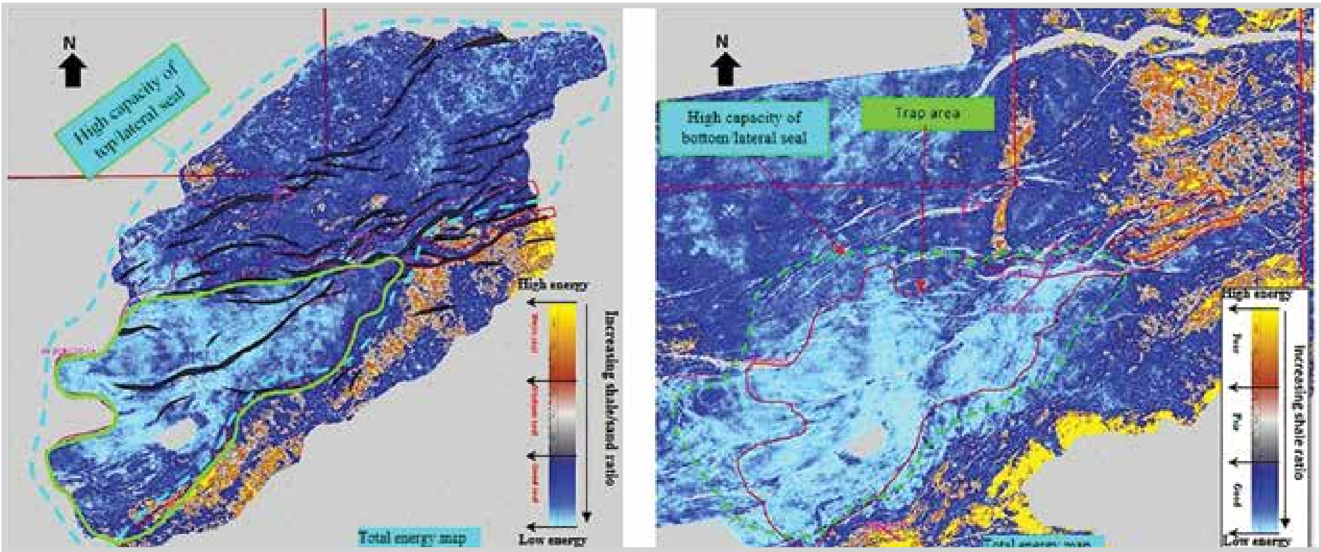

(a) (b)

Figure 8. *Sealing capacity prediction for top seal (a) and bottom/lateral seal (b) for the stratigraphic fan trap in Block 09-2/09 using seismic attribute analysis. Both seismic attribute maps show that there is high possibility of shale distributions over the trap area represented by low total energy anomalies.*

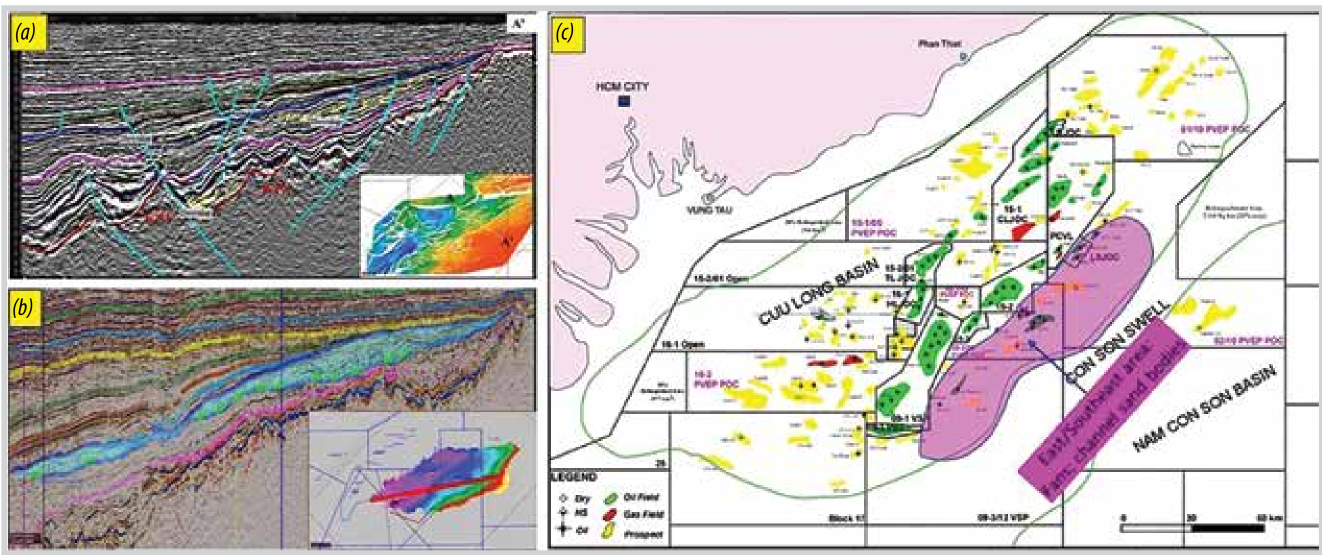

Figure 9. *Possible distribution of stratigraphic traps in southeastern margin of Cuu Long basin. NW-SE seismic section showing progradation of reflections toward the basin centre (a); E-W section showing seismic characteristics that could be related to prograding deltaic depositions (b); Predicted distribution of fan-shaped traps in Oligocene section of Cuu Long basin (c).*

the combination trap. These traps often have better reservoir heterogeneity and clearer reservoir boundaries than facies-changed stratigraphic traps. Therefore, this trap normally has good reservoir quality. This kind of stratigraphic traps is interpreted to distribute at the eastern margin of the basin as well as areas close to the basement highs (Figure 9c). It is, however, necessary to have a concrete prediction about lithology changes as well as to evaluate the petroleum system with great care on lateral and bottom seals just the same as facies-changed stratigraphic traps.

- Unconformity-related trap (truncation)

Beside the above-mentioned stratigraphic trap types, it is possible to identify the unconformity-related stratigraphic trap in the study area. By applying seismic analysis, this kind of stratigraphic trap is interpreted to be truncation trap (below unconformity). Seismic data analysis shows that strong erosion of highstand system tract (HST) of D sequence occurred in the eastern part of Block 09-2/09. These sandy sediments of HST in D sequence were then overlain by fine-grained sediments acting as top seal (Figure 10b). The bottom/lateral seal for the trap is determined to be fine-grained sediments in transgressive system tract of D sequence. Exploring these traps could be performed in the erosional areas of Oligocene strata adjacent to Con Son swell. However, further detailed studies focusing on top and lateral seals, reservoir distribution and hydrocarbon potential should be carried out in order to reduce risks in exploration activities.

5. Reservoir quality of stratigraphic/combination traps

As mentioned earlier, several kinds of stratigraphic/combination traps have been identified in the Oligocene section in the Cuu Long basin, most of which are located in the Southeastern areas of the basin. Some of them are confirmed by exploration drilling. This section shall focus on some evaluations of reservoir quality of the discovered stratigraphic/combination traps in the Southeastern margin of the Cuu Long basin.

5.1. Facies change traps

This kind of stratigraphic trap was confirmed by drilling in several places such as KTN (in C sequence) and SoN (in D sequence). In KTN wells, the reservoir interval has moderate to good oil shows while drilling [5]. Petrophysical interpretation shows that the reservoir interval is 20 - 30m thick with porosity ranging from 16 to 22 percent (Figure 11a) [5]. Results of petrographical analysis indicate that the lithology of reservoir interval consists of sandstones interbedded with shales and claystones. Sandstones are coarse - very coarse grain, poor - very poor sorted, subangular, subrounded to rounded. The rock composition is composed of mostly granitic fragments, quartz and quartzite, showing that the sediment supply is from nearby basement highs (Con Son swell). In addition, grain size is quite large (0.5 - 5mm), showing that the reservoir was formed in shallow water environment with high energy (Figure 11b) [18]. These analyses of well data reveal that the reservoir has moderate to good quality.

Seismic attribute analysis integrated with well log interpretation shows that the stratigraphic trap has fan-shaped distribution of more than 88km^2 (Figure 5a). The reservoir porosity of the trap is predicted by applying artificial neuron network theory using database of both seismic attributes and well log data. The result shows that the predicted porosities of trap's reservoir are from 12%

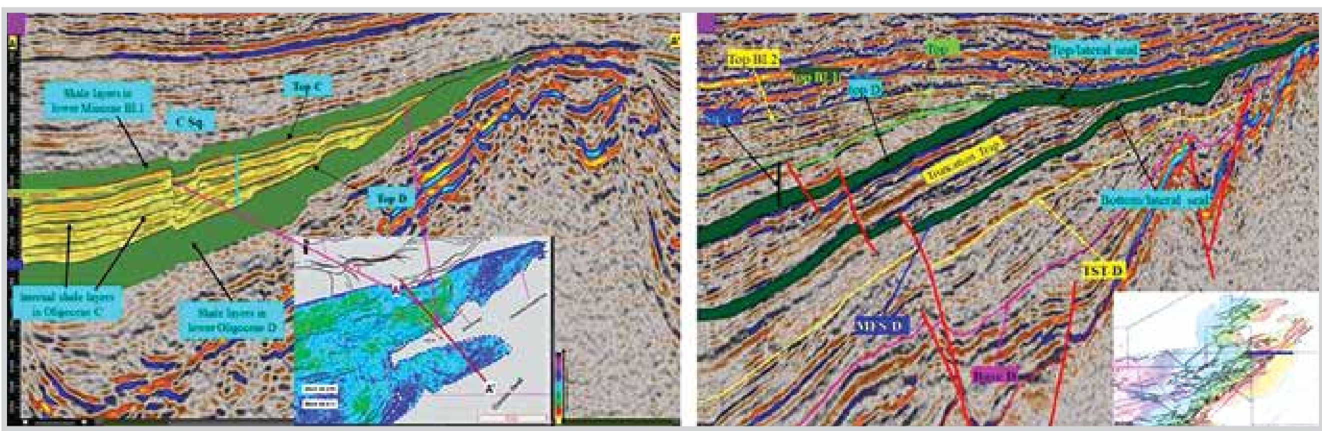

(a) (b)

Figure 10. *Interpreted seismic sections through the stratigraphic traps in the southeastern margin of Cuu Long basin: Pinch-out trap formed by the tapering off of sand layers landward or toward the horsts (a); Truncation trap formed by tectonic uplifting and truncation of underlying strata and later draping of fine-grained sediments over the trap (b).*

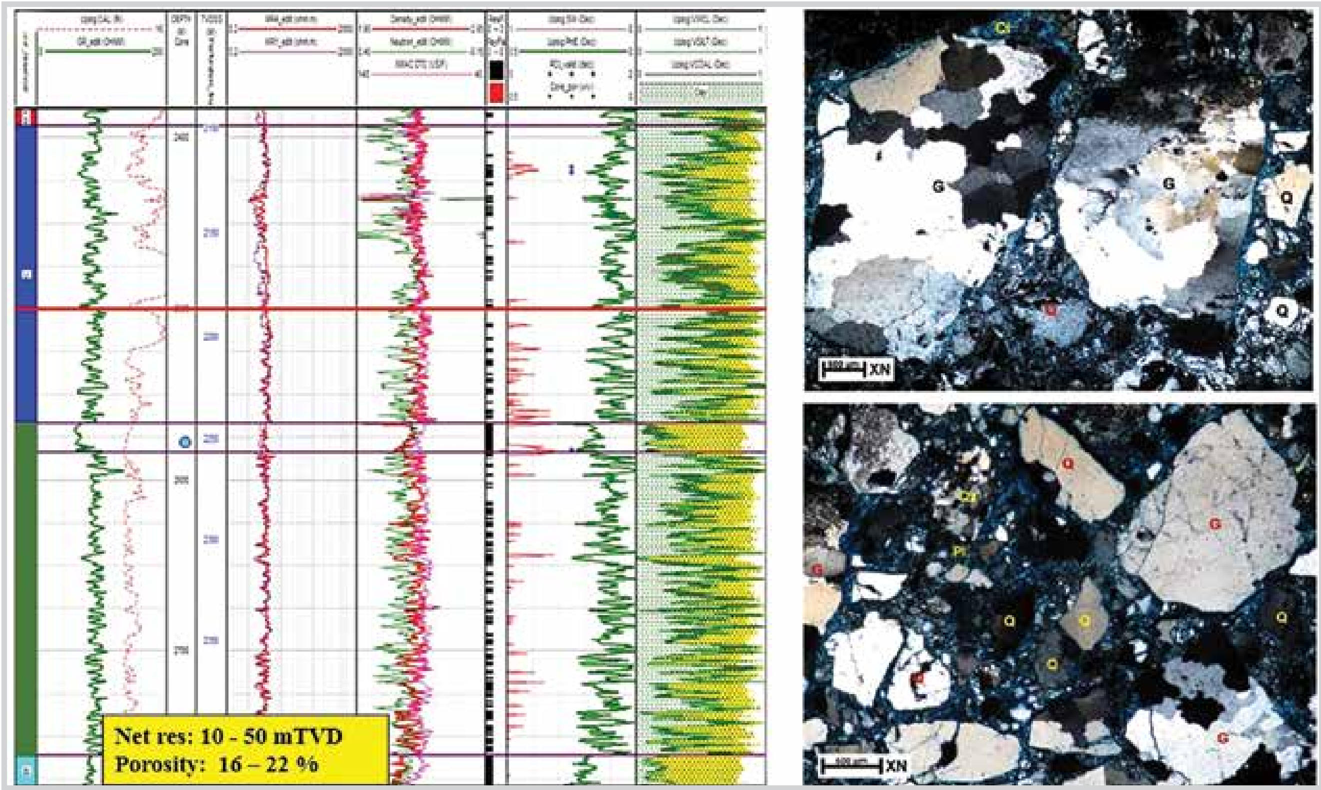

(a) (b)

Figure 11. *Reservoir characteristics of the fan trap in Block 09-2/09 on Kn-2 well data: Petrophysical interpretation (a). In Kn wells, the trap reservoir is interpreted to have about 10m to more than 50m reservoir and porosity from 16% to more than 20%; Petrographical analysis in reservoir interval showing mostly of coarse-grained and poor sorted sandstones (b) [18].*

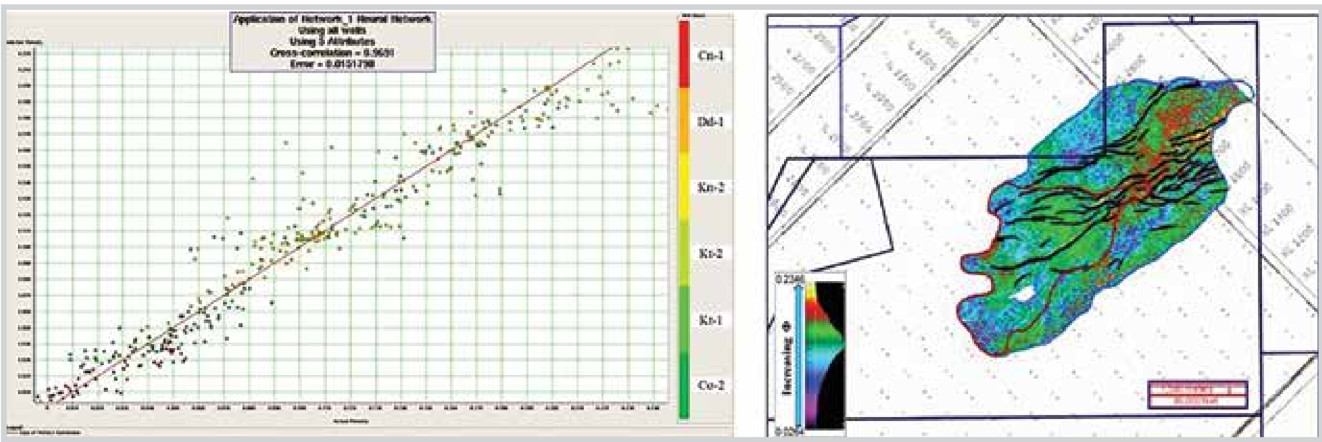

(a) (b)

Figure 12. *Prediction of reservoir porosity of stratigraphic fan trap in Block 09-2/09. Correlation between the predicted porosities and the actual porosities (a); Predicted porosity map of the trap's reservoir showing that the predicted porosities are from 12 to 19%, consistent with those derived from well log interpretation (b).*

to 19%, consistent with the calculated porosities derived from well log interpretation (Figure 12). This means that the porosity prediction for the trap's reservoir using seismic data is highly reliable.

5.2. Other stratigraphic traps

Other kinds of undrilled stratigraphic trap are also identified in the study area using seismic data analysis. They are pinch-out and truncation traps located in the Southeastern margin of the Cuu Long basin. Although these traps have not been penetrated by drilling, their reservoir distribution and other characteristics are also predicted in order to support further exploration of these traps in the future.

Primary stratigraphic traps - pinch-out: The result of porosity prediction for the reservoir of this trap type

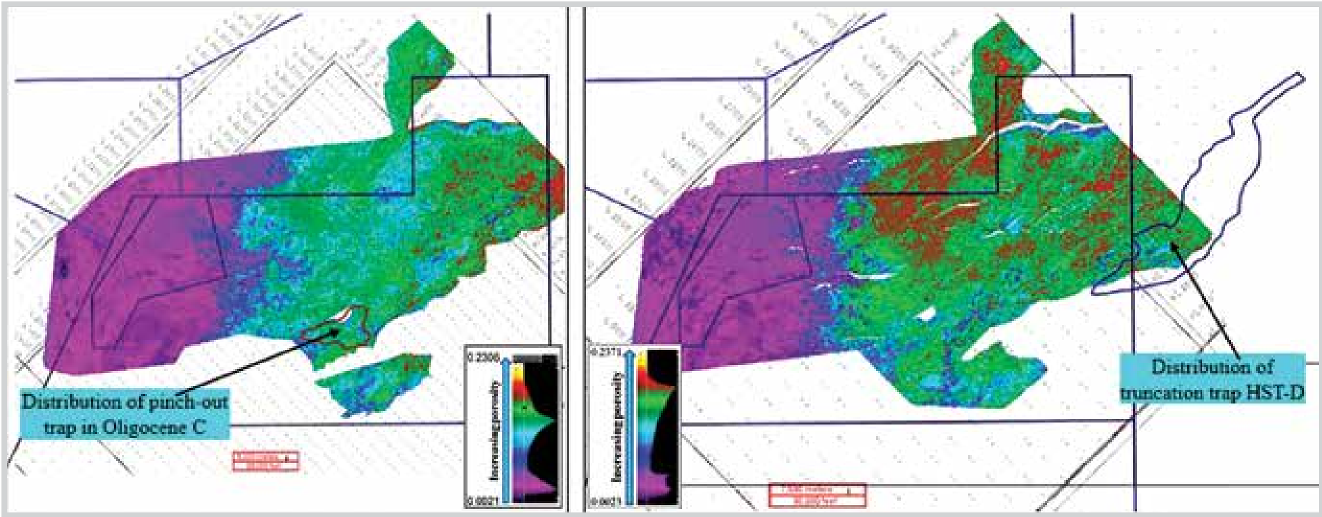

(a) (b)

Figure 13. *Reservoir porosity prediction for two stratigraphic traps in Block 09-2/09. Predicted porosity map of pinch-out trap. In the trap's area, the reservoir is predicted to have porosities from 9% to 16% (a); Predicted porosity map of truncation trap. In the trap's area, the reservoir is predicted to have porosities from 9% to 18% (b).*

shows that in the trap's area the predicted porosities are from 9% to 16%, 13% in average (Figure 13a). This reveals that the reservoir of the trap has medium quality.

Unconformity-related stratigraphic trap (truncation): As the above-mentioned forming mechanisms, these traps are predicted to distribute in the erosional areas close to Con Son swell. Stratigraphy in these areas are mostly sandy sediments deposited in the near-source areas. Therefore, the reservoir quality of these traps is predicted to be good. This is supported by porosity prediction for reservoir of the truncation trap in the study area (Figure 13b) ranging from 9% to 18%, 14% in average.

6. Conclusions

The presented study discussed the research methodology and practical issues associated with assessing different Oligocene trap types, trapping mechanisms and associated risks in exploration in the Cuu Long basin. Based on the results, several statements can be concluded as follows:

- Oil and gas in the Oligocene section were accumulated in both structural and stratigraphic traps with different forming mechanisms. The structural traps could develop widely in the Cuu Long basin. While the distribution of stratigraphic traps is evidenced in the Southeastern area of the basin. Some of which have been confirmed by drilling, thus making them important in oil and gas exploration.

- Structural traps were formed by post-depositional tectonic activities or draping over the existing topography highs with less risks in exploration except for fault seal and migration in some places. The key forming factor for stratigraphic traps is lithology changes, tapering off of sand layers or truncating of underlying strata. These stratigraphic traps have more risks in exploration than the structural ones, mostly are sealing capacity of both top and bottom ones. Although the stratigraphic traps' reservoir qualities are interpreted to be good, their distribution is one of the issues for prospecting these traps. Migration could also add more risks in exploring these traps in some places due to long distance to the source area.

- It could be said that the existence of Oligocene stratigraphic traps and their hydrocarbon bearing reservoirs confirm the importance of these traps and demand more attention to them in future exploration strategies and activities. However, further studies focusing on petroleum system, especially top and bottom seals, and the hydrocarbon potential of these stratigraphic traps need to be carried out in order to optimise the next-stage exploration strategy in the Cuu Long basin.

Acknowledgement

The authors thank the Vietnam Oil and Gas Group (Petrovietnam) and the Petrovietnam Exploration Production Corporation (PVEP) for the support and permission to publish this work. We also thank the Vietnam Petroleum Institute 40th anniversary conference's Organising Committee for giving us the opportunity to present this work. Contributions of technical assistance and comments for this manuscript by colleagues from the Exploration Department of Petrovietnam Domestic

Exploration Production Operating Company and from the Exploration Division of PVEP as well as Ha Noi University of Mining and Geology and Ho Chi Minh City University of Technology are greatly acknowledged and appreciated.

References

1. Trần Lê Đông, Phùng Đắc Hải. *Bể trầm tích Cửu Long và tài nguyên dầu khí*. Địa chất và Tài nguyên Dầu khí Việt Nam. Nhà xuất bản Khoa học và kỹ thuật. 2007; 9: trang 271 - 312.

2. Trần Mạnh Cường. *Đặc điểm hình thành và quy luật phân bố các bẫy phi cấu tạo khu vực Bắc bể Cửu Long*. Luận án Tiến sĩ, Đại học Mỏ - Địa chất. 2012.

3. EPC-VPI. *Stratigraphic combination trap study of block 01/10 & 02/10, offshore Vietnam*. Joint study with PVEP POC. 2014: 93p.

4. Đỗ Quang Đối, nnk. *Đánh giá tiềm năng dầu khí bể Cửu Long. Dự án "Đánh giá tiềm năng dầu khí trên vùng biển và thềm lục địa Việt Nam"*. Tập đoàn Dầu khí Việt Nam. 2012.

5. PVEP POC. *Updated appraisal plan for Kinh Ngu Trang Nam discovery*. Internal report to PVN and PVEP. 2014.

6. Ngô Thường San, Lê Văn Trương, Cù Minh Hoàng, Trần Văn Trị. *Kiến tạo Việt Nam trong khung cấu trúc Đông Nam Á*. Địa chất và Tài nguyên Dầu khí Việt Nam. Nhà xuất bản Khoa học và kỹ thuật. 2007; 4: trang 71 - 108.

7. R.M.Mitchum Jr., P.R.Vail, S.Thompson. *The depositional sequence as a basic unit for stratigraphic analysis: Section 2. Application of seismic reflection configuration to stratigraphic interpretation*. M26: Seismic Stratigraphy - Applications to Hydrocarbon Exploration. AAPG Special Volumes. 1977: p. 53 - 62.

8. Keith J.Myers, N.J.Milton. *Concepts and principles of sequence stratigraphy*. Sequence Stratigraphy. Blackwell Science Ltd. 1996: p. 11 - 41.

9. M.Turhan Taner. *Seismic attributes*. CSEG Recorder. 2001; 26(7): p. 48 - 55.

10. Satinder Chopra, Kurt Marfurt. *Seismic attributes - A promising aid for geologic prediction*. CSEG Recorder. 2006: p. 110 - 120.

11. Malcolm Rider. *The geological interpretation of well logs (2nd edition)*. Gulf Publishing Company. 1996: p. 64 - 260.

12. Robert Hall. *Cenozoic geological and plate tectonic evolution of SE Asia and the SW Pacific: Computer-based reconstruction, model and animations*. Journal of Asian Earth Sciences. 2002; 20(4): p. 353 - 431.

13. Tran Nhu Huy, Nguyen Quoc Thap, Hoang Ngoc Dang, Tran Manh Cuong, Tran Van Xuan, Nguyen Dinh Chuc, Nguyen Xuan Vinh and Tran Van Lam. *Factors controlling sedimentary and petroleum system of early syn-rift plays in faulted margin of continental rift basin: An example in the eastern edge Cuu Long basin, offshore Vietnam*. AAPG/SEG International Conference and Exhibition, Cancum, Mexico. 6 - 9 September, 2016.

14. Paul E.Olsen. *Tectonic, climatic, and biotic modulation of lacustrine ecosystems - Examples from Newark Supergroup of Eastern North America*. AAPG Memoir: Lacustrine Basin Exploration: Case Studies and Modern Analogs. 1990; 50: p. 209 - 224.

15. Robert J.Morley. *Palynological evidence for Tertiary plant dispersals in the SE Asian region in relation to plate tectonics and climate*. Biogeography and Geological Evolution of SE Asia. 1998: p. 211 - 234.

16. Robert J.Morley. *A review of the Cenozoic Palaeoclimate history of Southeast Asia*. Biotic Evolution and Environment Change in Southeast Asia. Cambridge University Press. 2012: p. 79 - 114.

17. Nguyễn Lâm Anh, Nguyễn Văn Khương, Nguyễn Hùng Anh. *Đặc trưng bẫy địa tầng trong trầm tích Oligoxen D tại phát hiện Cá Tầm, Lô 09-3/12, bồn trũng Cửu Long*. Tuyển tập báo cáo Hội nghị Khoa học kỷ niệm 35 năm ngày thành lập liên doanh Việt - Nga "Vietsovpetro" và 30 năm khai thác tấn dầu đầu tiên. Tập I. 2016: trang 102 - 120.

18. VPI. *Reports of petrographic and biostratigraphic analysis of wells in Kn*. Reports conducted for PVEP POC. 2014.

PETROVIETNAM JOURNAL
Volume 6/2019, p. 41 - 47
ISSN-0866-854X

Characterisation of acid treatment for damaged zone in fractured granitic basement of Bach Ho field

Nguyen Quoc Dung, Pham Trung Son, Nguyen Van Trung, Nguyen Van Nga
Vietsovpetro Joint Venture
Email: dungnq.rd@vietsov.com.vn

Summary

Bach Ho is the largest reservoir in the continental shelf of Vietnam. This field consists of numerous oil pay zones, from Lower Miocene, Upper Oligocene, Lower Oligocene to Cenozoic fractured basement, which is known for a unique oil zone with nearly 2,000m in thickness. This oil zone features a large number of naturally flowing wells with production rate of approximately 1,000 tons per day, contributing to over 90% of total production.

The oil pay zone in the fractured granitic basement is considered unconventional with extremely high degree of heterogeneity, anisotropy, and permeability. This requires more challenging production methods than those applied for conventional pay zones around the world. To achieve current optimal treatment methods, Vietsovpetro has been researching, selecting, and applying various acid treatment methods for damaged zones in this complicated basement. Nowadays, these treatment methods are successfully performed in most reservoirs in the continental shelf of Vietnam.

The success of research and application of acid treatment for pay zones in Bach Ho fractured granitic basement has made significant scientific and technological contribution not only to Vietnam but also to the South East region and the world. This paper will present the acid treatment methods applied for Bach Ho fractured basement reservoir and their techniques to optimise the production.

Key words: Near bottomhole, damaged, acid treatment, high temperature reservoir, mud acid, acid salt, acid-in-oil emulsion, non-acidic, acid-in-oil-gas emulsion, fractured basement, Bach Ho field.

1. Introduction

The basement reservoir at Bach Ho field is a reservoir granite volume of cavities and pores, with multiple cracks and micro-cracks acting as oil-filled channels. The cracks and micro-cracks are 0.3 - 3mm in size; the porosity ranges from 3 to 5%; the permeability greatly varies from 0.004 to 464D with an average of 0.135D. The reservoir temperature is relatively high, ranging from 130 to 155°C. The reservoir pressure measured at 3,650m ranges from 200 to 320atm. Results from minerology tests indicate that the basement rocks of Bach Ho field are composed of mostly granite, granodiorite, quartz - monzodiorite, diorite, and quartz - diorite.

Granite rocks at Bach Ho field are highly fractured and porous (mostly deal to cracks and micro-cracks). The dominated secondary minerals are zeolite and calcite.

Date of receipt: 16/4/2018. Date of review and editing: 16/4 - 1/6/2018.
Date of approval: 3/6/2019.

Granodiorite rocks features breccia form with debris of various shapes, colours, and sizes; this variety is deal to carbonitisation and zeolitisation processes. Cracks inside rocks also occur in various shapes; they are mostly filled with zeolite, carbonate, or chlorite. Their width can range from several millimetres to several centimetres.

In general, the basement rocks at Bach Ho field include:

- Neutral rocks (58 - 64% SiO_2) include diorite quartz biotite and diorite quartz amphibole - biotite presenting at the North East, North West, North and Centre Blocks;

- Weakly acidic rocks (64 - 68% SiO_2) at Jurassic Age include adamellite, granodiorite, granodiorite biotite, tonalite, monzonite, quartz monzonite and biotite - amphibole in the drilling wells located in the North West and North Blocks.

- Acidic rocks (68 - 74% SiO_2) before Late Cretaceous Age are mainly granite biotite in the drilling wells located in all of the blocks.

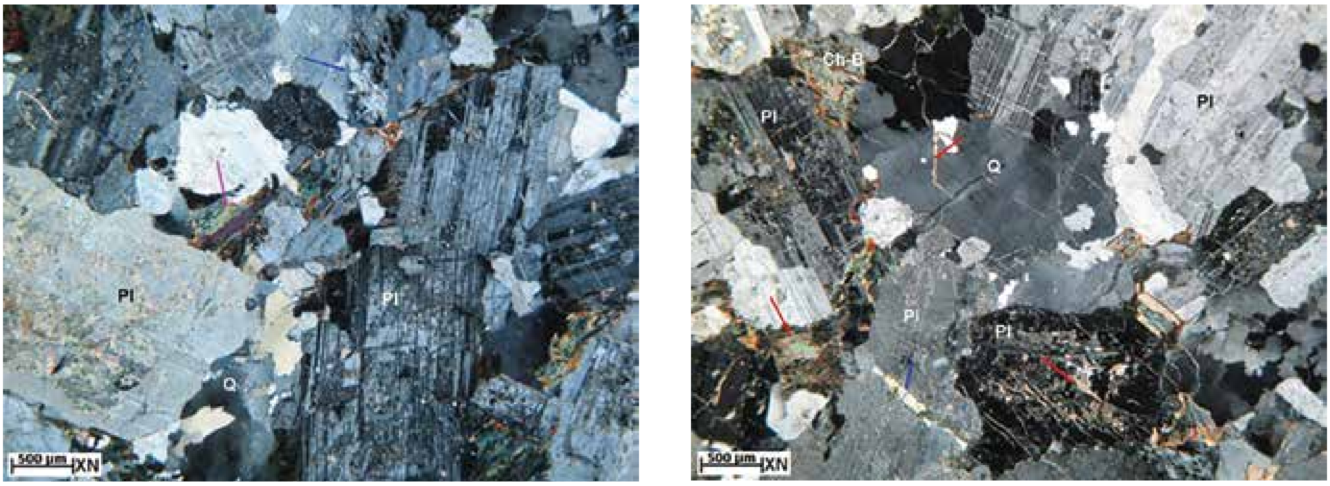

***Figure 1.** Minerology of gradiorite from XRD Red arrows: calcite, blue arrows: zeolite, pink arrow: chlorite.*

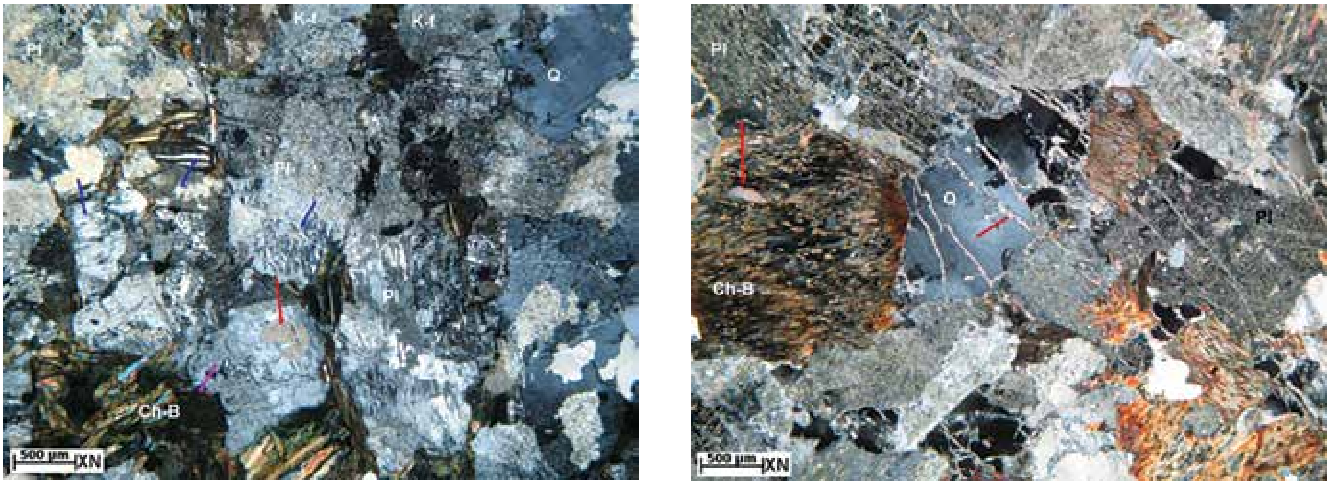

***Figure 2.** Minerology of gradiorite from XRD Red arrows: calcite, blue arrows: zeolite, pink arrow: chlorite.*

Lithologically, the basement rocks at Bach Ho field compose of granodiorite and granodiorite biotite cataclasis. They are light grey in colour, medium in size, poorly sorted, medium to highly fractured, and highly compacted. The minerals presented in the rocks include: plagioclase (35 - 54%), potassium feldspar (mainly microcline: 1 - 10%), and orthoclase (12 - 24%), quartz (13 - 27%), and biotite (13 - 21%).

2. Concept and causes of damage near bottomhole

2.1. Concept of damage near bottomhole

Near bottomhole zone is the reservoir area surrounding the wellbore which plays a crucial role in the pressure drop under the effects of formation damage factors (Figure 3). About 30 - 50% of pressure reduction occurs in this zone. The damaged zone is typically 0.9 - 1.5m (3 - 5ft) in radius. However, the most significant damaged zone, which is mainly responsible for the pressure drop, is no more than several inches (about 5 - 9cm) in radius. For drilling wells with casing diameter of 140mm and reservoir homogeneous permeability near the wells, the resistance force at the distance of 5cm from the wellbore is 8 times greater than that at the distance of 1m from the wellbore.

2.2. Causes of damaged zone

For a typical reservoir of sedimentary rocks, there are numerous causes of formation damage: damage resulted during drilling, production, well treatment, or workover process, etc. Based on the components of formation damage, 2 types of formation damage causes are distinguished: inorganic deposition and organic deposition. In reality, there is also the case where mixed organic and inorganic deposition occurs.

For the wells in the basement reservoir, formation damage occurs mainly during drilling and completion processes. The partial and total lost circulation problems during the drilling process can be solved by lost circulation

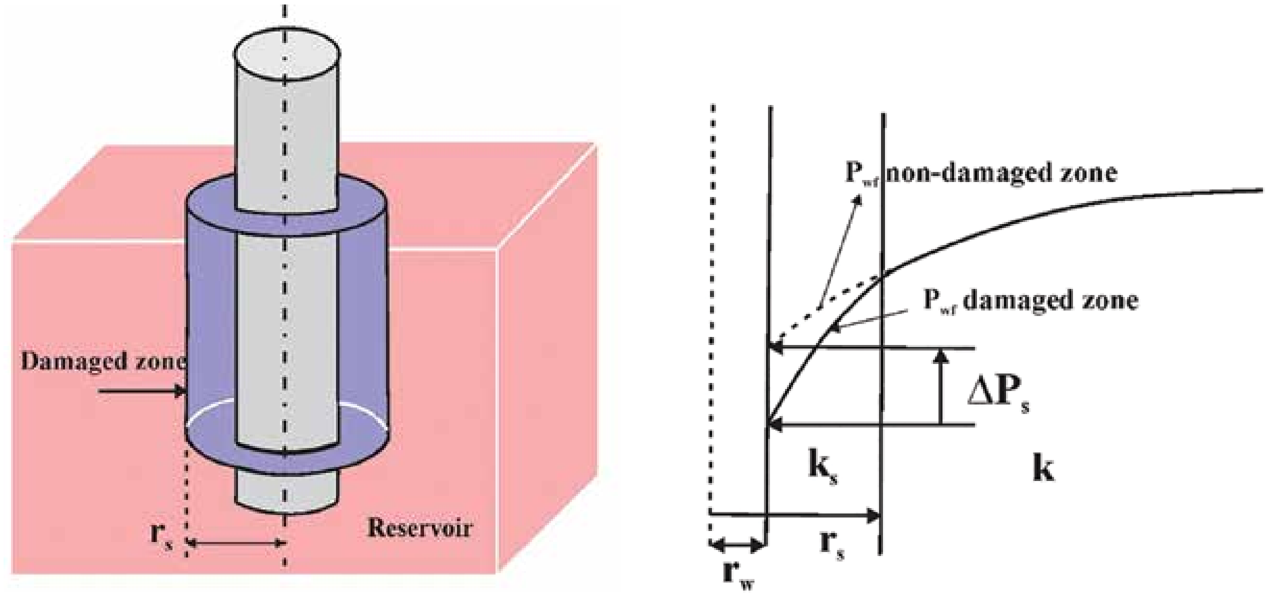

Figure 3. *Damaged zone and the pressure drop occurring in the damaged zone.*

Table 1. *Composition of different LCM solutions [1]*

No.	Composition of LCM solutions
1	Technical water + Bentonite API + Xanvis + Shell (d = 1 - 5mm) + $CaCO_3$ (F) + $CaCO_3$ (d < 0.3mm)
2	Technical water + Bentonite API + Xanvis + Shell (d = 1 - 5mm) + $CaCO_3$ (F) + $CaCO_3$ (d = 0.3 - 0.9mm)
3	Technical water + Bentonite API + Xanvis + Shell OBK (d < 1.5mm) + Shell (d = 1 - 5mm)
4	Technical water + Bentonite API + CMCLV + DUOVIS + $CaCO_3$ (F) + Glass bubble 3M (d ≤ 100µm) + Glass bubble 3M (d ≤ 200µm)
5	Technical water + Bentonite API + Xanvis + $CaCO_3$ (d < 0.9mm) + $CaCO_3$ (d < 1.25mm) + Shell (d = 1 - 5mm) + Nut plug (M) + Nut plug (F) + Kiwik seal (M) + KR22
6	Technical water + Bentonite API + Xanvis + OBK (d < 0.9mm) + OBK (d < 1.25mm) + Shell (d = 1 - 5mm) + Nut plug (M) + Nut plug (F) + Kiwik seal (M) + KR22

materials (LCM). The amount of LCM applied depends on the degree of the lost circulation. These LCM are stuffed into the channels and fractures, resulting in formation damage and thus preventing the fluid from flowing to the wellbore.

The LCM applied for the basement rocks are grains, fibres, or flakes. Researches on characterisation of fractures in the basement reservoir at Bach Ho field and practical results of LCM suggest that the optimal size of LCM grains for highly fractured formation are medium (74 - 200µm) and fine (≤ 74µm). The results also indicate that multiple sized LCM are more effectively filled into fractures than single sized LCM. Therefore, LCM with multiple sizes are used to solve lost circulation problems in the fractured basement reservoir.

To protect the reservoir, LCMs are preferably soluble in acid. Lost circulation experiments signify that the combination of different types of LCM (grain, fibre, and flake) in the solution also improves the effectiveness of the fracture filling. Hence, the LCM solution applied for the fractured basement reservoir consists of multiple types of LCM.

The applied LCMs include:

- Grain type: Scotchlite 3M Scotchlite (Scotchlite glass bubble 3M - HGS); $CaCO_3$ grains;

- Fibre type: Kiwik seal. Kiwik seal is a synthetic LCM fibre, proved to be highly effective in lost circulation solution;

- Flake type: $CaCO_3$ artificial flakes. They are highly soluble in acid but are expensive. Shells, which are abundant in Vung Tau sea, are more economical and more mechanically durable.

In addition to the mentioned types, nut plug type is widely applied around the world.

It is noticed that a large amount of secondary minerals present inside the fractures of the rocks such as calcite, zeolite, chlorite, and clays (Figures 1 and 2). These minerals reduce the permeability. As a result, the actual

Table 2. *The quality of different treatment methods for basement reservoir - Bach Ho field [2]*

Target area	Acid treatment methods	Production wells	
		Number of treated wells	Successful percentage (%)
Basement reservoir	Acid salt (HCl)	6	0
	Mud acid	90	78
	Acid salt + mud acid	6	100
	Acid-in-oil emulsion (clay based acid)	75	87
	Acid-in-oil-gas emulsion	6	83
	Acid + Chemical of DMC	38	63
	Acid-in-oil emulsion (acid based salt)	3	67
	Foam acid	3	67
	Non-acid	2	100
	Total	**229**	**72**

flow rates of the wells are significantly lower than the flow rates expected from good characteristics of the basement reservoir.

Therefore, the acid treatment job in the fractured basement rocks is considered successful when LCMs and the remaining secondary minerals within cracks and micro cracks are effectively dissolved.

3. Synthesis of acid treatment methods for damage near bottomhole applied for Bach Ho fractured granitic basement reservoir

Vietsovpetro has conducted researches, selected and applied numerous acid treatment methods for damaged zone in the fractured basement reservoir. Thus far, many treatment methods have yielded good results and have been applied for other oil and gas reservoirs owned by Vietsovpetro.

By the end of 2017, the production wells in the basement reservoir at Bach Ho field were treated 229 times, with the successful percentage of 72%.

4. Chemicals used in acid treatment for damaged zone

The main acid solutions applied for acid treatment are acid salt and clay acid solutions. The acid salt solution contains hydrochloric acid (HCl) and acetic acid (CH_3COOH); the mud acid solution contains hydrofluoric acid (HF), HCl, and CH_3COOH.

- HCl: dissolve calcite components and inorganic salt precipitation, dissolve partial clay components of secondary minerals causing formation damage. For clay acid, excess HCl prevents phenomena such as gel accumulation from iron compounds; precipitation of CaF_2 and MgF_2; and gel accumulation from $Si(OH)_2$. Technical HCl has the concentration of 28 - 32%.

- HF in the clay acid solution is highly hazardous and highly noxious (group III). Technical HF concentration is maintained below 30%. HF plays the main role of dissolving clay minerals, quartz minerals, and aluminosilicate in reservoir rocks or damaged surface and subsurface equipment.

- CH_3COOH: balance the pH of acid solution (≤ 2) to prevent the gel accumulation of iron hydroxide, aluminium hydroxide, and other metal ions. At the concentration > 4%, CH_3COOH helps reduce reaction rate, thus increase the affected depth.

In addition to those main chemicals, corrosion control chemicals, surfactants, and stabilisers are included in the acid salt and clay acid solutions. Corrosion control chemicals help reduce the corrosion effects of these acid solutions on wellbore equipment. Surfactants help lower the surface tension on the boundaries of fluid phases, distribute and extract solid from the reaction volume, prevent the precipitation of gudron (tar), reduce the permeability prevention effects, and prevent the precipitation of emulsion. Stabilisers help stabilise clay minerals, prevent the precipitation of iron and aluminium hydroxide, etc., and prevent the creation of hydroxide gel.

5. Acid treatment technology applied for fractured basement reservoir - Bach Ho field

As mentioned in Part 1, due to the unique characteristics of the geology of the reservoir rocks, the acid treatment technology applied for the basement reservoir faces multiple challenges:

- Great thickness of the pay zone (over 2,000m) which creates difficulties in controlling the acid flow into the reservoir.

- High reservoir temperature (130 - 155°C) which results in high reaction rate, thus shortens the affected depth.

- In addition, high reservoir temperature destabilises clay minerals and results in gel accumulation, which corrodes the wellbore equipment.

Therefore, corrosion control chemicals are added to minimise the corrosion rate under high reservoir temperature conditions.

The successful acid treatment methods applied for the basement reservoir are required to solve those problems (Table 2):

- Treatment methods using clay acid + acid salt;
- Treatment methods using non-acid solution to create acid solution at bottomhole;
- Acid-in-oil emulsion (clay-based acid);
- Acid-in-oil-gas emulsion;
- Treatment methods using clay acid.

5.1. Treatment method using combination of acid salt and mud acid solutions

Acid salt solutions are mainly applied for reservoir rocks with high percentage of $CaCO_3$ and $CaMg(CO_3)_2$. For granite reservoir, a combination of HF, HCl solutions and additives is used. HF mainly reacts with SiO_2 (silicic oxide) components and $H_4Al_2Si_2O_9$ (kaolinite).

Mud acid solution is used for reservoir rock with calcite percentage < 0.5%. If this acid reacts with carbonate or dolomite, the products are undissolved salts:

$$2HF + Ca^{2+} = CaF_2 + 2H^+$$

For reservoir rocks with clay, it is important to control the concentration of each type of acid in the acid solution that can affect clay heave, resulting in permeability reduction. The rate of reaction between soluble clay and HF is significantly slow. Therefore, the amount of HF needs to be sufficient for the reaction; in addition, CH_3COOH is required to increase the affected time of the solution to the rocks.

To eliminate the salt produced: CaF_2 and MgF_2. The acid salt treatment is conducted prior to the main acid treatment as reservoir rocks contain a great percentage of Ca and Mg.

Figure 4 illustrates a typical schema for treatment method using combination of acid salt and mud acid.

5.2. Acid treatment methods using non-acid solution to create acid solution at the bottomhole

The basis of this method is to treat the damaged zone by acid solution created at the bottomhole by pumping non-acidic components into the wellbore. This technique is called non-acid treatment method [3].

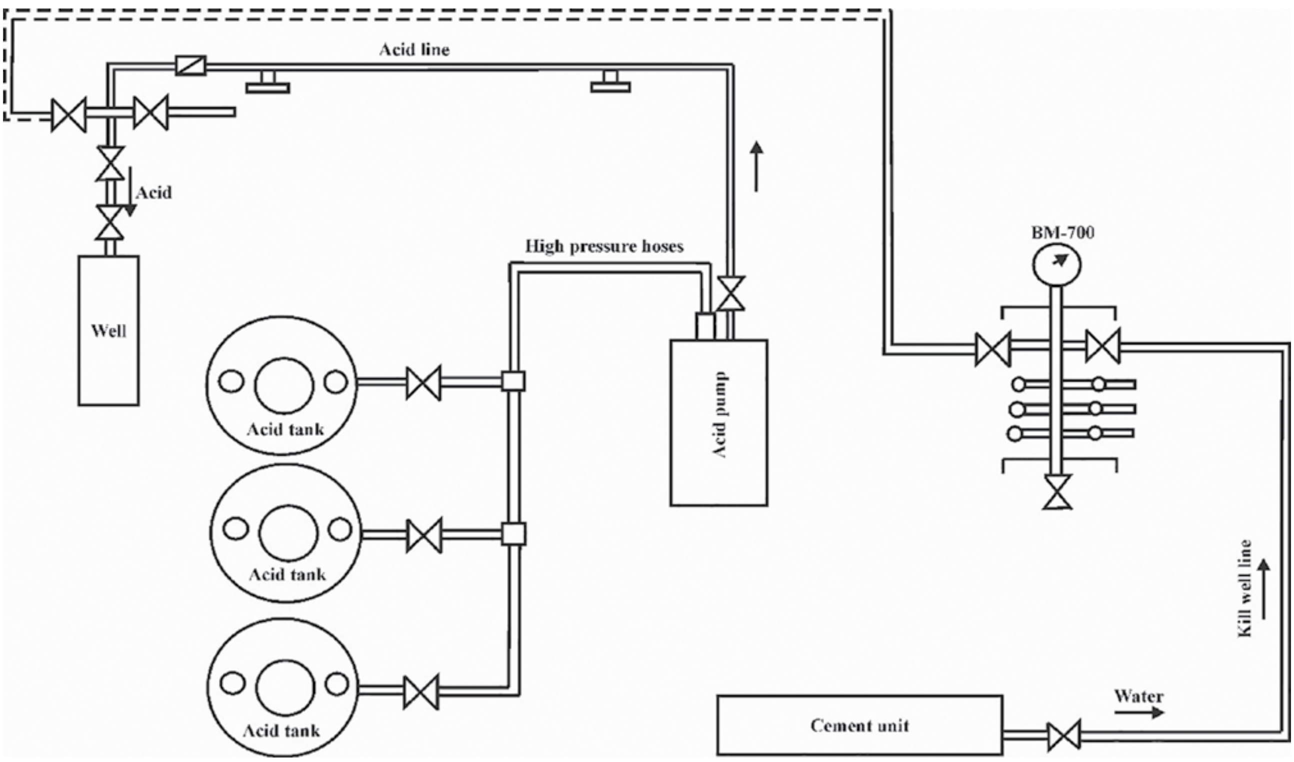

Figure 4. *Schema of acid treatment for damaged zone - Clay acid + acid salt method [2].*

Acid is created in the formation when HBF_4 and water are pumped to the damaged zone. The acid product of the reactions is HF:

$$HBF_4 + H_2O = HBF_3(OH) + HF \quad (1)$$

$$HBF_3(OH) + H_2O = HBF_2(OH)_2 + HF \quad (2)$$

In a particular time, only a limited amount of HF is created in the solution. The solubility of HBF_4 is relatively high (8% HBF_4 is equivalent to 2% HF). Under reservoir conditions, this acid duo acts similarly to the HF/HCl duo (with the concentration of HF below 1%).

Compared to a typical HF/HCl duo, the acid duo produced from HBF_4 and H_2O reaction has many advantages: lower rate of corrosion of borehole equipment and casing, good acid concentration maintenance, and prevention of precipitation.

Figure 5 illustrates a typical schema for the non-acid treatment method.

5.3. Acid treatment methods using acid-in-oil emulsion (mud-based acid)

Acid-in-oil emulsion includes two phases: acid and hydrocarbon (which can be either crude oil or diesel). Acid is the dispersed phase; crude oil is the dispersion medium.

When the area of surface boundaries between acid in the acid-in-oil emulsion and the reservoir rocks decreases, the solution will invade deeper into the formation compared to normal acid solution, the rate of metal corrosion by acid solution will also decrease.

Depending on the fluid ratio, there are different types of acid-in-oil emulsions. Typically, there are 60 - 70% acid and 40 - 30% crude oil. The acid solution is normally clay acid.

Depending on the geologic - technical condition of the wells, suitable schema for the treatment is selected (Figure 6).

5.4. Acid treatment methods using acid-in-oil-gas emulsion

Bach Ho field is a high temperature reservoir. When the area of surface boundaries between acid in the acid-in-oil emulsion and the reservoir rocks decreases, the solution will invade deeper into the formation as compared to normal acid solution, and the rate of metal corrosion by acid solution will also decrease. The gas phase in acid-in-oil-gas emulsion supports the swab process after the treatment.

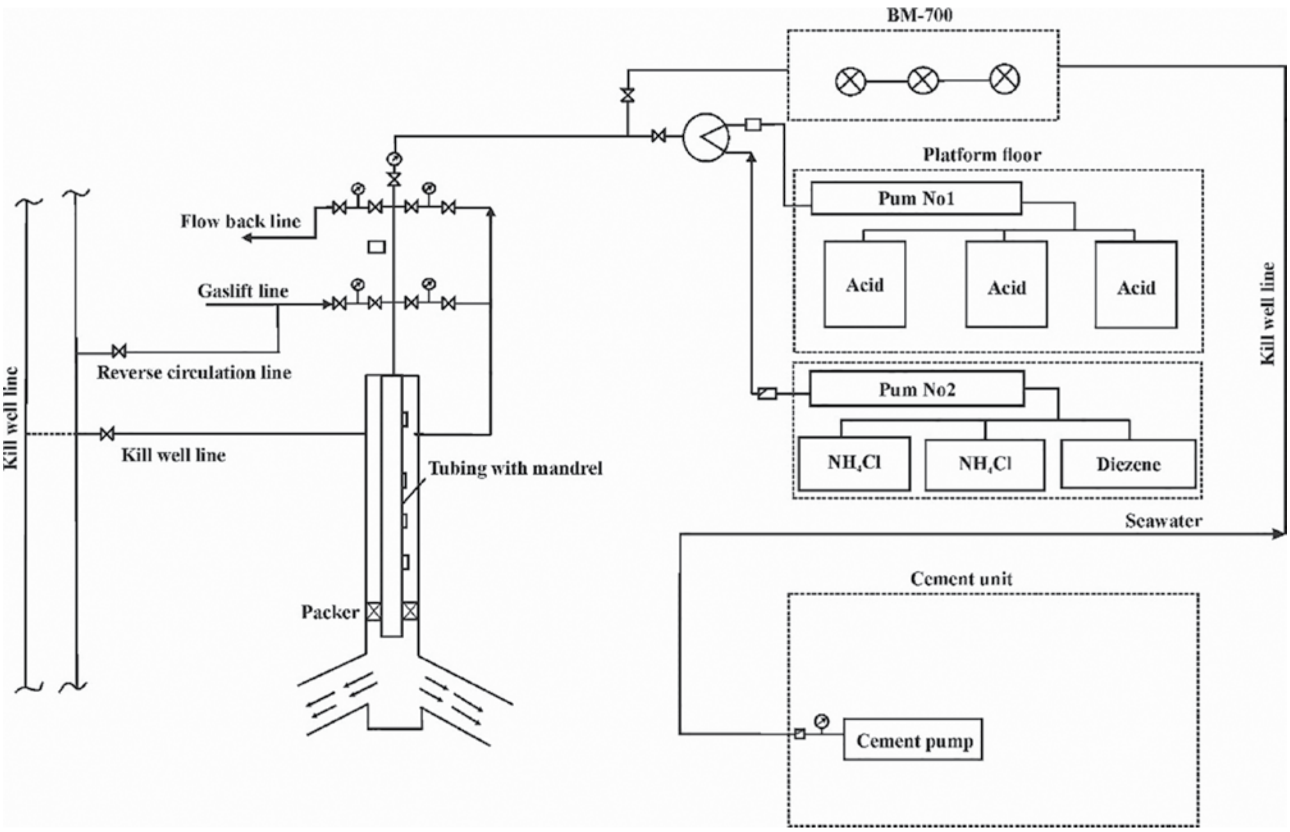

Figure 5. *Schema of acid treatment for damaged zone - non-acid solution method [3]*

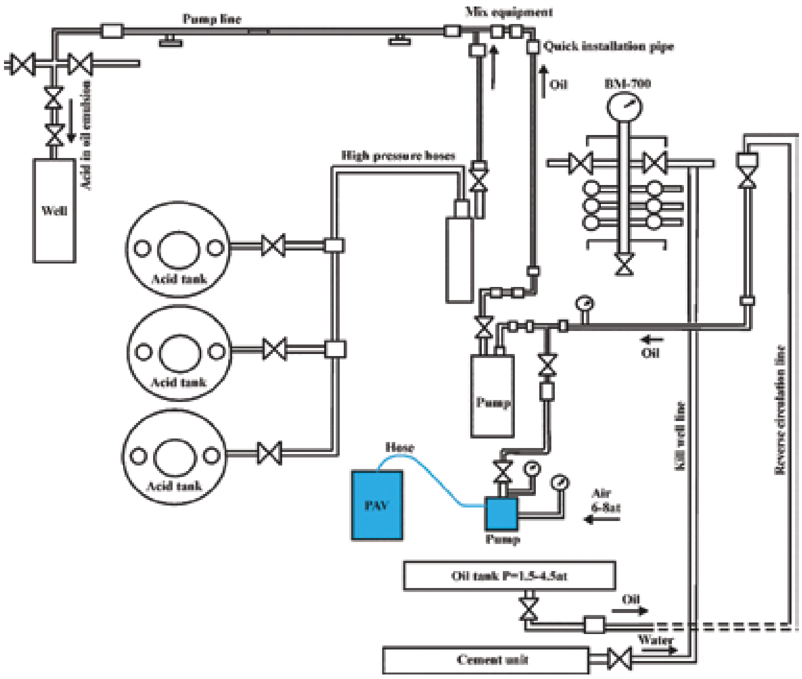

Figure 6. *Schema of acid treatment for damaged zone - acid-in-oil emulsion methods on fixed platform [2].*

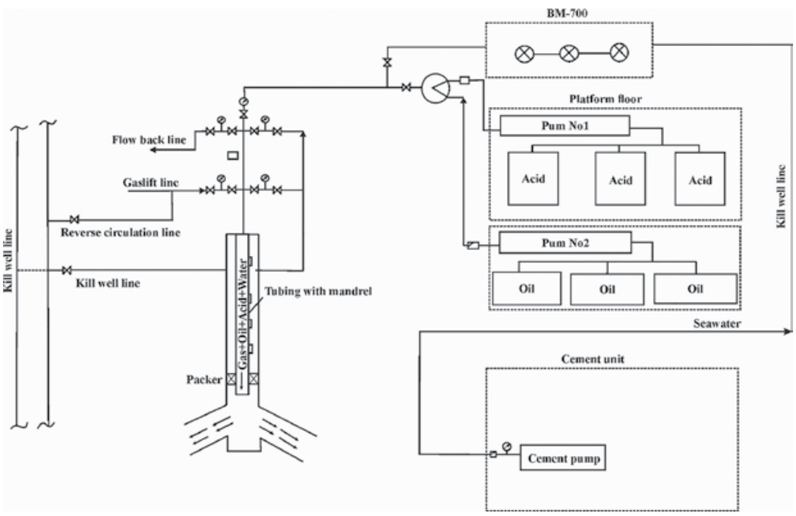

Figure 7. *Schema of acid treatment for damaged zone - acid-in-oil-gas emulsion method [4].*

The acid-in-oil-gas emulsion treatment method was proposed by Vietsovpetro experts to target the production wells in the basement reservoir. This method is performed by simultaneously or continuously pumping each component of the emulsion (acid, oil, diesel or separated oil, and gas) into the wellbore (Figure 7).

The ratio of the components and their order of pumping are selected to achieve the optimal gas solubility in the emulsion solution and maximise the travel distance of the emulsion solution into the formation. For the wells under low reservoir pressure, after the acid treatment, the damaged zone is strongly swabbed; the impurities and reaction products will follow the flow to the wellbore.

6. Conclusion

On the basis of researches and practical application of formation damage treatment, a number of treatment methods has been selected and recommended: treatment methods using combination of acid salt and clay acid solutions, acid-in-oil emulsion (clay-based acid), acid-in-oil-gas emulsion, and non-acid solution. These treatment methods are applied to the basement of other reservoirs with similar characteristics located in the continental shelf of the South of Vietnam and yield great economic results.

The success of selecting optimal acid treatment methods for the fractured basement reservoir with high temperature as well as unique geological and mineralogical features contribute greatly to the big picture of the oil and gas production for the reservoirs in their late time in Vietnam and around the world.

References

1. Hoang Hong Linh, Tran Xuan Dao. *Research the relationship between lost circulation and fractured characteristics of Bach Ho basement for selecting the suitable LCM pill recipes to fight against lost circulation and protect the reservoir*. Science and Technics Publishing House. 2018.

2. Từ Thành Nghĩa, Nguyễn Thúc Kháng, Lê Việt Hải, Dương Danh Lam, Nguyễn Quốc Dũng, Nguyễn Văn Trung, Phan Đức Tuấn. *Công nghệ xử lý vùng cận đáy giếng ở thềm lục địa Nam Việt Nam*. Nhà xuất bản Đại học Quốc gia Việt Nam. 2016.

3. Dương Danh Lam, Lê Việt Hải, Nguyễn Quốc Dũng, nnk. *Phương pháp xử lý axit bằng thành phần non-acid để tạo axit ở đáy giếng*. Giải pháp sáng kiến sáng chế. 2012.

4. Dương Danh Lam, Nguyễn Thúc Kháng, nnk. *Phương pháp xử lý vùng cận đáy giếng bằng nhũ tương khí-dầu-axit trong các giếng mỏ Bạch Hổ có áp suất cao*. Vietsovpetro. 13 July, 1997.

PETROVIETNAM JOURNAL
Volume 6/2019, p. 48 - 57
ISSN-0866-854X

An applied machine learning approach to production forecast for basement formation - Bach Ho field

Tran Dang Tu[1], Nguyen The Duc[1], Le Quang Duyen[2], Pham Truong Giang[1], Le Vu Quan[1], Le Quoc Trung[1], Tran Xuan Quy[1], Pham Chi Duc[1]
[1]Vietnam Petroleum Institute
[2]Ha Noi University of Mining and Geology
Email: tutd@vpi.pvn.vn

Summary

Oil production forecast is a major challenge in the oil and gas industry. Simulation model and prediction results play an important role in field operation and management. Currently, production forecast problems are resolved mainly by using pure traditional prediction methods. Generally, production forecast by dynamic simulations does not provide reliable results in case where a lot of uncertain parameters remain when the dynamic model is constructed.

In fact, in Vietnam, the dynamic models of fractured reservoirs give unreliable results and differ with actual performance. It is a challenge to build and design reasonable production plans for fractured granite reservoirs in Vietnam. In order to replace the disadvantages of simulation model by different methods, a growing trend of research in the world is constructing predictive tools by using machine learning algorithms.

The paper introduces the applicability of machine learning through the artificial neural network to predict oil production for basement formation - Bach Ho field. The research results show that Artificial Neural Network (ANN) model has improved the ability to predict production with high accuracy.

Key words: Artificial Neural Network, machine learning, oil production, reservoir management, Bach Ho field.

1. Introduction

Machine learning (ML) is the scientific study of algorithms and statistical models that computer systems use to effectively perform a specific task without using explicit instructions, relying on models and inference instead. It is seen as a subset of artificial intelligence. Machine learning algorithms build a mathematical model of sample data, known as "training data", in order to make predictions or decisions without being explicitly programmed to perform the task [2, 3]. Machine learning is closely related to computational statistics, which focuses on making predictions using computers. The study of mathematical optimisation delivers methods, theory and application domains to the field of machine learning. Data mining is a field of study within machine learning and focuses on exploratory data analysis through unsupervised learning. In its application across business problems, machine learning is also referred to as predictive analytics [4].

Date of receipt: 20/2/2019. Date of review and editing: 20/2 - 1/4/2019.
Date of approval: 3/6/2019.

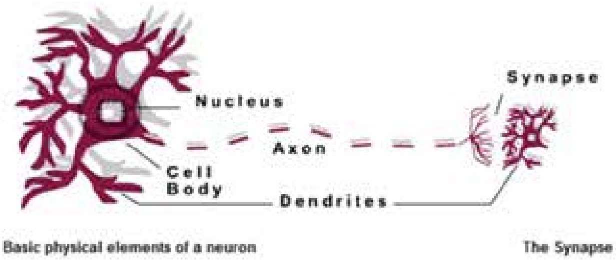

Figure 1. *Basic physical elements of a biological neuron [1].*

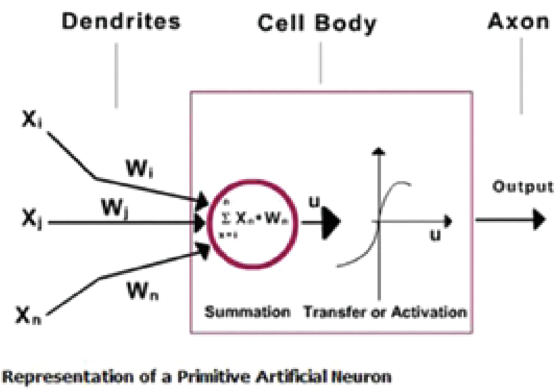

Figure 2. *Representation of neuron in ANN [1].*

One of the most popular machine learning methods - ANN is employed for this purpose. In computer science, ANN is formed of computer architecture, inspired by biological neural networks (the central nervous systems of animals, particularly, the brain) and used to estimate or approximate functions that can depend on a large number of inputs and are generally unknown. ANN is generally presented as systems of interconnected "neurons" which can compute values from inputs and are capable of machine learning or pattern recognition, thanks to their adaptive nature. Figures 1 and 2 show the basic biological neuron structure and representation of artificial neuron.

2. Neural networks

The most popular ANN model is the multi-layer perceptron (MLP) architecture trained using the feedforward backpropagation algorithm. The MLP architecture is composed of at least three layers vector and the last layer consists of the output vector. The intermediate layers, called hidden layers, represent neural pathways and modify the input data through several weighted connections.

There are three major phases to network training with backpropagation. During the initial phase, the input vector is presented to a network, which is activated via the forward pass. This generates a difference (error) between the input of the network (error backward pass). During the output layer back, through the hidden layers, to the input layer. This process is repeated until the connection weights produce an output which is with a predetermined tolerance of the desired output [2].

The selection of an optimum architecture of a model is a difficult task requiring a procedure of trial and error [5]. Thus, several networks with various numbers of hidden units, training algorithms, and activation functions are attempted and the generalisation error is estimated for each. The network with the minimum estimated generalisation error is chosen.

3. Production data of basement formation of Bach Ho field

The basement formation of Bach Ho field has produced commercially since 1988. Based on the well test results of wells 2, 401, 401, and 417, which were the first exploration, appraisal, and production wells, the initial reservoir pressure was 417atm at 3,650m TVDSS. In the first production stage, reservoir drive mechanisms were rock or compaction drive and solution gas without water drive and water injection supply. After several years of production the reservoir pressure decreased significantly to 280atm. Pressure maintenance by water injection was initiated in 1993 when a few production wells were converted to injection wells and connected with the water injection system. As of May

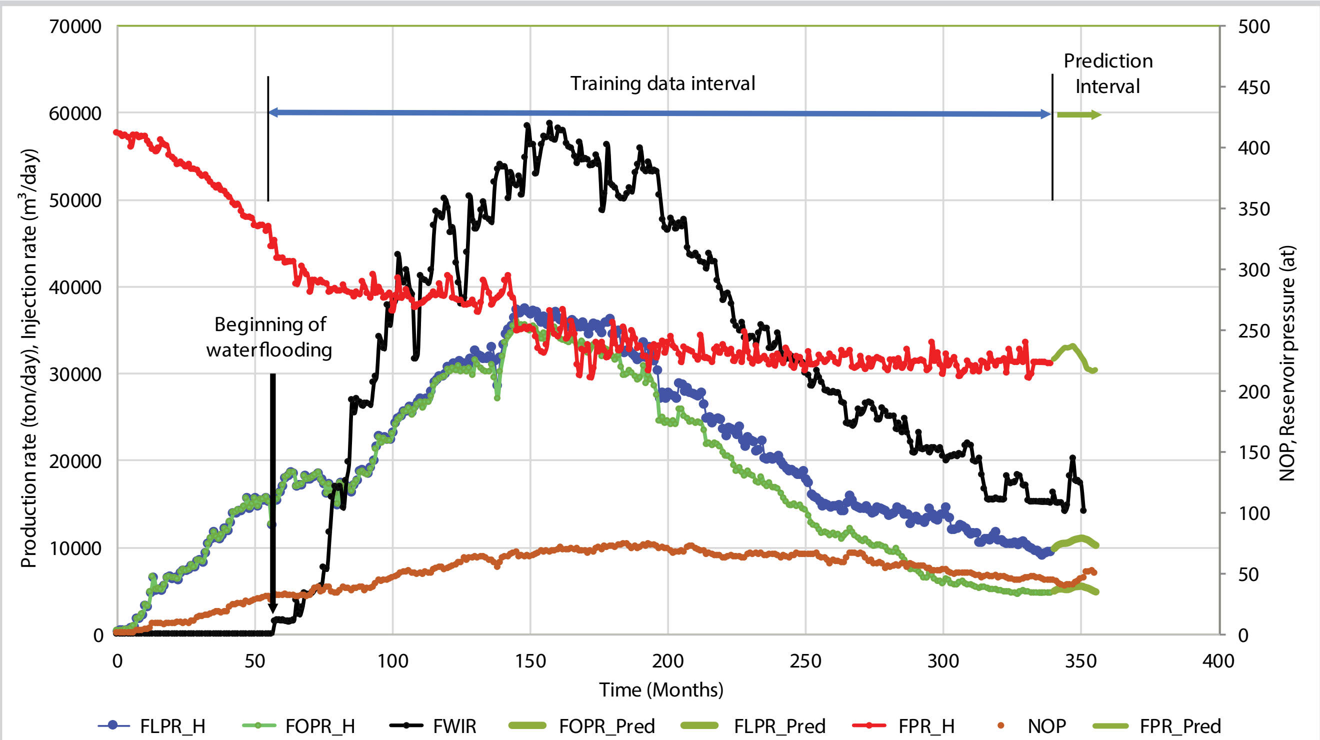

Figure 3. *Reservoir oil production from September 1988 to May 2018.*

2018, the reservoir had achieved a cumulative oil production of 180 million tons, accounting for 86% of Vietsovpetro's total oil production, with an average oil rate of 6,000 tons per day, and an average water cut of 60% [6].

4. Network architecture

Neuron architecture is composed of five inputs and three outputs. The inputs are the average field oil production rate (FOPR) at time t, the average field liquid production rate (FLPR) at time t, the average reservoir pressure (FPR) at time t, the average water injection rate (FWIR) at time t+1 and the number of production wells (NP) at time t+1. The outputs are the average field oil production rate (FOPR) at time t+1, the average field liquid production rate (FLPR) at time t+1, the average reservoir pressure (FPR) at time t+1. The selection of an optimum neuron network architecture can be achieved using a trial and error approach. Figure 3 shows the oil production rate from September 1988 to May 2018.

4.1. Short-term production prediction

- Data pre-processing

Normally, an accurate network model can be achieved without adequate data. Therefore, before training model, production data have to guarantee high reliability to avoid peculiar answers from trained network model. However, depending on the problem, there may be special features from the data that are able to test its quality. One way to check the quality is to view the graphical representations of the data in question, in the hope of selecting a reasonable subset while eliminating problematic portions. As presented in Figure 3, the oil field production rate is time-dependent and was split into two sets. The first set (from May 1993 to December 2016) used 284 data months to build the network model. The second set (from January 2017 to May 2018) used 15 data months to predict the average oil production rate, liquid production rate, and reservoir pressure.

To avoid overfitting or underfitting results and improve the generalisation of the network model, the first set was subdivided randomly into three parts: training, validation, and testing. The training set used 190 data months (67%) to compute the gradient and update the network weights and biases. The validation set used 47 data months (16.5%) to evaluate the quality of the training process. Training can be stopped when the performance of the model on the validation dataset provides a minimum error. The testing set used 47 data months (16.5%) to fine-tune the network model. It is not applied for training and validation process, only used to identify optimum network architecture, to select a suitable network model and assess their performance.

- ANN network architecture

The best results were obtained from ANN model consisting of 2 hidden layers and 50 neurons for each one. The node in the hidden and output layers is activated through Sigmoid function and trained by the Backpropagation Neural Network algorithm (BPNN).

4.2. Long-term production prediction

- Data pre-processing

The first set used 236 data months (from May 1993 to December 2012) to build a network model. The second set used 60 data months (from January 2013 to December 2017) to predict oil production rate, liquid production rate, and reservoir pressure. The training set used 160 data months (67%) to calculate gradient and update the network weights and biases. The validation set used 38 data months (16.5%) to evaluate the quality of the training process. Training can be stopped when the performance of the model on the validation dataset provides a minimum error. The testing set used 38 data months (16.5%) to fine-tune the network model. It is not applied for training and validation process, only used to identify optimum network architecture, to select a suitable network model and assess their performance.

- ANN network architecture

The best results were obtained from ANN model consisting of 1 hidden layer and 60 neurons for each one. The node in the hidden and output layers is activated through Sigmoid function and trained by the Backpropagation Neural Network algorithm (BPNN)

5. Assessing and comparing the production prediction results of ANN model and those of the dynamic simulation model

5.1. Evaluating short-term production prediction results from the ANN model

The statistic method is used to assess the accuracy of the ANN model in the training, validation, and testing processes (Table 1) through the average absolute error (AE) and average relative error (ARE) of three parameters: oil production rate, liquid production rate, and reservoir pressure:

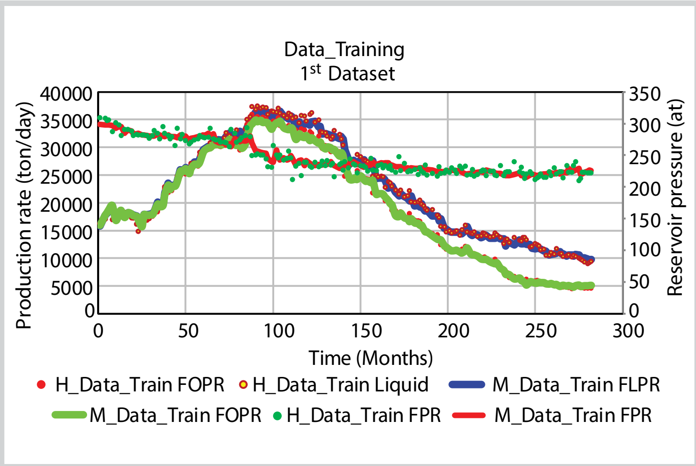

Figure 4. *Performance of short-term prediction training set.*

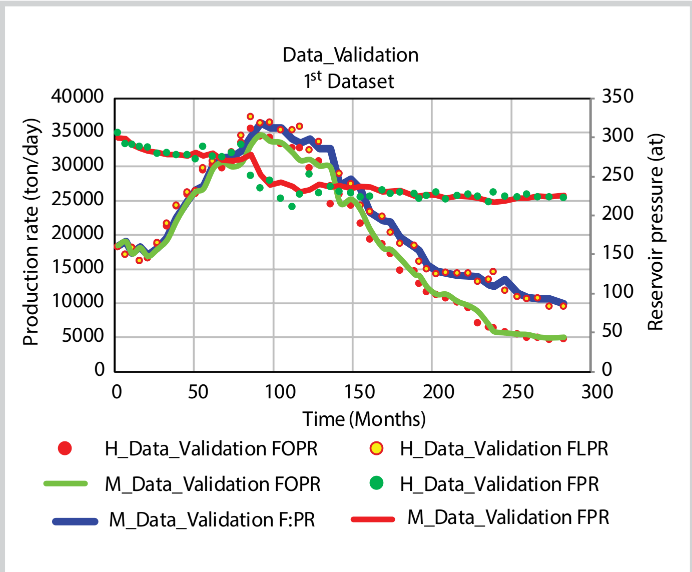

Figure 5. *Performance of short-term prediction validation set.*

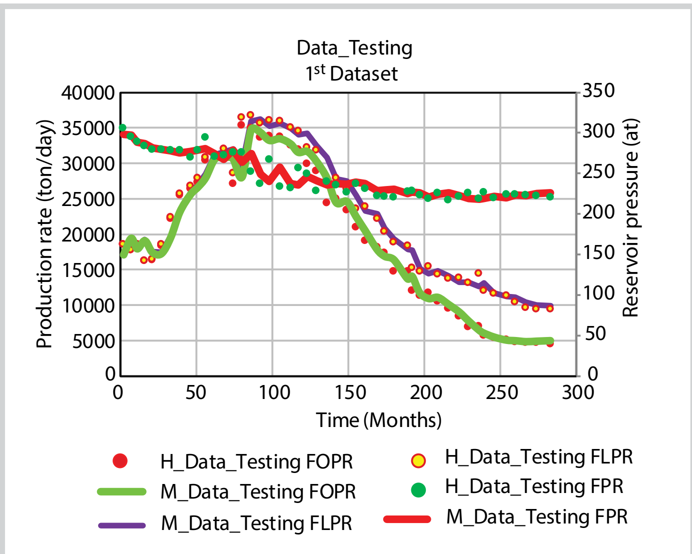

Figure 6. *Performance of short-term prediction testing set.*

- Training set:

+ AE: 526 tons/day, 637 tons/day, 6at;

+ ARE: 3.11%, 3.13%, 2.47%;

- Validation set:

+ AE: 998 tons/day, 1112 tons/day, 6.67at;

+ ARE: 5.51%, 5.26%, 2.76%;

- Testing set:

+ AE: 1157 tons/day, 1165 tons/day, 6.12at;

+ ARE: 6.46%, 5.54%, 2.5%.

The errors are in the allowable limit. The results of training, validation and testing processes are described in Figures 4, 5 and 6.

To study the robustness and accuracy of the network approach, with respect to predicting oil reservoir production, the second dataset was used to predict the reservoir oil production. The predicted reservoir oil rate values agree with the historical values indicating the training network can serve as a practical robust reservoir production management tool (Figure 7). The network provides reservoir oil rates with an average AE of 255 tons/day and average ARE of 4.82%, as illustrated in Table 1.

5.2. Evaluating long-term production prediction results from the ANN model

The statistic method is used to assess the accuracy of ANN model in the training, validation, and testing processes (Table 1) through the average absolute error (AE) and average relative error (ARE) of three parameters: oil production rate, liquid production rate, and reservoir pressure:

- Training set:

+ AE: 553 tons/day, 644 tons/day, 5.25at;

+ ARE: 2.79%, 2.78%, 2.1%;

- Validation set:

+ AE: 1001 tons/day, 1025 tons/day, 6.34at;

+ ARE: 4.91%, 4.4%, 2.52%;

- Testing set:

+ AE: 1215 tons/day, 1261 tons/day, 7.69at;

+ ARE: 5.6%, 5.43%, 3.13%.

Table 1. Statistical analysis of network model accuracy for short-term production prediction

		FOPR H	FOPR ANN	AE1	ARE1 (%)	FLPR H	FLPR ANN	AE2	ARE2 (%)	FPR H	FPR ANN	AE3	ARE3 (%)
DATABASE I	**TRAINING**												
	Average	19523	19421	526	3.11	22410	22273	637	3.13	245	245	6.00	2.47
	Standard deviation	10034	9914	485	2.79	8815	8656	522	2.63	26	25	5.37	2.23
	Minimum	4521	4765	4	0.01	9081	9719	10	0.04	210	216	0.08	0.03
	Maximum	35959	34902	2496	17.84	37452	36707	2765	14.81	309	298	33.11	15.62
	VALIDATION												
	Average	19469	19558	998	5.51	22289	22270	1112	5.26	245	247	6.67	2.76
	Standard deviation	9973	9649	995	4.92	8772	8411	1020	4.45	28	26	7.08	3.02
	Minimum	4669	4901	15	0.23	9438	9902	20	0.14	211	216	0.16	0.06
	Maximum	35478	34648	5407	23.20	37204	36382	5480	20.22	305	299	27.86	12.69
	TESTING												
	Average	19380	19523	1157	6.46	22216	22250	1165	5.54	246	247	6.12	2.50
	Standard deviation	10015	9794	1281	4.98	8765	8531	1218	4.72	27	25	6.47	2.59
	Minimum	4525	4900	6	0.11	9464	9947	65	0.19	217	218	0.02	0.01
	Maximum	35367	34801	7271	20.56	36778	36267	6883	18.88	306	298	26.70	10.18
DATABASE II	**PREDICTION**												
	Average	5280	5277	254.50	4.82	11095	10615	573	5.00	220	228	10.38	4.83
	Standard deviation	350	173	111.78	2.13	726	312	504	4.13	7	7	8.68	4.15
	Minimum	4692	4951	30.54	0.56	9464	9947	66	0.63	206	216	0.35	0.15
	Maximum	5848	5538	434.59	8.71	12097	11041	1637	13.54	234	237	24.78	11.83

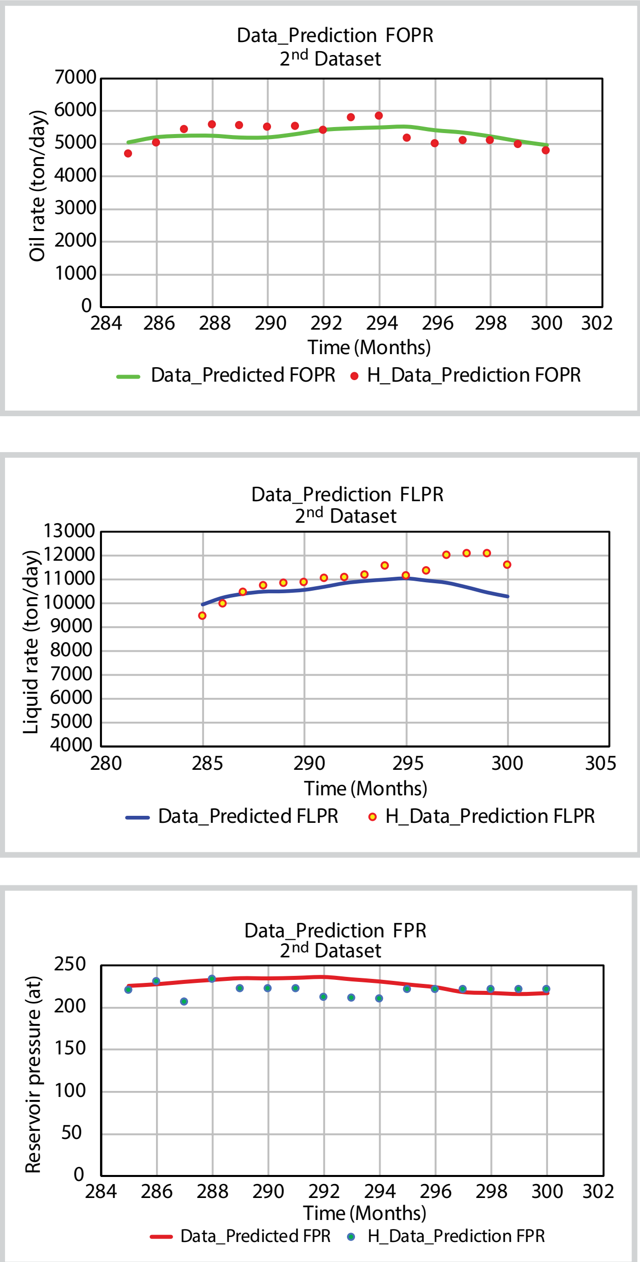

Figure 7. *Prediction of average oil production rate, liquid production rate and reservoir pressure (from January 2017 to April 2018).*

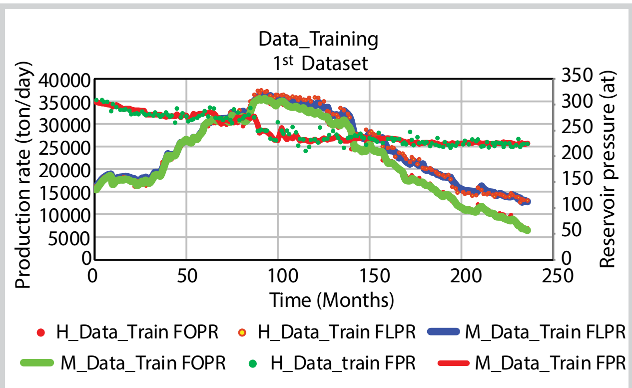

Figure 8. *Performance of long-term prediction training set.*

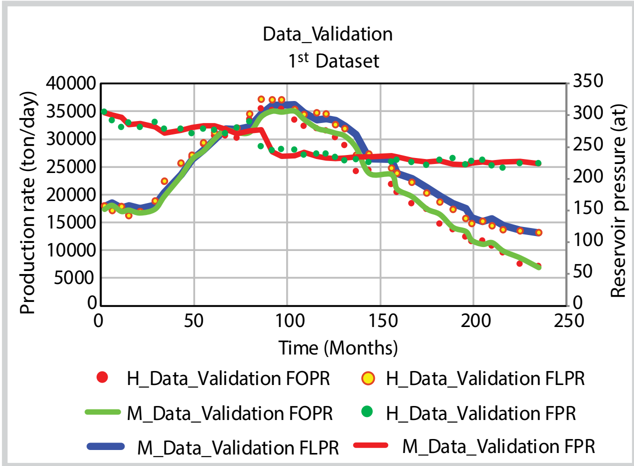

Figure 9. *Performance of long-term prediction validation set.*

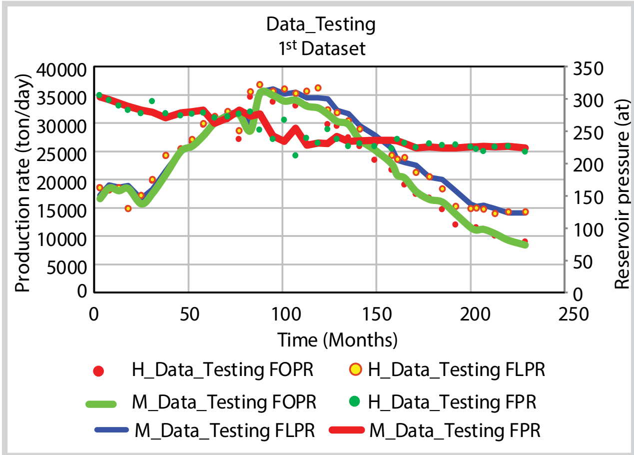

Figure 10. *Performance of long-term prediction testing set.*

The errors are in the allowable limit. The results of training, validation and testing processes are described in Figures 8, 9, and 10.

To study the robustness and accuracy of the network approach, the second dataset was used to predict the reservoir oil production. The predicted reservoir oil rate values agree with the historical values indicating the training network can serve as a practical robust reservoir production management tool (Figure 11). The network provides reservoir oil rates with an average AE of 698 tons/day and average ARE of 12.61%, as illustrated in Table 2.

5.3. Comparing the production prediction results of ANN model and dynamic simulation model results in the short term and in the long term

\- Comparing the results of short-term production prediction and those of long-term production prediction

From Figures 12 and 13, it is obvious that short-term oil production prediction of ANN model (284 data

Table 2. Statistical analysis of network model accuracy for long-term production prediction

		FOPR H	FOPR ANN	AE1	ARE1 (%)	FLPR_H	FLPR ANN	AE2	ARE2 (%)	FPR H	PR ANN	AE3	ARE3 (%)
DATASET I	TRAINING												
	Average	22342	22302	553	2.79	24599	24498	644	2.78	250	249	5.25	2.10
	Standard deviation	8365	8571	478	2.45	7820	7475	551	2.45	27	26	5.41	2.14
	Minimum	6864	6498	6	0.06	12650	12748	9	0.04	211	223	0.02	0.01
	Maximum	35959	35569	3941	16.11	37452	36606	3693	13.62	309	304	34.37	12.94
	VALIDATION												
	Average	22430	22633	1001	4.91	24633	24668	1025	4.40	250	252	6.34	2.52
	Standard deviation	8729	8666	844	3.97	8149	7644	794	3.45	27	27	5.01	1.95
	Minimum	7083	6852	58	0.18	13167	13137	12	0.08	217	222	0.24	0.11
	Maximum	22430	22633	1001	4.91	24633	24668	1025	4.40	250	252	6.34	2.52
	TESTING												
	Average	22563	22753	1215	5.60	24779	24796	1261	5.43	250	251	7.69	3.13
	Standard deviation	8236	8300	1307	5.68	7804	7367	1216	5.53	27	26	9.02	3.89
	Minimum	8935	8453	30	0.27	14021	14080	95	0.38	212	224	0.25	0.11
	Maximum	34899	35255	5887	23.91	36778	36052	5963	27.26	306	303	42.64	20.11
DATASET II	PREDICTION												
	Average	5405	5238	697.84	12.61	11302	11899	1254	11.44	222	241	19.60	8.94
	Standard deviation	630	863	559.05	10.08	1369	638	761	7.29	7	15	16.88	7.90
	Minimum	4521	4419	16.73	0.26	9081	11281	9	0.08	206	224	0.00	0.00
	Maximum	7031	7697	2628.28	52.67	14553	13755	2758	25.71	240	278	66.92	31.73

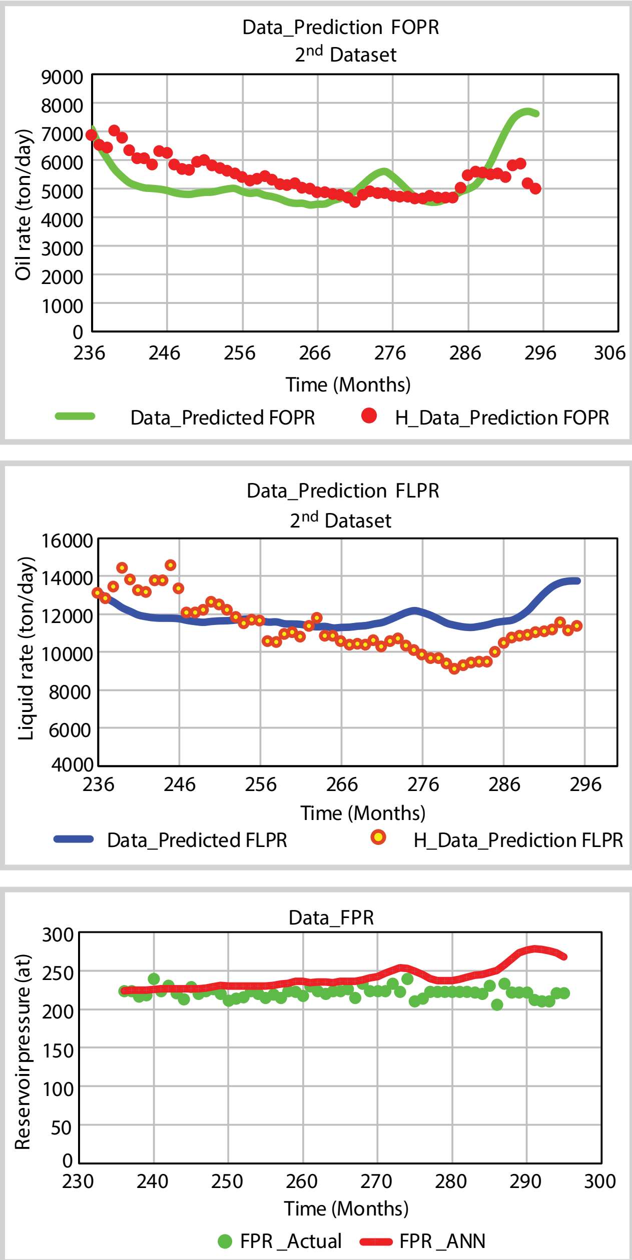

Figure 11. *Prediction of average oil production rate, liquid production rate and reservoir pressure (from January 2013 to December 2017).*

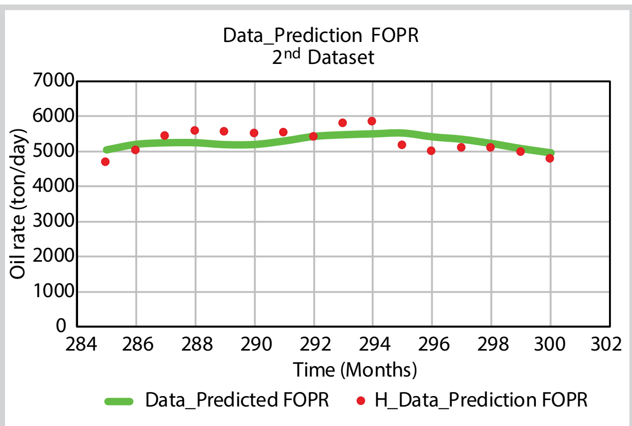

Figure 12. *Short-term oil production rate prediction.*

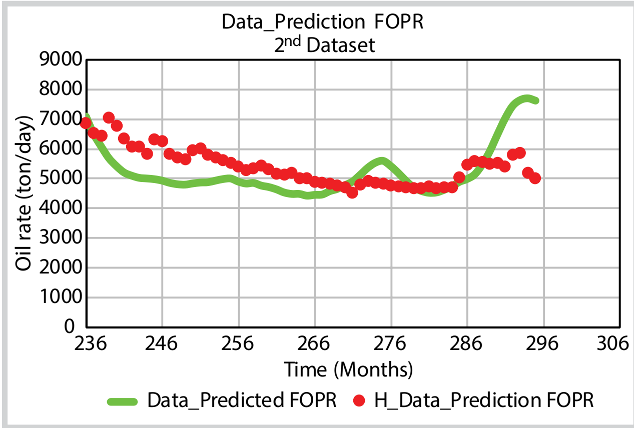

Figure 13. *Long-term oil production rate prediction.*

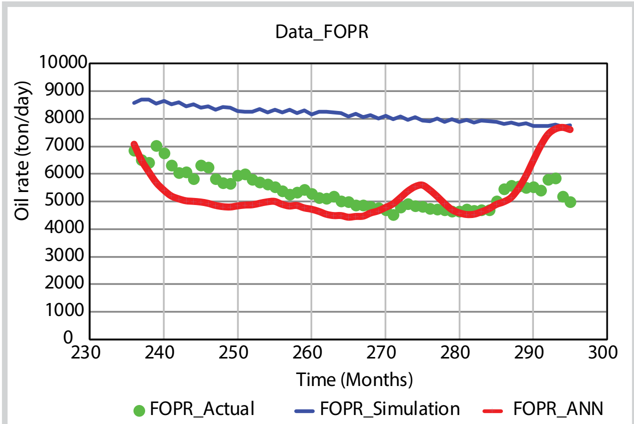

Figure 14. *The results of oil production rate prediction.*

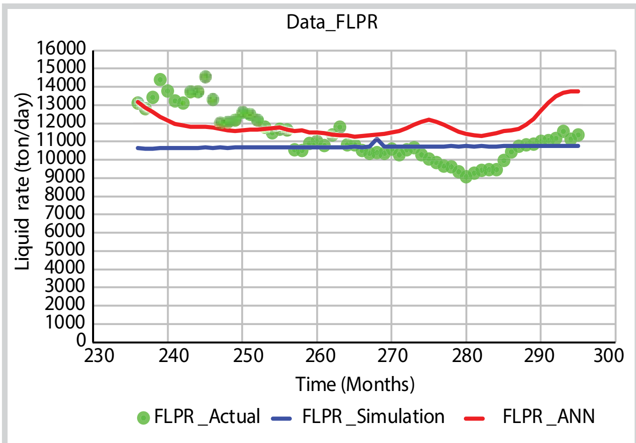

Figure 15. *The results of liquid production rate prediction.*

months) gives better results than long-term oil production prediction of ANN model (236 data months).

- Comparing the results of long-term production prediction of ANN model and dynamic simulation model results

- In comparison with traditional prediction method, the artificial neural network method can learn arithmetic problems which the in-out relationship is non-linear with

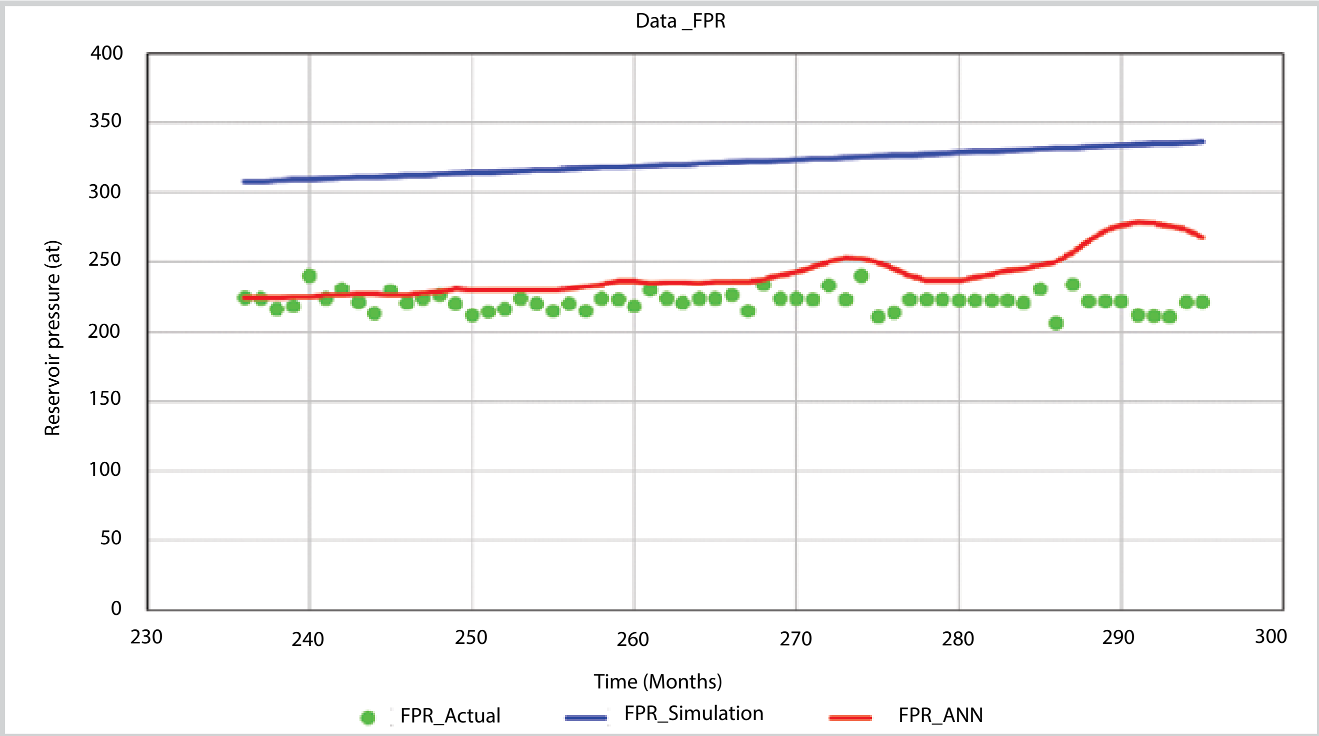

Figure 16. *The results of reservoir pressure prediction.*

high accurate prediction, corresponding to production input data. The ANN method forecasts input data without being based on the subjective experiment of professors. After the training process, the ANN model will actively determine weights for each input parameter and their relationship. Accordingly, the results of the ANN model are more trustworthy than the traditional prediction method.

- In the training set, the network will regulate input parameters to satisfy mean squared error value, ANN's convergence ability depends on original arguments, so many sensitivity scenarios must be run to choose the best original arguments. On the other hand, the training in complicated networks becomes more difficult than shallow and narrow networks, in which case the optimisation is more likely to converge to some useless local optima. Ideally, we would like to design a model of reasonable complexity but powerful representation for the data we feed into it. Moreover, to avoid overfitting the model, the size of the training data has also to be considered in the designing. Therefore, taking all these concerns into account and after several trials on the validation dataset, one layer of the hidden layer with the proper number of neurons fits the best.

- Figures 14, 15 and 16 show comparison between the results of long-term production prediction of the ANN model and those of the dynamic simulation model.

Observation: From the experimental results, the performance of the two models was assessed, showing:

- Dynamic simulation model:

The model is controlled by a constant value of liquid production rate (LPR) in the period from January 2013 to December 2017. As a matter of fact, LPR did not remain stable due to production operation (well shut-in, facility maintenance, weather conditions…). The precise assumption of production qualification depends on experiment, simulator's subjective and field development plan. On the other hand, the simulation oil production rate has high deviation compared with history at starting forecasting date, the model does not obtain reliability and neither does it capture geological complication, rock property distribution, fracture network, and hydrodynamic connectivity of granite basement. Until now, there is not a granite basement simulation method that is accurate, reliable and widely recognised.

- ANN model:

The parameters: oil production rate, liquid production rate, and reservoir pressure are very close to the actual data, the trend of results and actual production match closer than the dynamic model. Nevertheless, the confinement of the ANN model only applies to predict short term.

6. Conclusion and recommendation

This research work aims to present a new approach to predict oil production rate based on the historical production data. The results of methodology show prediction problem generalisation ability on the ANN model, become an effective implement to resolve variable problems in operation and management field production techniques. The ANN model has many features: data learning possibility, adaptation, a decision with deficiency or noise data, which are a significant advantage compared with numerical simulation.

- ANN application will be more effective when the first stages such as training samples, extracting characteristics and pre-processing are well done;

- ANN model postulates more time to train and adjust network argument;

- As for the future work, other particularly different algorithms and input data effected to production prediction such as well bottom hole pressure, choke size, and gas lift rate will be integrated.

Acknowledgement

This work is supported by the Ministry of Industry and Trade of Vietnam, project No. CNKK.001/19.

References

1. Q.Cao, R.Banerjee, S.Gupta, J.Li, W.Zhou, B.Jeyachandra. *Data driven production forecasting using machine learning*. SPE Argentina Exploration and Production of Unconventional Resources Symposium, Buenos Aires, Argentina. 1 - 3 June, 2016.

2. Brian D.Ripley. *Pattern recognition and neural networks*. Cambridge University Press. 1996.

3. John R.Koza, Forrest H.Bennett, David Andre, Martin A.Keane. *Automated design of both the topology and sizing of analog electrical circuits using genetic programming*. Springer. 1996: p. 151 - 170.

4. Jerome H.Friedman. *Data mining and statistics: What's the connection*. Computing Science and Statistics. 1997.

5. Jeff Heaton. *Introduction to neural networks for java (2nd edition)*. Heaton Research. 2008.

6. Trần Văn Hồi, Nguyễn Văn Đức, Phạm Xuân Sơn. *Tìm kiếm thăm dò và phát triển dầu trong đá móng mỏ Bạch Hổ: Tư liệu, sự kiện và bài học kinh nghiệm*. Vietsovpetro. 2018: trang 7 - 20.

7. Yunan Li, Yifu Han. *Decline curve analysis for production forecasting based on machine learning. SPE Symposium: Production Enhancement and Cost Optimisation, Kuala Lumpur, Malaysia*. 7 - 8 November, 2017.

8. A.Mirzaei Paiaman, S.Salavati. *The application of artificial neural networks for the prediction of oil production flow rate. Energy Sources, Part A: Recovery, utilization, and environmental effects*. 2012; 34(19): p. 1834 - 1843.

PETROVIETNAM JOURNAL
Volume 6/2019, p. 58 - 62
ISSN-0866-854X

Predicting water influx for gas production wells of Lan Do field using material balance method

Vu Duc Ung[1], Le Vu Quan[1], Tran Dang Tu[1], Nguyen Van Thinh[2], Trieu Hung Truong[2]
[1]Vietnam Petroleum Institute
[2]Hanoi University of Mining and Geology
Email: ungvd@vpi.pvn.vn

Summary

Lan Do gas field (Block 06-1 in Nam Con Son basin) started producing gas and condensate in October 2012. The cumulative production up to February 2018 was 6,854 billion cubic metres of gas and 0.09 million barrels of condensate which account for 62% and 41% of the reserve, respectively. At present, there is no water influx phenomenon in Lan Do production wells. However, it is necessary to forecast water influx period for reservoir production and management strategies. This paper analyses and forecasts this phenomenon for the production wells of Lan Do field and proposes optimal production strategy.

Key words: Lan Do field, water influx, water-gas ratio, gas-water contact.

1. Introduction

Lan Do field started producing gas and condensate in October 2012 with two production wells LD-1P and LD-2P. The production rate of Lan Do field in 2013 reached 925 million m^3 (0.033 trillion ft^3) of gas and 0.014 million barrels of condensate. In the 2014 - 2017 period, gas production rate reached over 1.2 billion m^3 per year (0.04 trillion ft^3) and condensate production rate was 0,17 million barrels per year. By the end of October 2018, the cumulative production of Lan Do field was 6,854 billion m^3 of gas and 0.09 million barrels of condensate [1].

The produced water of Lan Do is the amount of condensed water in the gas, so the chloride content of produced water is quite low, averaging 80 - 110ppm. When the chloride content in the produced water of the field increases and exceeds the permitted level (150ppm), that means gas-water contact (GWC) is gradually approaching the perforation interval of production wells. The current water-gas ratio (WGR) of Lan Do field is 0,45 barrel/million ft^3 (Figure 1).

In this paper, the authors analyse and calculate the current GWC, forecast the possibility of water influx to production wells based on the principle of material balance method and propose solutions to improve production in Lan Do field more effectively.

Date of receipt: 14/6/2018. Date of review and editing: 14/6 - 25/10/2018.
Date of approval: 3/6/2019.

2. Determination of reservoir drive mechanisms and prediction of water influx for gas production wells of Lan Do field

2.1. Determination of reservoir drive mechanisms

The reservoir pressure support of Lan Do field is very good. From 2012 to February 2018, the reservoir pressure reduced by 63psi, from 1,948psi to 1,885psi. With the declining trend of reservoir pressure (Figure 2), the cumulative gas production at the end of production will reach 0.39 trillion ft^3, while the reservoir pressure will decline to 1,858psi at 1,132m TVDss.

For gas condensate reservoirs, the reservoir drive mechanism can be determined by the relationship between reservoir pressure (or P/z ratio) and cumulative gas - condensate production (G_p) [4].

For gas reservoirs produced by natural drive mechanism without aquifer, the relationship between reservoir pressure and accumulated gas - condensate production is linear and can be expressed as:

$$\frac{P}{z} = -\frac{Pi}{ziG} G_p + \frac{Pi}{zi}$$

For the reservoir produced by water drive mechanism, the relationship between reservoir pressure and accumulated gas-condensate production is nonlinear because the reservoir pressure decreases during production is smaller than the reservoir pressure produced by the natural drive mechanism without aquifer (Figure 3).

From the results of the reservoir pressure measurements, the construction of P/z curve (Figure 4) shows that the wells of Lan Do field have the volume of aquifer which supports Lan Do is 250Bbbl.

2.2. Prediction of water influx

Production in Lan Do field is on-going with stable flows without water influx into the production wells. However, the reservoir has a large aquifer which can accumulate water influx. Therefore, analysis and forecast of the water influx are very important to improve the efficiency of operation and production.

The gas-water contact (GWC) during production and at the end of production is determined through the amount of water influx into the reservoir, based on the material balance equation [4].

$$G(B_g - B_{gi}) + GB_{gi}\left[\frac{C_w S_{wi} + C_f}{1 - S_{wi}}\right]\Delta\bar{p} + W_e = G_p B_g + B_w W_p \qquad (1)$$

In which:

G: Gas and condensate initially in place;

B_g: Gas formation volume factor;

B_{gi}: Initial gas formation volume factor;

B_w: Water formation volume factor;

C_w: Water compressibility;

C_f: Rock compressibility;

S_{wi}: Initial water saturation;

W_e: Cumulative water influx;

W_p: Cumulative water production.

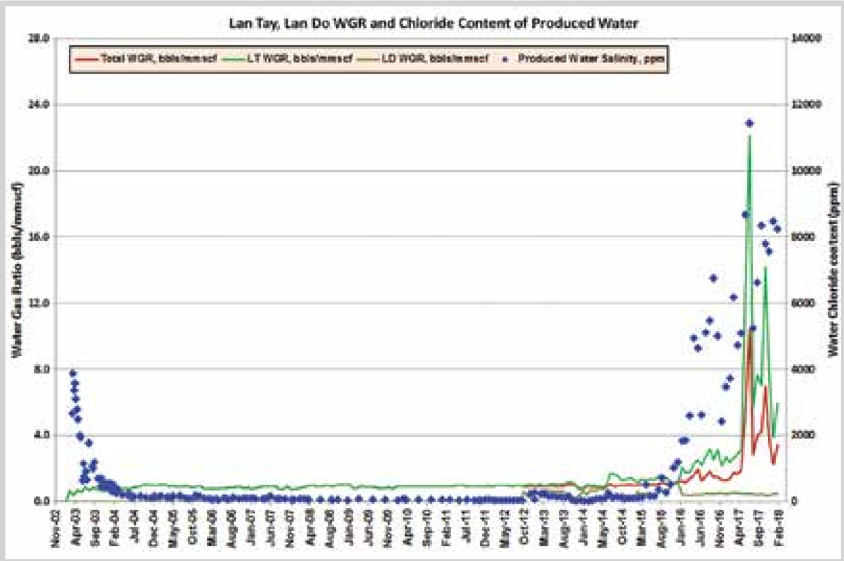

Figure 1. *Lan Tay, Lan Do water-gas ratio and chloride content of produced water [2].*

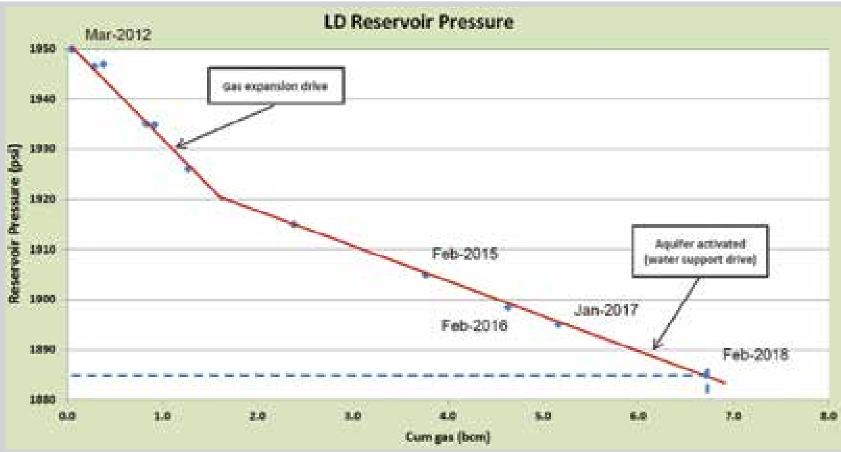

Figure 2. *Reservoir pressure and cumulative gas production [3].*

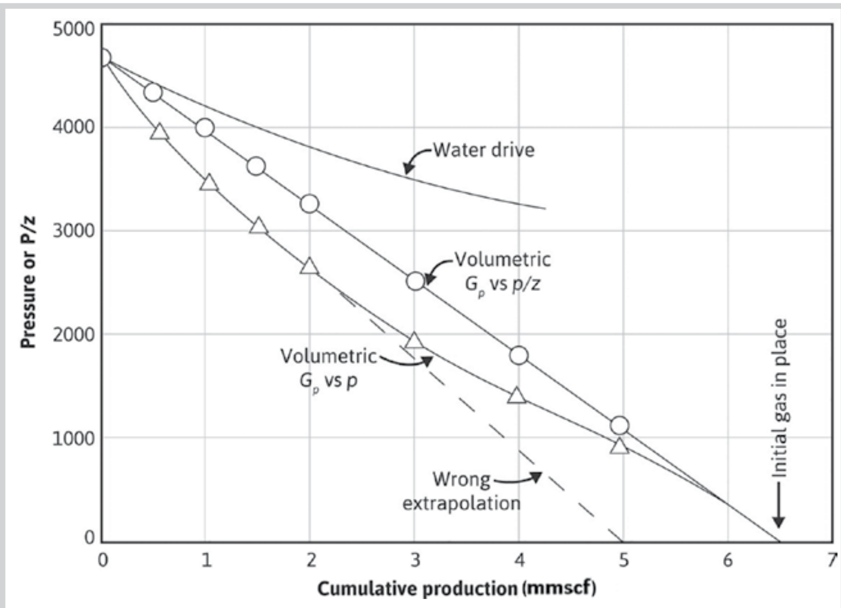

Figure 3. *Relationship between P/z and G_p for gas field in case of production reservoir with the aquifer and volumetric reservoir [4].*

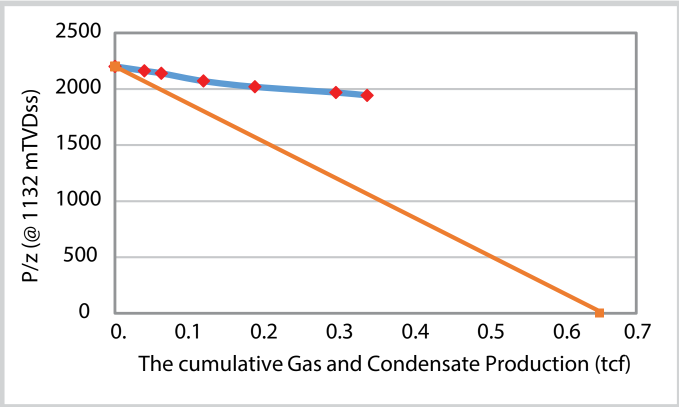

Figure 4. *Relationship between P/z ratio and cumulative gas condensate production.*

Table 1. *Characteristics of fluid and reservoir*

Gas initially in place (trillion ft³)	0.65
Condensate initially in place (million barrels)	0.33
B_g (cuft/SCF)	0.008548733
B_{gi} (cuft/SCF)	0.007874
C_w (psi^{-1})	3.46×10^{-6}
S_{wi}	0.05
C_f (psi^{-1})	6.30×10^{-6}
Rock porosity Φ, (%)	37.5
Initial bulk rock volume - BRV (million m³)	1,518
B_w, rb/stb	1.01537
Water-gas ratio - WGR (barrel/million ft³)	0.45
Residual gas saturation	0.283
Compression factor z	0.87
Reservoir pressure at 1,132m TVDss (psi)	1,885
Reservoir temperature (°F)	157
Initial reservoir pressure at 1,132m TVDss (psi)	1,948
Initial compression factor Z_i	0.88
Pressure gradient (psi/ft)	0.04

2.2.1. Determination of gas-water contact

By February 2018, the cumulative production of Lan Do reached 0.2420 trillion ft³ of gas (equivalent to 62% of the reserve) and 0.09 million barrels of condensate (equivalent to 41% of the reserve). Cumulative water production is 30.7 thousand barrels. The magnitude of the reservoir pressure which decreases with the cumulative production of Lan Do field is shown in Figure 2 and the reservoir pressure in February 2018 was about 1,885psi at 1,132m TVDss. The parameters showing the properties of fluid and reservoir are presented in Table 1 [5].

Condensate production and water production are converted via the below equation [4]:

- For condensate production:

$$GE = V = \frac{nR'T_{sc}}{p_{sc}} = \frac{350.5\gamma_0(10.73)(520)}{M_{wo}(14.7)} = 133{,}000\frac{\gamma_0}{M_{wo}} \quad (2)$$

in which:

$$M_{wo} = \frac{5954}{\rho_0\, API - 8.811} = \frac{42.43\gamma_0}{1.008 - \gamma_0} \quad (3)$$

- For water production:

$$GE_w = \frac{nR'T_{sc}}{p_{sc}} = \frac{350.5 \times 1.00 \times 10.73 \times 520}{18 \times 14.7} \quad (4)$$

$$= 7{,}390\ SCF/surface\ barrel$$

- The converted condensate production via equation (2) và (3) is 0.074 billion ft³;

- The converted water production via equation (4) is 0.227 billion ft³

Thus, the total gas production included converted water and condensate, G_p = 0.2423 trillion ft³.

Water influx into the reservoir (W_e), which is determined by material balance equation (1), is 290.3 million barrels (46.2 million m³).

So, the remaining bulk rock volume: BRV = initial BRV - [W_e/Φ x (1-S_{wi}-S_{gr})] = 470 million m³.

Thus, by the end of February 2018, the gas water contact, which is determined by Figure 5, is 1,153m TVDss.

2.2.2. Calculation of gas-water contact at the end of production when the expected cumulative gas production G_p = 0.39 trillion ft³

According to Lan Do prediction, the cumulative gas and condensate production are 0.39 trillion ft³ and 0.22 million barrels respectively at the end of production and the average reservoir pressure at that time is expected to reach 1,858psi at 1,132m TVDss.

- Gas reserves: 0.39 trillion ft³

- Cumulative water production: 43.8 thousand barrels

- Condensate reserves: 0.22 million barrels

- Converted condensate reserves: 0.18 billion ft³

- Converted water production: 0.32 billion ft³

Thus, the total gas production including the converted water and condensate reserves is G_p = 0.391 trillion ft³.

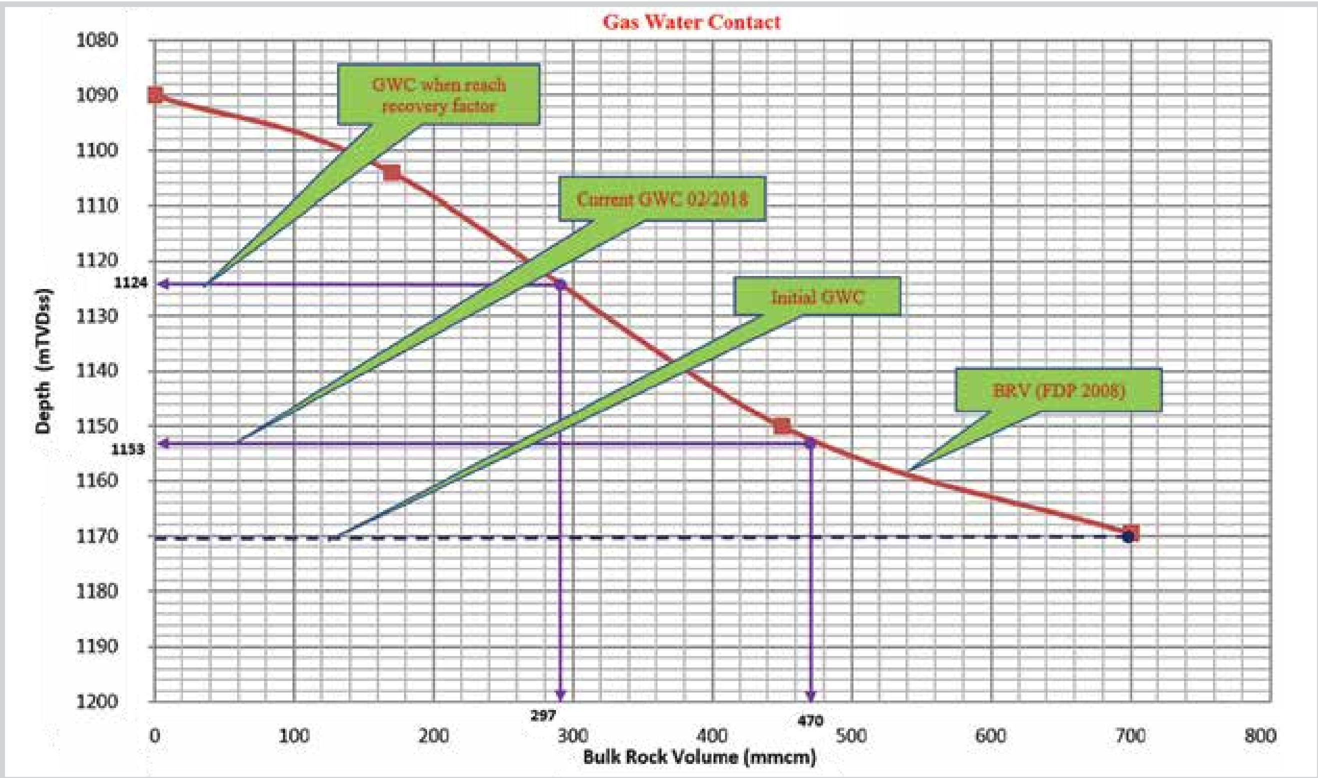

Figure 5. *Determination of gas water contact via BRV [5].*

Table 2. *The results of calculating the amount of water influx based on accumulated gas and condensate production*

Cumulative gas and condensate production (billion ft^3)	Water influx into reservoir (million barrels)
32.7	0.57
44.6	12.6
84.7	61.7
134.4	132.6
228.2	271.03
242.3	290.3
390	508.9

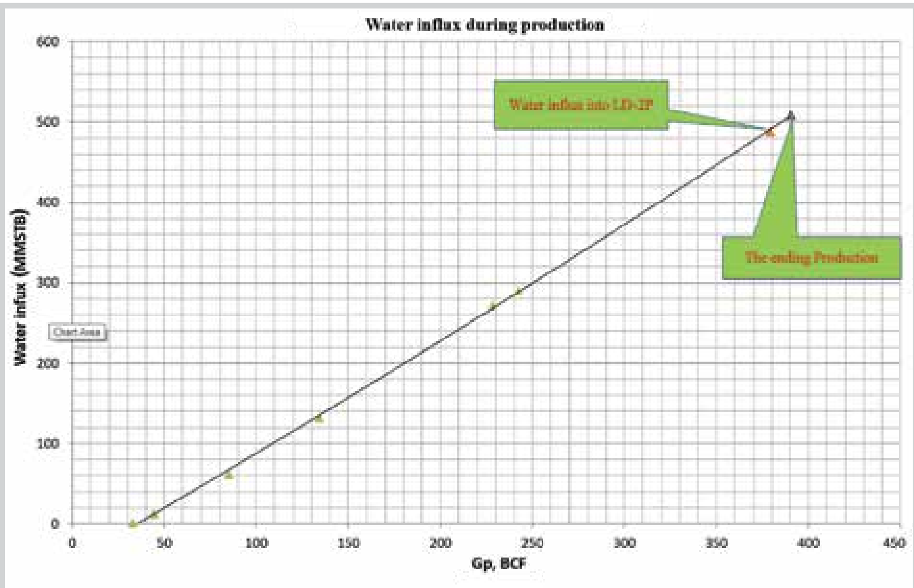

Figure 6. *Prediction of water influx during production.*

Water influx into the reservoir (W_e), which is determined by material balance equation (1), is 508 million barrels (81 million m^3)

The remaining bulk rock volume: BRV = initial BRV - [W_e/Φ x (1-S_{wi}-S_{gr})] = 297 million m^3.

Therefore, the gas-water contact at the end of production is 1,124m TVDss (Figure 5)

The amount of water influx into the reservoir during production is calculated by the material balance equation and it has a close relationship with the cumulative gas and condensate production. The results of forecasting the water influx into the reservoirs via the cumulative gas and condensate production are shown in Table 2 and Figure 6.

With the bottom hole depths (TD) of wells LD-1P and

Table 3. Lan Do GWC estimation

Depth (m TVDss)	Bottom hole depth (m TVDss)		Water-gas contact (m TVDss)		
	LT-1P	LT-2P	Initial	February 2018	At G_p = 0.39 trillion ft^3
1,080					
1,090					
1,100	1,101				
1,110					
1,120					1,124
1,130		1,138			
1,140					
1,150				1,153	
1,160					
1,170			1,170		
1,180					

Table 4. Prediction of water influx into the Lan Do wells

Well	Depth (m TVDss)	BRV at well depth (million m^3)	Water influx volume at the time of flooding		Cumulative production (trillion ft^3)	Time of starting to flood
			million m^3	million barrels		
1P	1,101	140	132	832	0.62	N/A
2P	1,138	370	78	490	0.38	August 2020

LD-2P are 1,101m TVDss and 1,138m TVDss respectively and GWC in February 2018 is 1,153m TVDss, the water will be present in well 2P before the end of production (Table 3).

Prediction for water influx is calculated with the assumption that the average annual production of Lan Do is 1,642 billion m^3 of gas and 0.02 million barrels of condensate to the end of field life. At the end of production, when cumulative production G_p = 0.39 trillion ft^3, well LD-2P will be flooded with water. The results of predicting time and cumulative production at the time wells start to flood are presented in Table 4.

3. Conclusion

The prediction of water influx for Lan Do field is calculated based on the reservoir and fluid parameters, the reservoir pressure prediction and calculations based on the material balance method with the average annual production of 1,642 billion m^3 of gas and 0.02 million barrels of condensate. From the results, the gas-water contact will move upwards and the earliest flooded well is LD-2P (in August 2020). Therefore, it is necessary to consider adjusting the production with reasonable rate of LD-2P to slow the water produced time and prolong the time of production of Lan Do field.

Reference

1. Viện Dầu khí Việt Nam. *Nghiên cứu phục vụ quản lý khai thác các mỏ dầu khí do nhà thầu nước ngoài điều hành tại Việt Nam*. 2017.

2. Hoang Vu Nam. *Block 06.1 PSC monthly production report*. Rosneft Vietnam. 2018.

3. Nguyen Tuan Anh. *Block 06-1 production quarterly review with PVN*. Rosneft Vietnam. 2018.

4. B.C.Craft, M.F.Hawkins. *Applied petroleum reservoir engineering (2nd edition)*. 1991.

5. BP Oil Company. *Block 06-1 Lan Tay - Lan Do development plan*. 2008.

PETROVIETNAM JOURNAL
Volume 6/2019, p. 63 - 67
ISSN-0866-854X

Corrosion threats and strategy to secure mechanical integrity of Dung Quat refinery

Mai Tuan Dat
Binh Son Refining and Petrochemical JSC
Email: datmt@bsr.com.vn

Summary

This article summarises some key results of several analysis of corrosion issues in Dung Quat refinery and the selected strategic action plan for this critical matter. Since corrosion is a natural process which happens along the lifetime of the plant, the strategy for securing its mechanical integrity will be updated time by time in line with the site conditions and the company's inspection and corrosion policy.

Key words: Corrosion under insulation (CUI), corrosion under pipe support, corrosion of dead legs, risk-based inspection (RBI).

1. Introduction

Dung Quat refinery, well known as the first refinery installed in Vietnam, was successfully commissioned in 2009 and started its commercial operation since May 2010. The plant was designed to process Bach Ho (a local light sweet crude oil) and a mixed crude of Bach Ho and Dubai (at 85%/15%) at a capacity of 6.5 million tons per year. The refinery is sited on the coast of Viet Thanh bay and under the equatorial monsoonal climate [1].

Similar to other refineries and petrochemical plants, corrosion is a real challenge to the plant operator. Thanks to low sulphur feedstocks, internal corrosion at Dung Quat refinery plant would principally not be as serious as in the refineries processing high sulphur crudes. In contradiction to internal corrosion, due to severe conditions of the coastal weather, external corrosions have been confirmed as the most serious problem threatening safe and reliable operation of the plant.

In order to secure the operational availability of the refinery, a vision of achieving zero corrosion incidents was set by the plant operator. Establishment of a pro-active risk mitigation culture supported by effective corrosion management systems and advanced technologies are the key strategies applied in BSR.

Date of receipt: 18/9/2018. Date of review and editing: 18/9 - 25/12/2018.
Date of approval: 3/6/2019.

2. Corrosion challenges in Dung Quat refinery

There are many different types of corrosion recognised in industries. According to API 571, there are more than sixty damage mechanisms listed to refinery and petrochemical plants [2]. In order to effectively manage the mechanical integrity of the plant, a risk-based inspection (RBI) study was conducted to identify which damage mechanisms happened at what level of vulnerability for each or groups of equipment and piping sections.

Based on analysis of the occurrence frequency and the potential impacts of corrosions in the plant since the commercial operation, three groups of external corrosion issue were identified as the most harmful to the mechanical integrity of the plant. The next paragraphs will provide some brief descriptions of these matters by its level of risk to the plant.

Firstly, corrosion under insulation (CUI) was recognised as a "silent killer" mechanism in the plant due to a high number of damages recorded. Mentioned in NACE Standard Practice SP0198, "Corrosion under insulation has been occurring for as long as hot or cold equipment has been insulated for thermal protection, energy conservation, or process stabilisation" [3]. In Dung Quat refinery plant, the level of threat by CUI was fast-tracked by the local weather conditions with a high humidity and salty air and a very long monsoon season (approximate of two months continuously). In addition, it is believed that the existence of chlorides in the atmosphere accelerates CUI damages.

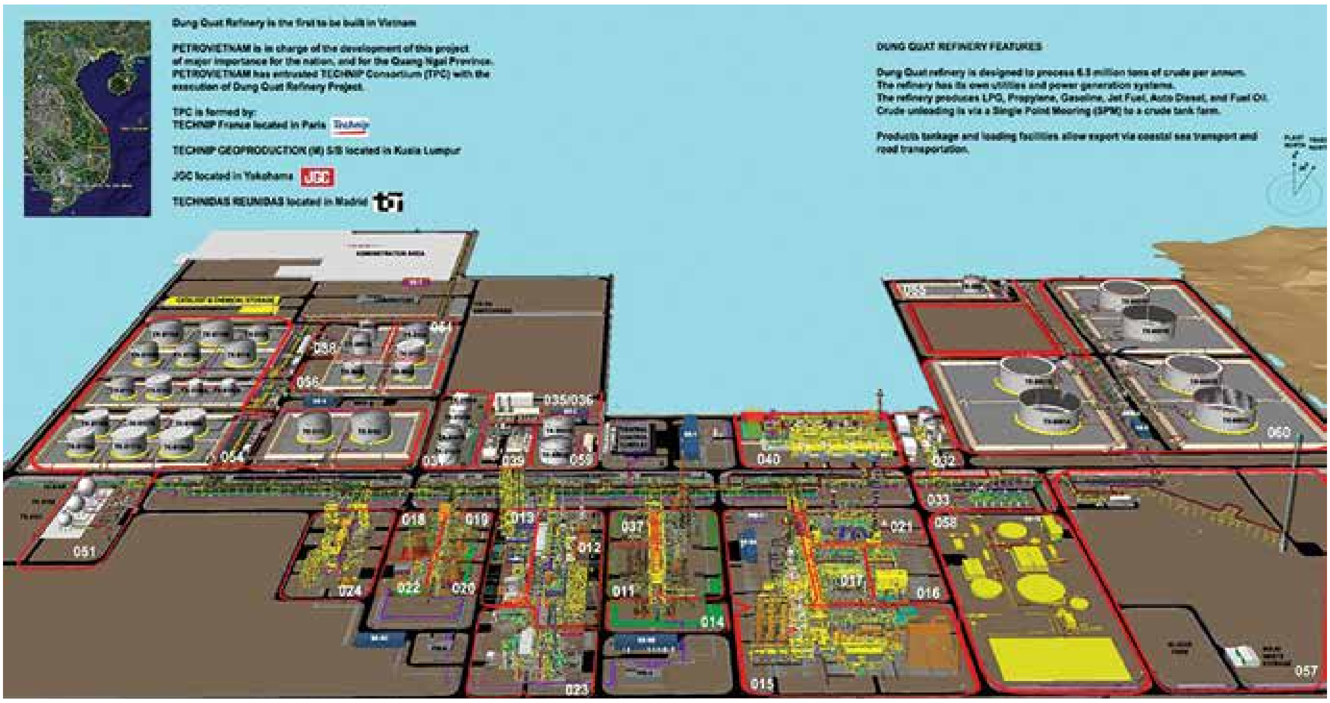

Figure 1. *Dung Quat refinery plant.*

Secondly, corrosion under pipe supports (CUPS) was acknowledged as a critical damage factor to the piping system. Similar to CUI, local climate and weather conditions facilitate CUPS damage. As a result of high corrosion rate to a large number of pipe's supports, mitigation of CUPS requires huge resources from maintenance team.

Thirdly, corrosion of dead legs attracts great attention of inspection teams because of a concentration of additional damage mechanisms in comparison with the remaining sections of the pipelines and equipment. For example, while microbiologically induced corrosion is commonly present in most of the dead legs, the by-pass spool of a control valve may additionally contain some layers of sediment which causes corrosion under deposit or, in case of drains normally may accumulate water which facilitates galvanic corrosion, etc. Subsequently, numerous amounts of dead legs fixed in the plant introduce real tangible challenges for inspection and operation teams in terms of management.

Other from above, failure mechanisms which have a significant frequency of occurrence or are potentially existing in the system but their impact to the plant availability have not yet been confirmed or have been resolved are not listed in detail. Some of them can be named herein such as refractory degradation, erosion-corrosion, atmospheric corrosion, wet H_2S damage (blistering/HIC/SOHIC/SSC), fuel ash corrosion, ammonium chloride corrosion, thermal fatigue, mechanical fatigue, amine corrosion, amine stress corrosion cracking, and high temperature hydrogen attack (HTHA), etc. In order to secure the mechanical integrity of the plant, an effective and systematic corrosion strategy is critically required.

Figure 2. *Image of a CUI.*

3. Strategies to overcome corrosion challenges in BSR

By consolidating related data, relevant analysis has been conducted to set up strategies to overcome the corrosion challenges of the plant. The key strategic management actions for some next few years focus on: i) competency development or employment of inspectors; ii) implementation of inspection management system;

and iii) application of new technologies for early risk detection and proactive risk migration. In parallel, the technical strategy to effectively handle the most concerned corrosion mechanism is highly required. Successful implementation of the strategy allows the company to take full advantages of operating the plant at maximum uptime, efficiency, and safety.

3.1. Management strategy

Corrosion and inspection management system (CIMS) is the essential tool for managing inspection plan of a very large quantity of stationary equipment and pipelines installed in the plant. BSR has fully utilised a dedicated CIMS software as the central tool for corrosion and inspection management in accordance with API RP 580 [4]. All mechanical assets are registered into the system together with their related engineering data. Then, on the basis of risk-based inspection study, detailed inspection plans will be developed for each of the equipment or piping system. A very simple workflow will be configured to the system allowing convenient usage by inspection engineers. Subsequent inspection data will be uploaded into CIMS system for detailed analysis using software built-in functions. Analysis results will then be used by corrosion engineers for determining next inspection date of the concerned asset.

A mechanical integrity dashboard was additionally developed by BSR inspectors providing main KPIs such as the number of assets having a remaining lifetime of less than 4 years, re-certification compliance, and inspection schedule compliance rate, etc.

As an important part of the management system, inspection procedures and guidelines perform a critical role in guaranteeing the quality and effectiveness of mechanical integrity management. The risk-based concept is the key to ensure resources are allocated to equipment and piping ranked as high risk. Therefore, inspection procedures are updated with detailed strategies for more effective management of corrosion threats.

Based on the concept of "incidents are preventable", a monitoring system was intensively upgraded in order to detect signs of corrosion as earlier as possible. The corrosion parameter monitoring system was configured to screen real time process data from the plant's Distributed Control System and Laboratory Information Management System. Data analysis will be conducted and advanced inspection technologies will be used in order to verify any potential signs of damages. All identified corrosion threats will be updated to the CIMS system for immediate actions.

3.2. Advanced technology employment strategy

Since corrosion is mostly hidden to human eyes, the utilisation of new technologies is essential to identify and confirm the existence of damage. BSR inspectors were en-

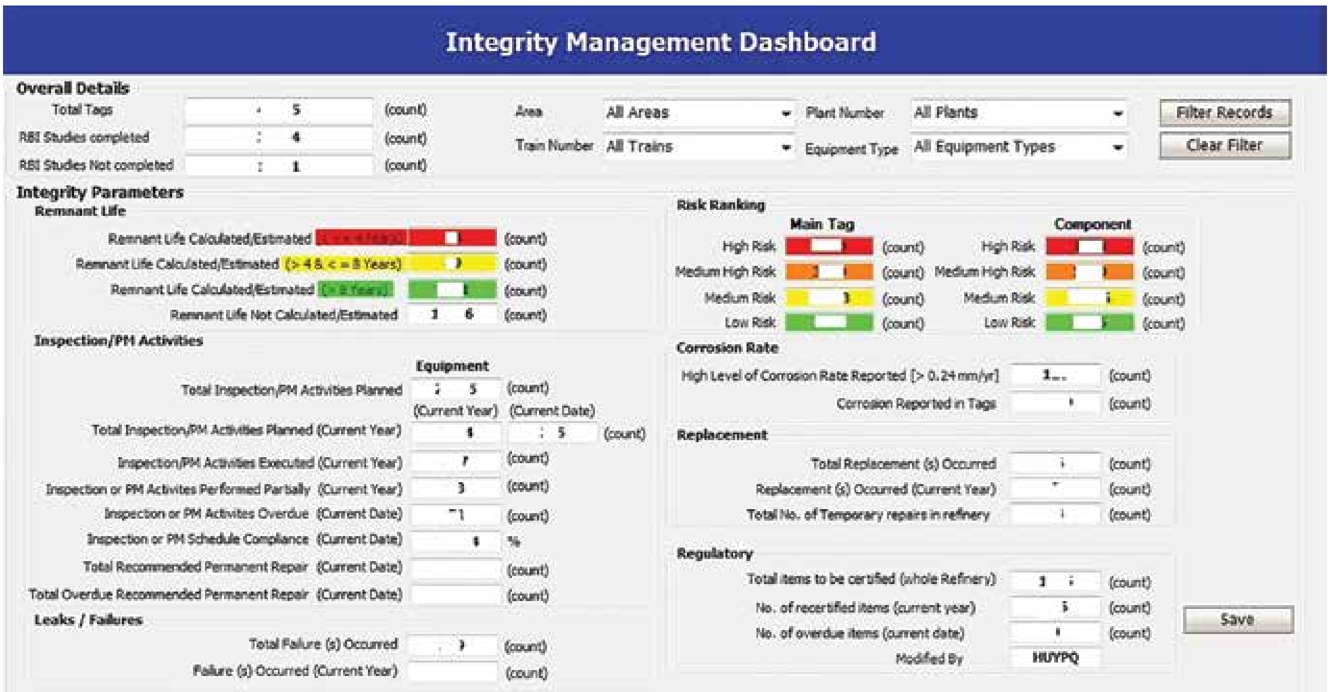

Figure 3. CIMS dashboard window.

couraged to discover the newest technologies available in the market and study for the application.

From 2016, BSR inspectors have completed their study for using a combination of thermographic camera and gamma scan together with the traditional ultrasonic thickness measurement to evaluate refractory degradation.

In 2017, in order to detect "phantom chlorides", BSR laboratory settled the in-house procedure for testing organic chloride.

Recently, BSR inspection team is completing its study for deep exploitation of infrared thermography and guided wave ultrasonic testing techniques which help to detect CUI in a very short time and at very high accuracy without spending a lot of time and money to open insulation.

In the meantime, and with effective supports of the upgraded inspection management system, strategic technical solutions were developed with high priority in order to mitigate the mechanical integrity risks caused by the most severe mechanism as mentioned above.

The intensive CUI surveillance programme uses three layers of data, including visual inspection, thermography images and guided wave ultrasonic testing. By taking great advantage of thermography and ultrasonic techniques, the process for finding suspected CUI location was shortened hundreds of times while delivered much higher accuracy and was extremely cost-effective compared with the traditional method. Furthermore, this in-house CUI inspection method was able to find suspected CUI locations in a straight section of pipelines and equipment which is normally out of any traditional guidelines. By investigating the identified CUI corrosion, a systematic improvement was adopted in order to mitigate risks by CUI from the plant. Some of the main improvement areas include the strength of the protective layer, the application of thermal sprayed aluminium, and preventive maintenance for insulation, etc.

CUPS issue has been deeply investigated by the company's corrosion committee and resulted in a strategy. For the avoidance of CUPS, immediate actions are required such as the installation of protective media between the pipe and support. In long-term and future projects, main-

No.	Item	Unit	Spec	Min	Max	Average	Quick comment
1	Iron	mg/kg	**1.00 max.**	0	0.58	**0.12**	Very low iron content & stable pH: corrosion situation is on moderate level
2	pH	-	**8 - 10**	9	9	**9**	
3	Chloride	mg/kg	**10 - 20**	2.30	16.30	**7.28**	
4	Ammonia	mg/kg	**2000 max.**	1,023	1,375	**1,254**	
5	Sulfide	mg/kg	**2000 max.**	348	724	**498**	
6	Delta P overhead	Kg/cm^{2}g		0.54147	0.65272	**0.60**	Stable delta P, a certain NH_4Cl salts deposition forms in the system but not fouling, removed by water
7	Electrical conductivity	µS/cm				**5,079**	

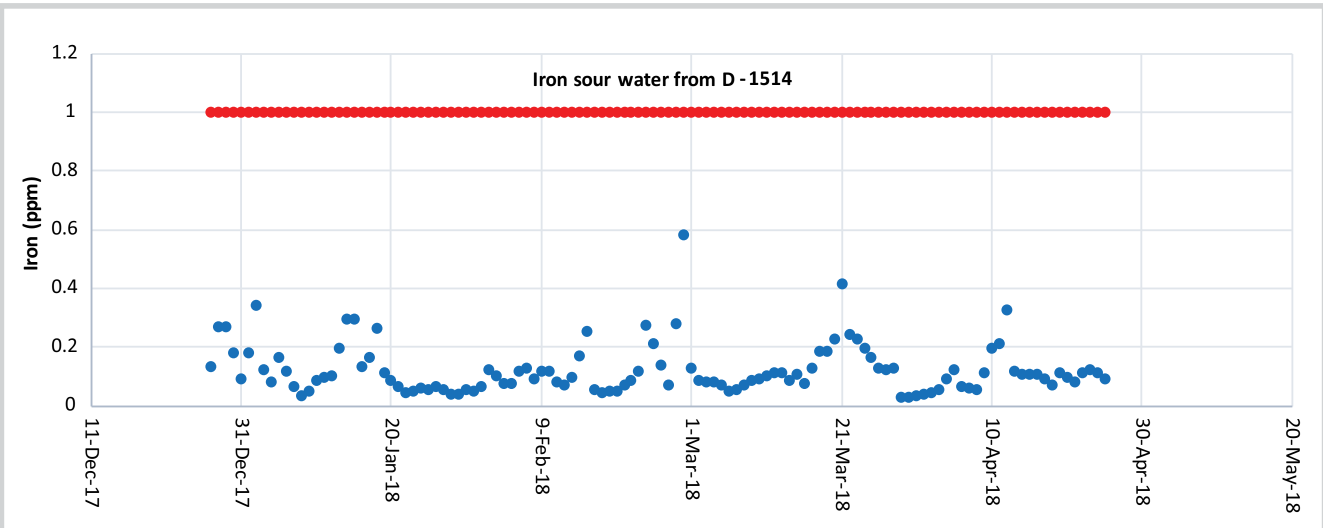

***Figure 4.** An example of corrosion monitoring of sour water.*

Figure 5. *Surveillance of wet insulation (area in red) by thermography camera.*

taining unique practices by having the shoe at the contact location of the pipe and support will help avoidance of CUPS.

The strategy for dead legs was recently reviewed and updated in accordance with API RP 2611 [5]. By employing the definition of dead leg in API PR 2611, some additional type of dead leg was added to the list. The updated list of dead legs demanded to enrich the inspection and testing methods for the detection of corrosion in these specialised objects. As soon as the inspection strategy was approved, all applicable solutions and practices such as line flushing or even removal of dead legs where possible, etc. were implemented in the plant.

4. Conclusions

Thanks to RBI study and utilisation of the modern monitoring system, corrosion threats have been properly addressed by BSR and appropriate strategies have been developed in a timely manner to secure the mechanical integrity of the plant. In parallel with enrichment of the management system, employment of advanced technologies is highly required in order to timely and effectively detect corrosion. Since the operational availability of the plant was maintained in the second quartile, as the latest result of refinery ranking by a well-known international organisation, it is understood that the strategy for securing the mechanical integrity of BSR has been successfully initiated.

Now and in the future, "aging equipment present a challenge to managing the integrity of plants" [6]. In order to maintain the mechanical integrity of the plant, in addition to implementation of the management system and new technologies, BSR needs to focus on developing and continuing the pro-active risk mitigation culture with the involvement of all employees. The culture will drive the continuous improvement process for the better mechanical integrity of the refinery and the sustainable development of the company.

References

1. Markus Kottek, Jürgen Grieser, Christoph Beck, Bruno Rudolf, Franz Rubel. *World Map of the Köppen-Geiger climate classification updated. Meteorologische Zeitschrift*. 2006; 15(3): p. 259 - 263.

2. API Recommended Practice 571. *Damage mechanisms affecting fixed equipment in the refining industry*. API Publishing Services.

3. NACE SP0198-2010. *Standard Practice: Control of corrosion under thermal insulation and fireproofing materials - A systems approach*. NACE International. 2010.

4. API Recommended Practice 580. *Risk-based inspection*. API Publishing Services. 2009.

5. API Recommended Practice 2611. *Terminal piping inspection-inspection of in-service terminal piping systems*. API Publishing Services. 2011.

6. The Center for Chemical Process Safety. *Dealing with aging process facilities and infrastructure*. Wiley. 2018.

PETROVIETNAM JOURNAL
Volume 6/2019, p. 68 - 76
ISSN-0866-854X

Renewable energy business in oil companies - Case studies in Japan

Doan Van Thuan[1], Tu Vi Sa[2]
[1]Vietnam Petroleum Institute
[2]Vietnam Oil and Gas Group
Email: satv@pvn.vn

Summary

Renewable energy has been the top preference among new business domains of Japanese oil companies. Applying qualitative research method, the paper aims to analyse the practices of renewable energy projects in these companies, highlighting various influential factors on investment decisions in this field.

The fact is that five among seven Japanese oil companies choose at least one renewable energy sector as new business, including hydrogen stations, fuel cells, bio-fuel, biomass, solar energy, wind energy and geo-thermal. It is stakeholders concerned such as governmental agencies, consumers, users, suppliers, competitors, shareholders, investors, and employees that have impacts on a company's policies toward renewable energy. Especially, in Japanese oil companies, the important internal motivation is business transformation into total energy companies. Besides, national policies are the catalyst for renewable energy investment in most of the cases.

However, in order to retain the business, profits are the crucial element which could be granted through feed-in tariff (FIT) mechanism. Over the time, FIT, an economic instrument of the government, would be reduced as renewables become more cost competitive with traditional energy sources. In turn, companies' efforts to manage production cost and output quality as well as to enhance internal capacity or international co-operation would play a significant role in making renewable energy business become sustainable in the long run.

Key words: Renewable energy business, total energy companies, feed-in tariff (FIT), triple bottom line, Japanese oil companies.

1. Introduction

In the 21st century, noticeable fluctuation in crude oil prices and larger decline in this natural resource have been frequently observed. In the petroleum companies of which the business greatly depends on crude oil importation from overseas as in the case of Japanese oil companies or on crude oil exploration and production such as the Vietnam Oil and Gas Group (PVN), there has been an orientation toward renewable energy as the possible synergic options.

Based on available data, interviews and observations obtained from JCCP training course in 2017 together with recent public statistics and documents, we would analyse the best practices in the Japanese oil companies in terms of (i) identifying driving forces for renewable energy projects; (ii) determining whether or not renewable energy could be sustainable business. These might give some useful implications and reflections to PVN in the context of crude oil price changes and exhaustion of these stock resources, and the renewable energy business of PVN might be taken into consideration.

Date of receipt: 3/8/2018. Date of review and editing: 3/8/2018 - 25/2/2019.
Date of approval: 3/6/2019.

2. Theoretical framework

The most well-known concept of sustainability was first introduced in the Brundtland Report [1], stating that sustainable development is to meet the needs of the

Figure 1. *The triple bottom line [3].*

***Table 1.** Application of renewable energy [7]*

Solar	Power generation	Photovoltaic	Si, Ga-As, CIS, others
		Steam turbine	Tower
			Trough
		Updraft tower	
	Heat	Hot water, hot air	
Wind	Power generation	Mountain, land	
		Onshore	
		Offshore	Fixed-bottom floating
Biomass	Power generation	Direct combustion	
		Methane fermentation	
	Heat	Direct combustion	
		Methane fermentation	
	Transportation fuel	Bio-ethanol Bio-diesel, bio-aviation fuel	
Hydro	Power generation	Low heat hydro power	
Geothermal	Power generation	Binary turbine	Hot water
		Flush type	Steam
Snow & Ice	Cold energy		
Thermal energy conversion	Ocean	Binary turbine	
	River		
Underground heat	Air conditioning	Geothermal heat pump	
Ocean	Power generation	Wave, tide power, tide current	

present without compromising the ability of future generations to meet their own needs. Since that landmark record, there have been various definitions of sustainable development. The Organisation for Economic Co-operation and Development (OECD) presented the idea of developing in a way that benefits different sectors, across borders and even between generations. The central of sustainable development is to deal with three pillars together: society, economy and environment [2].

In the spectrum of sustainability, from the business point of view, the notion of the triple bottom line has been widely used. One is the traditional quantity of corporate profits. The second is the bottom line of people account, a measure in how socially responsible an organisation has been throughout its operations. The third is the line of the planet account, a degree of being environmentally friendly [4]. The triple bottom line captures the essence of sustainability by measuring the impact of an organisation's activities including both profitability, shareholder values and its social, human and environmental capital.

From the environmental science perspective, natural resources can be classified between stock and flow resources [5]. Whereas stock reserves such as plants, animal populations and mineral deposits, have the characteristic that today's use has implications for tomorrow's availability; flow resources, solar radiation, power of wind, of tides, of flowing water for instance, are naturally replenished, using more renewable resources today does not itself have any implications for the availability of those tomorrow. Renewable energy projects have some unique features besides the common characteristics of industrial projects. Although most forms of renewable energy are naturally available and cheap to operate, they are relatively expensive to install, as they have to take dispersed energy and concentrate it into a useful form. Regarding technology aspect, this often required the technical design feasibility of advanced technologies and adequate quality, preferably approved systems (i.e. following a defined standard). About the project site, an investor must be assured to have access to the site for construction and operation of facilities for the term of contracts. Another important feature is the off-take agreement, a PPA (Power Purchase Agreement) or other agreements including the terms of energy sale, and any other outputs of the project that generate funds [8].

The following section would study actual operating results of renewable energy projects in Japanese oil companies.

3. Analysis

The Japanese oil industry consists of seven private companies supplying around 50% of primary energy, relying on overseas resources mainly from the Middle East. In recent years, the industry faces significant competition

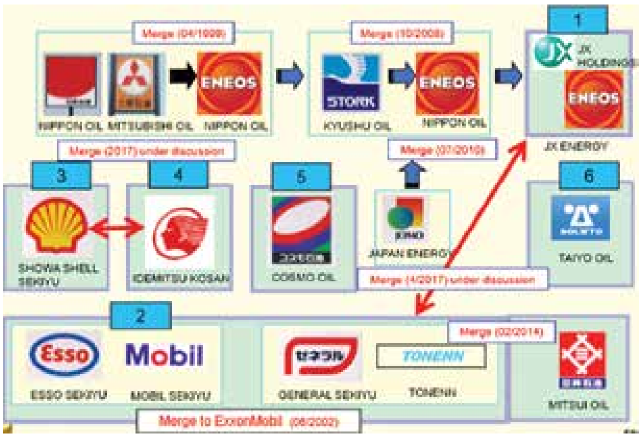

Figure 2. Oil companies in Japan [9].

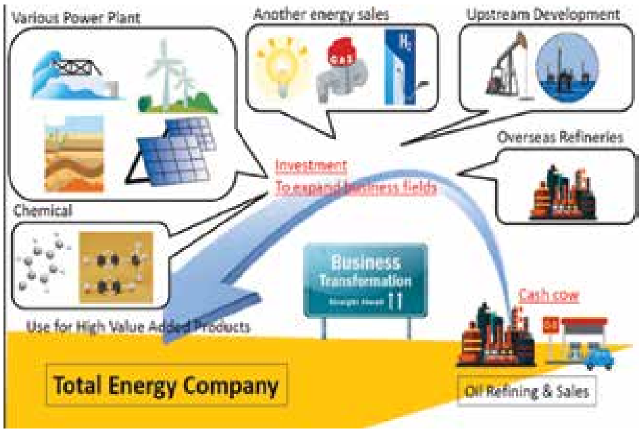

Figure 3. Toward total energy companies [9].

Table 2. New business domains of Japanese oil companies [9]

Company	Petrochemical	Crude Oil Exploration	IPP	EV Station	Hydrogen[1] Station	Bio Fuel	Fuel[2] Cell	Solar	Wind	LNG	Geothermal	Solvent	Specialty Chemical	Power Supply	Steam Supply	Electric Devices	Coal	GTL	Uranium Mining
JX	Y	Y	Y	Y	Y	Y	Y	Y	Y	Y		Y	Y	Y			Y	Y	
Idemitsu	Y	Y	Y	Y	Y	Y		Y	Y		Y	Y	Y	Y	Y	Y	Y		Y
Showa Shell	Y		Y	Y	Y		Y	Y		Y				Y	Y				
Cosmo	Y	Y	Y	Y	Y	Y	Y	Y	Y	Y						Y		Y	
Exxon Mobil	Y		Y									Y	Y						
Taiyo	Y	Y																	
Mitsui	Y	Y									Y								

Y Top runners   Y Cooperating with national policies   Y Doing business   No business

and shrinking in the domestic oil market. Therefore, most of them have been seeking diversification and business transformation to be more efficient. The latest trend is to become total energy companies.

There have been six among nine renewable energy categories depicted in Table 1, occupying one third of new business domains of Japanese oil companies, including: 1. hydrogen station, 2. fuel cells, 3. bio-fuel, biomass, 4. solar energy, 5. wind energy, 6. geo-thermal. Five among seven companies choose at least one renewable energy sector as a new business. The below part reviews missions and strategies of these five oil companies about renewable energy.

3.1. JXTG Nippon Oil and Energy Corporation, "a comprehensive energy company, supplying various forms of energy to meet customers' need" [10]

Hydrogen stations, fuel cells:

- Hydrogen stations[3]: As of 31 July 2016, JXTG has operated 37 hydrogen stations in 9 prefectures of Japan, accounting for about half of all hydrogen stations in Japan.

- Fuel cells: JXTG has proposed a dedicated fuel for fuel cell vehicles, also focused on new business utilising in- house technology, SOENE house fuel cells with the target of 300 thousand cells to be sold per year [9].

Solar power: In 2016, JXTG operated 14 mega solar

[1]The Government of Japan and Tokyo Metropolitan Government have announced to showcase the potential of hydrogen to the world at the Tokyo 2020 Olympic and Paralympic Games. Thereafter they will spread the technology worldwide so as to promote a hydrogen - based society. [2]Fuel cells have high environmental compatibility that release no hazardous materials because power is generated by reaction between hydrogen and oxygen. [3]JXTG is a Tokyo 2020 Gold Partner to encourage fuel-cell vehicles (games official vehicles and buses connecting venues) and developing hydrogen supply systems in the Olympic Village (hydrogen stations, hydrogen pipelines).

power plants across Japan, with a total generating capacity of around 40 million kWh/year.

Bio-fuel

- Kawasaki Biomass Power Plant (28,000kW) of which power generated will be purchased by JX that leases the land for the plant [10].

- JX, IHI Corporation, and Denso Corporation formulated the Council to promote the growth of micro algae fuel in June 2012. A structure of 10 private companies, encompassing these 3 companies, will hasten the application of micro algae fuels by starting up an integrated production system for such fuels by 2020.

Wind power: In March 2005, JXTG opened wind generation facilities in Kashima Oil Refinery. These facilities produced 3,685 million kWh of electricity. However, it was the last wind turbine built by the group.

3.2. Idemitsu Kosan Co. Ltd. has been making efforts to “introduce renewable energy that has less impacts on the environment than conventional energy” [12]

Bio-fuel, biomass:

- Biofuel business: cultivating, securing feedstocks, producing, distributing and marketing fuel in Southeast Asia. Currently, Idemitsu is studying cassavas, palm oil in Indonesia, Malaysia and founded bioethanol business in Cambodia.

- Biomass power generation: Tosa Green Power Co. Ltd. with an output capacity of 6,250kW, 50% of its shares are held by Idemitsu. Fukui Green Power Co., Ltd. with an output capacity of 7,000kW, 10% of its shares are held by Idemitsu. Both are in operation.

Wind power: Jointly operating Futamata Wind Development Co., Ltd. with Japan Wind Development Co., Ltd., which is the first wind power plant combined battery in Japan.

Hydrogen: Joining phase 2 of JHFC[4] as a co-operative company; a commercial hydrogen station has been constructed at Narita Airport.

Geothermal:

- Since March 2017, setting up a 5MW geothermal power plant in Japan’s south-western prefecture of Oita.

- Carrying out surveys in Amemasudake district of Hokkaido prefecture, Oyasu district of Akita prefecture, Bandai district of Fukushima prefecture

Solar power: Starting 3 solar power plants, namely "Moji" in Fukuoka prefecture in November 2013, "Himeji" in Hyogo prefecture in March 2014 and "Onahama" in Fukushima prefecture in November 2014.

3.3. Showa Shell Sekiyu Group's goal is to be “an energy solution provider supplying safe and sustainable energy” [13]

Solar power: The group began developing solar technologies since the oil crisis in the 1970s, containing crystalline and amorphous silicon. Then the group uncovered the advantages of CIS (Copper-Indium-Selenium) which were put in commercial production in 2007. Since this event, Atsugi Research Centre, a world-record-setting R&D facility, and a new production plant followed in 2009. By early 2011, the group had initiated the world’s first gigawatt-scale CIS production facility and had been active in the global market.

Hydrogen stations, fuel cells: Participated in JHFC: (1) validated technologies to resolve issues: high-pressure recharging to extend cruising distances, quick refueling; (2) created initiatives to rationalise regulations on building hydrogen supply infrastructure. Since 2017, the Group and Idemitsu have been under negotiation for merging. As a result, they have loosen their mind in this sphere.

3.4. Cosmo Energy Holdings, “a vertically integrated global energy company, focuses on renewable energy to diversify the energy supply” [14]

Wind power: Since 2014, Cosmo Oil has become a head of shareholders of EcoPower (formed in 1997). It has power generation capacity of 184,000kW at its 22 areas, as of 31 March 2016, and ranks third in the domestic industry based on generation capacity. The group plans to expand business over the long term by broadening land-based sites together with participating in offshore projects. The Akita offshore wind farm project is a large-scale one led by the private sector. The total wind power generation capacity of Cosmo was expected to reach about 230,000kW in 2017.

Solar power: CSD Solar, which was established jointly with another company, had been steadily supplying power at 8 locations nationwide, as of July 2016.

[4]JHFC: Japan Hydrogen and Fuel Cell Demonstration Project, http://www.jari.or.jp/portals/0/jhfc/e/jhfc/index.html. [5]The first Fuel Cell Vehicles (FCVs) on the road with type IV tanks were the Toyota FCHV, Mercedes-Benz F-Cell and the GM HydroGen4.

Biofuel: In 2007 Japan's petroleum industry kicked off a demonstration project for trial sales of bio-gasoline, a regular gasoline mixed with bio-ETBE. The trial was expanded in 2008 to involve 100 service stations, enclosing 9 owned by Cosmo Oil. The company also conducted R&D in bioethanol and BTL (biomass to liquid). However, the group found biofuel not attractive right now because of high costs.

Hydrogen stations, fuel cells: As part of JHFC, Cosmo began operating Yokohama-Daikoku hydrogen station in 2002. In 2008, the group began the type IV hydrogen tanks for compressed hydrogen at 700 bars (70MPa; 10,000psi). In the stationary fuel cell business, based on the results of a demonstration project carried out in 2005, Cosmo intended to bring LPG fuel cell systems to the market in 2009. However, in 2013 the company closed its demonstration site of hydrogen station in Yokohama, along with the LPG fuel cell system.

Table 3. *Renewable laws and policies in Japan from 1995 to present, excluding hydraulic power*

In general	Energy policy is to ensure stable supply (Energy Security) at low cost by enhancing efficiency (Economic Efficiency) on the premise of Safety. It is also important to make efforts to pursue environment suitability (Environment) (3E + S)[16].
In 1995, the Electric Utilities Industry Law was revised to let corporations with electric generation capabilities sell electric power to utilities. In 2000, further revisions allowed direct sale of electricity to major users. In 2012, the Act on Purchase of Renewable Energy Sourced Electricity by Electric Utilities introduced a feed-in tariff (FIT) regime, by requiring electric utilities to purchase electricity generated from renewable energy sources based on a fixed-period contract with a fixed price. In 2015, the Government published a Long-term Energy Supply and Demand Outlook to present the ideal structure of energy supply and demand for 2030. Energy efficiency and renewable energy were expected to take an essential part. The Act on Special Measures Concerning Procurement of Renewable Energy Sourced Electricity by Electric Utilities (2011) promoted the use of renewable energy sources for electricity. The Act was amended on 03 June 2016, announcing a new certification system for FIT eligibility and a tender bid system for FIT, initially for large-scale solar projects [17].	
Incentive programmes for wind energy	The government has committed to the construction of a high voltage transmission network to help wind producers gain grid access. In 2016 and 2017: FIT and relaxed rules for onshore wind farms in harbours and ports have been proposed.
Incentive programmes for solar energy	In 2016, METI (Japanese Ministry of Economy, Trade and Industry) FIT pricing committee stated to reduce rates by 11.15% for over 10kW solar usage, which was a sign of tightening government budgets and a period of decreased incentives. To promote the use of photovoltaic cells in households, the Government offered installation cost subsidies.
Incentive programmes for biomass/bio-fuel	As for biofuel, which are mostly imported, the government continues the introduction of such fuel while taking into account international situation and technology trend concerning next-generation biofuel. For woody biomass power generation: increase biomass energy by pursuing scale merit and adopting mixed combustion at existing thermal power plants. It refers to regionally-distributed energy sources in addition to keeping up Japan's precious forests and vitalising forest industry [16].
Incentive programmes for hydrogen	1. Japan Hydrogen and Fuel Cell Demonstration Project - JHFC (supported by METI): Objectives of phase 1 (2002 - 2005): (i) clarified the high energy efficiency of FCV; (ii) defined "Well to Wheel" efficiency: from the mining of the primary energy, production, transportation and filling, driving vehicles with demonstration data of FCVs and hydrogen stations. Objectives of phase 2 (2006 - 2010): (i) resolved issues in practices; (ii) set up regulations, codes, standards; (iii) public relations, dissemination, promotion; (iv) verified energy saving (fuel economy) and environmental impacts; (v) determined technology, policy trends of FCVs, small fuel-cell powered vehicles and hydrogen engine vehicles with hydrogen infrastructures. 2. Strategic Roadmap for Hydrogen and Fuel Cells (2014) of METI has set a target to build around 160 hydrogen stations by the year 2020 [18]: Phase 1: expand the applications for fuel cell technology (fuel cells for households, FCVs), target to achieve dramatic energy conservation plus acquire a new global market (scheduled to begin in 2014). Phase 2: create a system for supplying hydrogen using unconventional energy resources imported from other countries. At the same time enhance energy security measures, full-fledged introduction of hydrogen power generation (time frame: putting the technology into practice by the late 2020s). Phase 3: organise a carbon-dioxide-free hydrogen supply system using renewable and other energy (time frame: putting the technology into practice around 2040).
Incentive programmes for geo-thermal	Geothermal energy is expected to increase to 1.0 - 1.1% of primary energy by 2030 [19]. METI is considering 36 geothermal projects in addition to the 537MW of capacity at the 17 facilities which currently exist. Moreover, METI is targeting to raise geothermal capacity by another 50MW by 2020. The FIT was also suggested in 2012 to accelerate geothermal power [17].

3.5. Mitsui has been working on geothermal energy by leveraging their experiences in E&P

The company has begun the business by conducting a joint survey in Hokkaido and Akita prefecture in 2012. At present, it has participated in 5 projects in Hokkaido and Tohoku area. Among these, for the Matsuo-Hachimantai Project in Iwate prefecture, the company decided to move to the development phase in February 2017 and constructed a geo-thermal power plant [15].

In order to explore Japanese oil companies' motivations into renewable energy, a preview of legal documents since 1995 has been made as in Tables 3 and 4.

We can see that each company has its own motivations which fall into three categories as noticed in Table 2: (i) co-operating with national policies, (ii) doing business or (iii) private options.

Regarding hydrogen and fuel cells, four companies have complied with JHFC: JXTG is the top runner, consistently expands hydrogen supply business (advancement of small size and highly efficient hydrogen production equipment using petroleum-based fuels such as LPG, naphtha and kerosene). Moreover, the group founded the ENEOS Hydrogen Trust Fund in 2006 (with the initial contribution of USD 14 million) for innovative and pioneering research. Each year this fund provides up to USD 500 thousand or USD 900 thousand per project. Idemitsu joined phase 2 of JHFC as a co-operative company, building one hydrogen station. While Showa Shell is not interested in this field anymore and Cosmo closed the demonstration site in 2013. The reasons are that hydrogen stations are considerably expensive and that lack of demand (expansion of fuel cell cars) restricts investment in building hydrogen stations. Currently, only 101 hydrogen stations are in operation among 34,000 gas stations.

Considering bio-fuel, Idemitsu takes the lead in feedstocks, production, distribution and marketing in Southeast Asia. Whereas JXTG has involved through leasing the land for the biomass power plant, and been at the initial stage of producing algae. From Cosmo's perspective, biofuel is not attractive right now because of high costs.

On the other hand, there are four companies doing well with solar power generation. Since the FIT system was launched in 2012, Idemitsu has been running three solar power plants. JXTG has been actively engaged in the mega solar power generation business using its idle lands. It has been developing next-generation CIS thin-film solar cell technologies and manufacturing solar panels with the total production capacity of more than 1,000MW per year. Solar Frontier (a subsidiary of Showa Shell) provides solar energy solutions and sells the CIS panels all over the world (Europe, the U.S, the Middle East, and Asia). Showa Shell's ambition is to become not only a mega solar operator, but also a global PV panel supplier. Cosmo recognises mega solar power generation as part of their green power business.

Concerning wind power generation, Cosmo is the pioneer, steadily running power generation facilities and achieving higher earnings over time. Wind power is another zone of Idemitsu green power whilst JXTG has not operated any wind turbine since the last one in Kashima refinery.

Last but not least, about geothermal, Mitsui Oil Exploration Co., Ltd. has been in partnership with Idemitsu Kosan Co. Ltd. to pursue commercialisation studies on geothermal power generation since 2011. The current project of Idemitsu in Oita (5MW geothermal power plant) will be one of the largest binary power plants in Japan.

In summary, it is obvious that Japanese oil companies' strong commitments to the environment and society

Table 4. *Tariffs for solar PV, wind power, geothermal power [20]*

		Solar PV		Wind power		Geothermal power	
Procurement category		≥ 10kW	< 10kW (purchase of excess electricity)	≥ 20kW	< 20kW	≥ 15,000kW	< 15,000kW
Costs	Installation cost (USD/kW)	2,593	3,954	2,778	11,574	7,315	11,389
	O&M costs (USD/kW/year)	83.4	39.8	55.6	-	305.6	444.4
Pre-tax IRR		6%	3.2%	8%	1.8%	13%	
Procurement price/kWh	Tax inclusive (UScent/kWh)	36	38	22	55	18.6	40
	Tax exclusive (UScent/kWh)	33.3	35.2	20.4	51	24	37
Duration		20 years	10 years	20 years	20 years	15 years	15 years

could be defined as one of the first driving forces toward renewable energy. Besides, national policies are the catalyst for renewable energy investment. However, in order to retain the business, returns are the crucial element.

4. Discussion

This section focuses on the driving forces toward renewable energy and discusses to what extent renewable energy could be sustainable business.

4.1. From the government point of view, in 2016, Japan ratified UNFCCC-Paris Agreements, aiming to attain a reduction of 26% in greenhouse gas emissions. It is global trends, international treaties which are driving renewable energy policies forward. In Japan, social attention is another influential factor. Prior to the Fukushima nuclear accident (initiated primarily by the Tsunami following the Tōhoku earthquake in 2011), nuclear power generated approximately 30% of Japan's energy. Since the disaster, almost all Japan's nuclear power stations have been switched off due to people's concerns and there have been unprecedented renewable energy opportunities in Japan [17].

From the company aspect, stakeholders such as political and governmental affairs, consumers, users, suppliers, competitors, shareholders, investors, and employees have vital influences on the company's policies. Companies run for profits (as desired by shareholders, investors, etc.) at the same time make great efforts for environmental protection (as expected by the government, consumers for instance). Particularly in Japanese oil companies, conserving nature is set as their own mission to fulfill. The other internal motivation of Japanese oil companies is business transformation toward total energy companies and renewable energy is top consideration among their new business domains.

Moreover, it is essential to emphasise that in most Japanese oil companies, the key making changes happen in investment for renewable energy is profits which are mostly effected by FIT. This is an instrument of governments to provide renewable energy producers long-term contracts to purchase energy at a set price, normally based on the cost of production plus an additional incentive. The approach actually have two different offers: (1) providing a price high enough to promote the desired investment; (2) guaranteeing the stability of that price rather than forcing investors to face market uncertainties [6]. The "well-adapted feed in tariff regimes are generally the most efficient and effective support schemes for promoting renewable electricity" [21]. In Japan, for instance, the share of renewable electricity, which was 9% in 2011, has increased to 15% in 2016 (Figure 4), due to the enforcement of the FIT Act (2012). Accordingly, renewable energy has become the third largest energy source after liquefied natural gas (LNG) and coal. In fact, the FIT Act has opened new perspectives toward making renewable energy the main energy source in Japan [16].

4.2. The second question of whether or not renewable energy could be profitable business and sustainability would be tough to clarify. Except the case of hydrogen and fuel cells which are in the R&D and pilot stage, the others have already been in the commercial scale, facing certain obstacles:

Financial challenges: In Japan, at the moment, the country has one of the most generous FIT schemes in the word [17]. For example, the tax exclusive procurement price is 20.4 cents/kWh for wind power projects with the capacity above 20kW or 51 cents/kWh for wind power capacity below 20kW (Table 4). However, this tariff would be decreased as renewables become more cost competitive with traditional energy sources. Consequently, dramatic change in the market is predicted as illustrated in Figure 5.

Technical challenges associated with the penetration

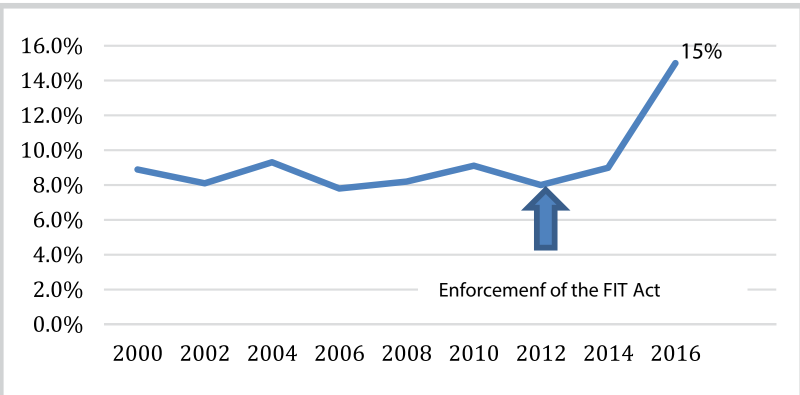

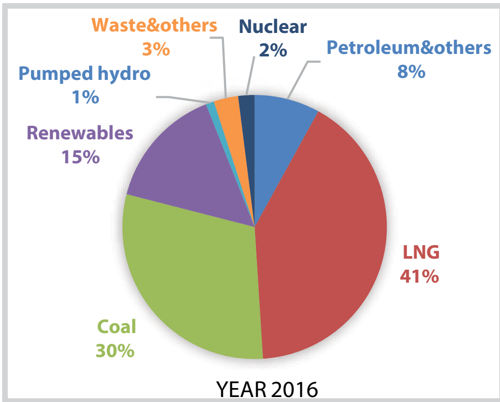

Figure 4. *Changes in the share of renewable energy in total electricity generated and purchased in Japan before and after the FIT Act [11].*

of renewable energy sources such as wind power are (i) lack of frequency regulation capacity, (ii) production of surplus power, (iii) increase in system voltage, (iv) insufficiency of available transmission capacity [22].

Site challenges: in the case of Cosmo wind power projects, the company had to go through 12 procedures and 11 related laws[6]. In the situation of geothermal, nearly 80% of Japan's geothermal resources are located within national parks or protected hot springs, designated restricted zones with limits on types and locations of work that can be done. It is strict regulations, complicated environmental impact assessments and zoning restrictions that continue to be barriers for geothermal power.

Overcoming these challenges is the necessity, but not the warranty for renewable energy to be sustainable business.

The companies could expect more incentives from the government, requesting FIT to be increased. However, for the time being, the overall trend for FIT as mentioned above is intended to be reduced as renewables become more cost competitive with traditional energy sources [21]. Alternatively, efforts from the company itself to reduce the costs are prerequisite. Cost reduction together with supports from the government would maximise companies' margins. For example, despite the fact that Japan

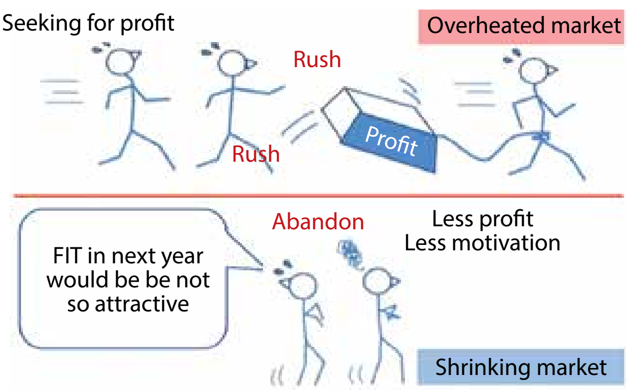

***Figure 5.** Basic image of FIT [7].*

is ranked first on the International Trade Administration list of top solar export markets in 2016, it has encountered increasing competition from Chinese manufacturers [17]. The oil companies doing business in this sector like JXTG, Showa Shell, Cosmo, and Idemitsu might need to reform in order to adapt in the competitive overseas market as well as changes in national policies (In 2016, METI FIT pricing committee stated to reduce rates by 11.15% for over 10kW solar usage, which was a sign of tightening government budgets and a period of decreased incentives, Table 3).

4.3. Further analysis in the best practices in Japanese oil companies would give some implications and reflections to PVN

In terms of cost management in renewable energy projects, in Cosmo's wind power projects for instance, all stages of development, EPC, power generation and O&M are carried out within the group. Some would suggest PVN utilise its own capacity in every stage of projects, or localise equipment and technologies. However, it might be not feasible because it is difficult for a Vietnamese company to manufacture all equipment while the local market is not big enough or it is not easy to self-implement in every phase of a project when internal factors and options for improvement are limited.

Referring to starting up a new business, it does take time. Showa Shell Sekiyu Group began developing solar technologies since the 1970s and had first commercial production 37 years later (2007). Also, in the 1970s, Idemitsu has involved in geothermal resources. After 26 years, in 1996 it began supplying geothermal steam to Kyushu Electric Power Co. Inc.'s Takigami Power Plant in Oita Prefecture. More than 10 years ago, so as to boost the hydrogen-based society and fuel cell industry, the Japanese government launched the demonstration project (JHFC), encouraging oil companies to participate. Since then, JXTG has been the top runner with the Hydrogen

6

Procedures to Japanese Government	*Related Japanese Laws*
Notification of land transaction	*National Land Planning Act*
Application for development permission	*City Planning Act*
Application for permission of diversion of agricultural land	*Agricultural Land Law*
Application for forest land development	*Forest Law*
Notification of deforestation and reforestation	*Forest Law*
Notification of civil engineering works of the land (archaeological culture asset)	*Law for the Protection of Cultural Properties*
Notification of change of the land character	*Soil Contamination Countermeasures Act*
Application for permission of new structure construction	*National Park Law*
Application for permission of structure installation in the riverside area	*River Law*
Environmental impact assessment	*Environmental Impact Assessment Law*
Necessary procedure pertaining to other laws	*Radio Law*
Necessary procedure pertaining to other laws	*Aviation Law*

Trust Fund for innovative research and gradually grew hydrogen supply business.

Other companies which did not have an early start, choose to collaborate with the pioneers. Cosmo, in 2014, has been a head of shareholders (89% share) of EcoPower (formed in 1997), ranking third in the domestic wind electricity industry. Mitsui, in 2012, has co-operated with Idemitsu in geo-thermal energy.

Some companies are taking their own advantages or experiences to start renewable energy business. For instance, JXTG is utilising technologies and know-how of petroleum refining to produce small size, highly efficient hydrogen production equipment using petroleum-based fuel. Whereas, Mitsui has been jointly working on geothermal energy by employing experiences in E&P.

These are some practical lessons which could be drawn for PVN, in terms of project management, internal capacity improvement, advantage ultilisation or international co-operation on the roadmap toward renewable energy business.

5. Conclusion

Case studies of oil companies from Japan have revealed the fact that renewable energy business has spread as a prevailing tendency but the speed substantially depends on the philosophy of each country, technology innovation and business models targeted by the companies. FIT, an economic instrument of the government is recognised as the most influential agent. In Japan, 9% share of renewable electricity in 2011 has risen to 15% in 2016, due to the enforcement of the FIT Act (2012). However, FIT would be reduced as renewables become more cost competitive with traditional energy sources. It is companies' efforts to manage production costs, output quality, enhance internal capacity that can play a significant role in making renewable energy business become sustainable in the long run.

References

1. Brundtland report. *World Commission on Environment and Development*. 1987.

2. Tracey Strange, Anne Bayley. *Sustainable development: Linking economy, society, environment*. OECD insights. 2008.

3. Trish Sissons. *Cause marketing and corporate social responsibility*. www.sponsifi.com.

4. Agnieszka Żak. *Triple bottom line concept in theory and practice*. Research papers of Wroclaw University of Economics. 2015; 387: p. 251 - 264.

5. Roger Perman, Yue Ma, James McGilvray, Michael Common. *Natural resource and environmental economics (3rd edition)*. Pearson Education Limited. 2013.

6. Tom Tietenberg, Lynne Lewis. *Environmental & natural resource economics (9th edition)*. Pearson Education Limited. 2011.

7. Bunsuke Kariya. *Renewable energy in Japan*. Japan Cooperation Center Petroleum. 2017.

8. US Department of Energy. *Developing renewable energy projects larger than 10 MWs at federal facilities - A practical guide to getting large-scale renewable energy projects financed with private capital*. Federal Energy Management Program. 2013.

9. Bunsuke Kariya. *Oil industry in Japan*. Japan Cooperation Center Petroleum. 2017.

10. CSR report. *JXTG Nippon Oil and Energy Corporation*. 2016.

11. Keiji Kimura. *Feed-in tariffs in Japan: Five years of achievements and future challenges*. Renewable Energy Institute. 2017.

12. www.idemitsu.com.

13. www.showa-shell.co.jp.

14. www.cosmo-oil.co.jp.

15. www.mitsui.com.

16. METI. Strategic energy plan. 2014.

17. DLA Piper. *Renewable energy in the Asia Pacific (4th edition)*. 2017.

18. METI. *Strategic roadmap for hydrogen and fuel cells*. 2014.

19. METI. *Long-term energy supply and demand outlook*. 2015.

20. Japan Oil, Gas, Metals National Corporation. *Current situation of geothermal power generation in Japan*. 2016.

21. David Timmons, Jonathan M.Harris, Brian Roach. *The economics of renewable energy: A GDAE teaching module on social and environmental issues in economics.* Global Development and Environment Institute, Tufts University, Medford, MA. 2014.

22. Norikazu Hatta. *Current status and issues of wind power business in Japan*. Cosmo Energy Holdings, Japan Cooperation Center Petroleum JCCP. 2017.

IEA consecutively cuts oil demand growth forecast

In its latest monthly Oil Market Report, the International Energy Agency (IEA) cuts its forecast for global demand growth in 2019 for a second consecutive month. It is now projected at 1.2 million barrels/day, reduced from 1.3 million barrels/day in the previous report and 1.4 million barrels/day in the April report.

2020 vision

In the Oil Market Report released in 14 June 2019 [1], IEA publishes their first outlook for 2020. So volatility has returned to oil markets with a dramatic sell-off in late May seeing Brent prices fall from USD 70/barrel to USD 60/barrel. Until recently, the focus has been on the supply side with the familiar list of uncertainties - Iran, Venezuela, Libya, and the Vienna Agreement - lifting Brent prices above USD 70/barrel in early April and keeping them there until late May.

IEA noted that the main focus curently is on oil demand as economic sentiment weakens. In May, the OECD published an outlook for global GDP growth for 2019 of 3.2%, lower than their previous assumption. World trade growth has fallen back to its slowest pace since the financial crisis ten years ago, according to data from the Netherlands Bureau of Economic Policy Analysis and various purchasing managers' indices. The consequences for oil demand are becoming apparent. In 1Q19, growth was only 0.3 million barrels/day versus a very strong 1Q18, the lowest for any quarter since 4Q11. The main weakness was in OECD countries where demand fell by a significant 0.6 million barrels/day, spread across all regions. There were various factors: a warm winter in Japan, a slowdown in the petrochemical industry in Europe, and tepid gasoline and diesel demand in the United States, with the worsening trade outlook a common theme across all regions. In contrast, the non-OECD world saw demand rise by 0.9 million barrels/day, although recent data for China suggest that growth in April was a lacklustre 0.2 million barrels/day. In 2Q19, IEA sees global demand growth 0.1 million barrels/day lower than in last month's Report. For now though, there is optimism that the latter part of this year and next year will see an improved economic picture. The OECD sees global GDP growth rebounding to 3.4% in 2020, assuming that trade disputes are resolved and confidence rebuilds. This suggests that global oil demand growth will have scope to recover from 1.2 million barrels/day in 2019 to 1.4 million barrels/day in 2020.

Meeting the expected demand growth is unlikely to be a problem. Plentiful supply will be available from non-OPEC countries. The US will contribute 90% of this year's 1.9 million barrels/day increase in supply and in 2020 non-OPEC growth will be significantly higher at 2.3 million barrels/day with US gains supported by important contributions from Brazil, Canada, and Norway. At the end of June, Vienna Agreement oil ministers, faced with short-term

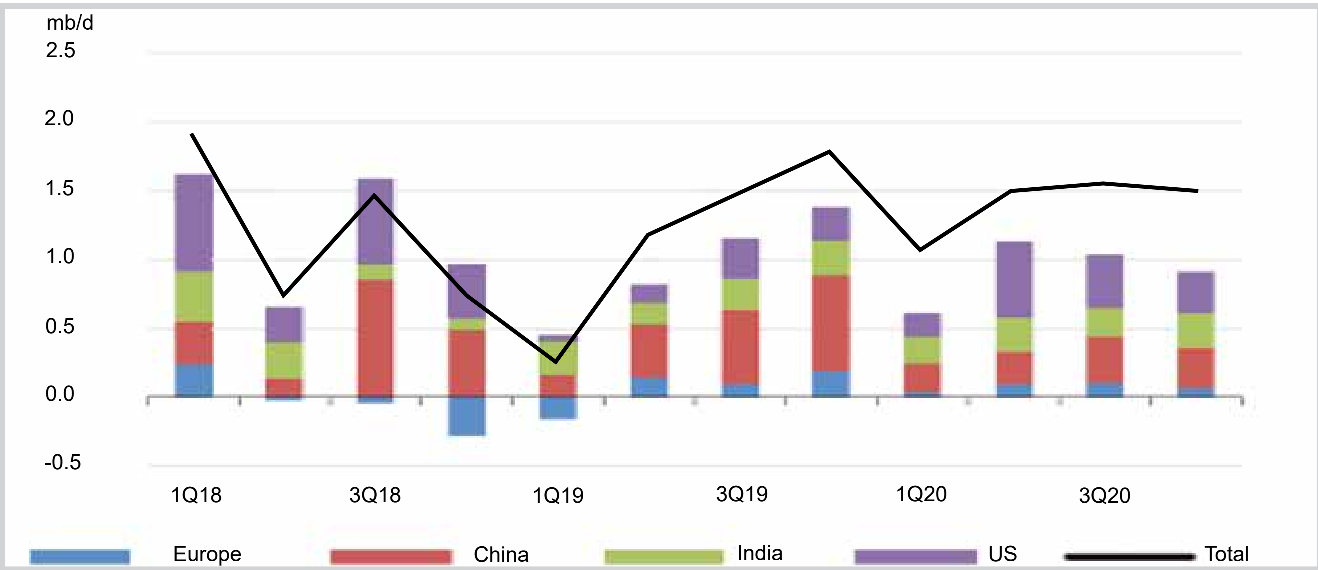

Figure 1. *Global oil demand growth, year-on-year (million barrels/day).*

uncertainty over the strength of demand and relentless supply growth from their competitors, are due to discuss the fate of their output deal. Ministers will note that OECD oil stocks remain at comfortable levels 16 million barrels above the five-year average. However, they will also note that although in 1Q19 weak demand helped create a surplus of 1.1 million barrels/day, in 2Q19 the market is in deficit by an estimated 0.4 million barrels/day, with the backwardated price structure reflecting tighter markets. This deficit is partly due to the fact that in May the Vienna Agreement countries cut output by 0.5 million barrels/day in excess of their committed 1.2 million barrels/day. In 3Q19, the market could receive further support from an expected pick-up in refining activity. Recently, high levels of maintenance in the US and Europe, low runs in Japan and Korea, and fallout from the Druzhba pipeline contamination contributed to weak growth in global refining throughput. This could be about to change: according to IEA's estimates, crude runs in August could be about 4 million barrels/day higher than in May. This might cause greater tightness in crude markets, particularly for sour barrels if the Vienna Agreement is extended and there is no change in the situations in Iran and Venezuela. Of course, much depends on the strength of oil demand later in the year.

A clear message from IEA's first look at 2020 is that there is plenty of non-OPEC supply growth available to meet any likely level of demand, assuming no major geopolitical shock, and the OPEC countries are sitting on 3.2 million barrels/day of spare capacity. This is welcome news for consumers and the wider health of the currently vulnerable global economy, as it will limit significant upward pressure on oil prices. However, this must be viewed against the needs of producers particularly with regard to investment in the new capacity that will be needed in the medium term.

Demand

For the second consecutive month, IEA has revised down their 2019 oil demand growth forecast, this time by 100 thousand barrels/day, to 1.2 million barrels/day. The bulk of the revision is in the OECD. IEA received lower March consumption statistics for the Americas, which drove their overall OECD 1Q19 growth estimate down by 360 thousand barrels/day versus last month's Report. Global oil demand is now estimated to have

***Table 1.** Global oil demand from 2018 to 2020 (million barrels per day).*

	1Q18	2Q18	3Q18	4Q18	2018	1Q19	2Q19	3Q19	4Q19	2019	1Q20	2Q20	3Q20	4Q20	2020
Africa	4.3	4.3	4.2	4.3	4.3	4.4	4.4	4.2	4.4	4.4	4.5	4.4	4.3	4.4	4.4
Americas	31.6	31.7	32.3	32.1	31.9	31.4	31.9	32.6	32.3	32.1	31.6	32.5	33.1	32.7	32.5
Asia/Pacific	35.0	34.7	34.3	35.1	34.8	35.4	35.2	35.2	36.1	35.4	36.0	35.9	35.9	37.0	36.2
Europe	14.8	15.0	15.5	14.9	15.1	14.7	15.2	15.6	15.1	15.2	14.7	15.3	15.7	15.2	15.2
FSU	4.5	4.6	4.9	4.8	4.7	4.7	4.8	5.0	5.0	4.9	4.8	4.8	5.1	5.0	4.9
Middle East	8.2	8.5	8.8	8.2	8.4	8.2	8.6	8.9	8.3	8.5	8.2	8.6	8.9	8.3	8.5
World	**98.5**	**98.8**	**99.9**	**99.4**	**99.2**	**98.7**	**100.0**	**101.4**	**101.2**	**100.3**	**99.8**	**101.6**	**102.9**	**102.7**	**101.7**
Annual Change (%)	2.0	0.7	1.5	0.7	1.2	0.3	1.2	1.5	1.8	1.2	1.1	1.5	1.5	1.5	1.4
Annual Change (mb/d)	1.9	0.7	1.5	0.7	1.2	0.2	1.2	1.5	1.8	1.2	1.1	1.5	1.5	1.5	1.4
Changes from last OMR (mb/d)	0.0	0.0	0.0	0.0	0.0	-0.4	-0.3	0.2	0.1	-0.1					

** Including biofuels*

risen by just 250 thousand barrels/day year-on-year (y-o-y) in 1Q19, the lowest annual growth registered since 4Q11, when the price of Brent crude oil averaged USD 109/barrel. Oil consumption fell in the OECD by 600 thousand barrels/day y-o-y and rose in non-OECD countries by 850 thousand barrels/day. A global economic slowdown, lower growth in the petrochemical industry and warmer than normal weather in the northern hemisphere were contributory factors. One should also bear in mind that annual growth in 1Q18 amounted to a significant 1.9 million barrels/day. This also contributed to low growth on a y-o-y basis.

This month, IEA has also revised down their 2Q19 growth estimates by 300 thousand barrels/day. China's April oil demand was 230 thousand barrels/day less than expected, owing to significant downgrades for diesel and LPG. However, these lower global estimates for 1Q19 and 2Q19 are partly offset by higher forecasts for 3Q19 (+200 thousand barrels/day) and 4Q19 (+80 thousand barrels/day) driven by lower oil prices and an expected rebound in petrochemical demand. IEA has also incorporated a new gross domestic product (GDP) forecast published by the OECD in May.

According to IEA, as for 2020, oil demand is expected to accelerate to 1.4 million barrels/day. Non-OECD countries will be the main drivers (+880 thousand barrels/day y-o-y), although the OECD will also contribute a significant 520 thousand barrels/day, helped by petrochemical cracker plant additions in the US and higher economic growth. On a fuel-by-fuel basis, diesel/gasoil will see solid expansion, as new rules implemented by the International Maritime Organisation (IMO) force ship operators to switch away from high sulphur fuel oil, the use of which will decline significantly.

Supply

According to IEA, stronger non-OPEC supply growth of 2.3 million barrels/day in 2020 - up from 1.9 million barrels/day this year - means the tightening of oil markets could prove short lived. The anticipated gains are such that even with higher demand growth versus 2019, the requirement for OPEC crude could drop to 29.3 million barrels/day in 2020, 650 thousand barrels/day below the group's production in May. In the near-term, global oil stock draws could be limited to 2Q19 and 3Q19, if OPEC output stays around current levels.

It is not as if OPEC has been pumping flat out. OPEC, Russia and nine other non-OPEC countries (OPEC+) have more than delivered on their 1.2 million barrels/day supply cut in the hopes of reversing the substantial stock builds of 2018. Output from the OPEC+ countries during May was 530 thousand barrels/day below their 44.3 million barrels/day target, which delivered compliance of 145%.

The over-performance is mainly from Saudi Arabia and Russia. Saudi Arabia led OPEC's compliance rate to 133% while the fallout from the Druzhba pipeline contamination saw Russia's output fall by 120 thousand barrels/day. OPEC+ is due to review its agreement at a meeting scheduled for 25 - 26 June in Vienna. Saudi Arabia has signalled that the curbs should be prolonged to avoid a market share battle with the US or a repeat of oil's collapse of five years ago.

The 2 million barrels/day reduction in OPEC+ supply since November's high, along with a combined loss of more than 1 million barrels/day from Iran and Venezuela, has helped clear the supply overhang. It has also left the producers with roughly 3.5 million barrels/day of spare capacity, 3.2 million barrels/day of which is held in OPEC. This is a useful insurance should Iranian and Venezuelan supplies fall further or in case of supply disruptions elsewhere. Output in Nigeria and Libya remains vulnerable due to ongoing civil unrest.

During May, global oil supply edged down 100 thousand barrels/day to 99.5 million barrels/day, nearly 3 million barrels/day below a November peak. The month-on-month (m-o-m) loss - led by Canada, Iran, Russia and Saudi Arabia - was mostly offset by higher supply from Brazil, the US, Iraq and biofuels. As for OPEC, plunging Iranian production and lower Saudi and Nigerian output cut crude supply by 230 thousand barrels/day to just under 30 million barrels/day, a five-year low. Non-OPEC supply rose 130 thousand barrels/day to 64 million barrels/day. Compared to a year ago, global oil supply was 620 thousand barrels/day higher. Driven by the US, non-OPEC output was up 2.1 million barrels/day, while OPEC was down 1.5 million barrels/day.

While supply growth in the US is forecast to slow to 1.3 million barrels/day in 2020 from 1.7 million barrels/day this year, expansions in other non-OPEC countries are set to accelerate. Norway is expected to show growth of 290 thousand barrels/day after declining by 130 thousand barrels/day this year and Brazil

Table 2. OPEC/Non-OPEC crude oil output[1] (Million barrels per day)

	Apr 2019 Supply	May 2019 Supply	Supply Baseline[2]	Agreed Cut	New Target	May Compliance (%)	Sustainable Production Capacity[5]	Spare Capacity vs May Supply[6]
Algeria	1.02	1.03	1.06	0.032	1.03	84	1.05	0.02
Angola	1.41	1.45	1.53	0.047	1.48	166	1.50	0.05
Congo	0.36	0.34	0.33	0.010	0.32	-150	0.35	0.01
Ecuador	0.53	0.53	0.52	0.016	0.51	-38	0.54	0.01
Equatorial Guinea	0.11	0.10	0.13	0.004	0.12	675	0.12	0.02
Gabon	0.20	0.20	0.19	0.006	0.18	-217	0.20	0.00
Iraq	4.65	4.78	4.65	0.141	4.51	-90	4.90	0.12
Kuwait	2.69	2.71	2.81	0.085	2.72	116	2.93	0.22
Nigeria[3]	1.75	1.69	1.65	0.053	1.60	-75	1.79	0.10
Saudi Arabia	9.81	9.70	10.63	0.322	10.31	290	12.02	2.32
UAE	3.05	3.05	3.17	0.096	3.07	123	3.39	0.34
Total OPEC 11	**25.58**	**25.58**	**26.66**	**0.812**	**25.85**	**133**		
Iran[4]	2.61	2.40					3.85	-
Libya[4]	1.16	1.16					1.10	-0.06
Venezuela[4]	0.83	0.81					0.81	0.00
Total OPEC	**30.18**	**29.95**					**34.55**	**3.21**
Azerbaijan	0.68	0.78	0.80	0.020	0.78	100		
Bahrain	0.21	0.21	0.22	0.005	0.21	120		
Brunei	0.13	0.13	0.12	0.003	0.11	-393		
Kazakhstan	1.70	1.77	2.03	0.040	1.99	637		
Malaysia	0.68	0.71	0.70	0.015	0.68	-60		
Mexico	1.92	1.91	1.99	0.040	1.95	195		
Oman	0.98	0.98	1.00	0.025	0.98	105		
Russia	11.57	11.44	11.75	0.230	11.52	132		
Sudan	0.08	0.08	0.07	0.002	0.07	-219		
South Sudan	0.16	0.14	0.12	0.003	0.12	-554		
Total Non-OPEC	**18.12**	**18.15**	**18.80**	**0.383**	**18.41**	**169**		

[1]OPEC figures are crude oil only. Non-OPEC figures are total oil supply (including NGLs); [2]Based on Oct-2018 production, except for Azerbaijan and Kuwait based on Sept-2018 and Kazakhstan Nov-2018 Non-OPEC supply baseline based on IEA estimates; [3]Nigeria supply baseline based on IEA estimates, which exclude Akpo and Agbami condensates; [4]Iran, Libya. Venezuela exempt from cuts; [5]Capacity that can be reached in 90 days and sustained for an extended period; [6]Spare capacity excludes Iranian crude supply that is offline due to sanctions.

is projected to ramp up by a further 330 thousand barrels/day following a 240 thousand barrels/day increase this year. Canada and Russia will also post gains assuming production restraints are lifted.

Overall, IEA has estimated that the global oil demand growth in 2019 is at 1.2 million barrels/day. In 1Q19, global growth was only 0.3 million barrels/day, and for 2Q19 the estimate is 1.2 million barrels/day. In 2020, global oil demand growth will rise to 1.4 million barrels/day, supported by solid non-OECD demand and petrochemicals expansion. The IMO switch will result in major changes to bunker fuel demand, sharply increasing gasoil demand from 4Q19. Non-OPEC supply growth will accelerate from 1.9 million barrels/day this year to 2.3 million barrels/day in 2020. The US leads the gains, but solid growth also comes from Brazil and Norway. In May, global oil supply eased by 0.1 million barrels/day to 99.5 million barrels/day, down 2.8 million barrels/day from the November peak. The call on OPEC crude drops to 29.3 million barrels/day in 2020, 650 thousand barrels/day below the May output level. OPEC supply fell to its lowest since 2014 as Iranian supply plunged due to sanctions and on lower Saudi and Nigerian output. OPEC's effective spare capacity was 3.2 million barrels/day.

Reported by **Quang Trung**

References

1. International Energy Agency (IEA). *Oil market report*. www.iea.org. 14/6/2019.